Für Ingo und Evelyn

Acknowledgements

First and foremost I wish to thank my parents for supporting me in all my endeavors, they deserve my deep gratitude.

I would like to thank my thesis supervisor Rüdiger Klein, who gave me the opportunity to work in a great scientific environment. I am grateful for his constant support and interest in my project and especially for his encouragement when I almost gave up.

I thank my thesis committee members, Rüdiger Klein, Francoise Helmbacher and Edgar Kramer for their interest, critical discussions and suggestions. Special thanks are dedicated to Francoise Helmbacher, who sparked my interest in motor neurons. I am grateful for her constant support in Munich and Marseille and for teaching me so many techniques.

I wish to acknowledge my collaborators for their excellent experimental contribution and scientific interest, especially Cathy Krull. I want to thank Artur Kania, Klas Kullander, Silvia Arber and Carlos Ibañes for providing mouse lines and constructs.

I thank all past and present lab members for a great working atmosphere, help whenever needed, discussions, criticism and lots of fun on retreats, ski-trips and Oktoberfest visits. My special thanks got to Francoise Helmbacher, Katrin Deininger, Irina Dudanova, Joaquim Egea, Christian Erlacher and Sónia Paixao.

My thanks go to the people of all the service units at the MPI, who make our work much easier. Special thanks to Anna Dengler, Bettina Hoisl und Patty Ziehlke from the animal facility for their excellent work.

I want to thank Till Marquardt for introducing me into the secrets of explant cultures and motor neuron tracings and for his interest, suggestions and scientific discussions.

Special thanks are dedicated to Irina Dudanova and Louise Gaitanos for critically reading this thesis and Tom Gaitanos, Katrin Deininger and Fabian Loschek for helping me with formatting matters.

Cooperation between GDNF/Ret and EphrinA/EphA4 signals for motor axon pathway selection in the limb

Dissertation

Der Fakultät für Biologie der Ludwig-Maximilian-Universität München

Eingereicht am 26.Oktober 2007 von Laura Franziska Knott aus München

Erstgutachter:	Prof. Dr. Rüdiger Klein
Zweitgutachter:	Prof. Dr. George Boyan

Tag der mündlichen Prüfung: 13.Dezember 2007

The work presented in this thesis was performed in the laboratory of Prof. Dr. Rüdiger Klein, Department of Molecular Neurobiology, Max-Planck Institute of Neurobiology, Martinsried, Germany.

Ehrenwörtliche Versicherung

Ich versichere hiermit ehrenwörtlich, dass die vorgelegte Dissertation von mir selbständig und ohne unerlaubte Beihilfe angefertigt ist.
Hiermit erkläre ich, dass ich mich anderweitig einer Doktorprüfung ohne Erfolg nicht unterzogen habe.

München, den ....
(Unterschift)

Table of Contents

Abstract

The vertebrate hindlimb has frequently been used as a model for the study of mechanisms involved in the establishment of specific neuronal connections. To select a specific trajectory, motor neurons have to make a series of axon guidance decisions involving the evaluation of different guidance cues in the periphery. Earlier studies showed that the pathway taken by the lateral fraction of the lateral motor column (LMC(l)) axons into the dorsal limb requires the EphA4 receptor, which mediates repulsion to ventrally expressed ephrinA ligands. This study implicates glial-cell-line-derived neurotrophic factor (GDNF) and its receptor, Ret, in the same axon guidance decision. In GDNF and Ret knockout mice, dorsally fated axons from the LMC(l) follow an aberrant ventral trajectory away from a GDNF-enriched dorsal territory, suggesting that the GDNF/Ret system provides an instructive signal for motor axon pathway selection. Conditional inactivation of Ret in the spinal cord leads to the same axon guidance phenotype, indicating a cell-autonomous function of Ret in motor neurons. This phenotype is enhanced in mutant mice lacking both Ret and EphA4 receptors, implying that signals from the two receptors cooperate to enforce the precision of the same binary choice in motor axon guidance. The idea of cooperation between Ret and EphA4 is supported by the observation that EphA4 and Ret receptors do not regulate the protein expression of each other. Moreover, preliminary experiments in transiently transfected cells have provided evidence for an activity-dependent interaction of the two receptors and an ability to phosphorylate each other. To study the sub-cellular localization in motor neurons and the behavior of their growth cones upon different stimuli, a culture system using explants or dissociated motor neurons was established.

Because ephrinAs have reverse signaling properties, it has been suggested that axonal ephrinAs expressed on limb innervating motor axons are functionally uncoupled from EphAs and mediate attraction toward the EphA4-positive dorsal limb mesenchyme. To test this hypothesis, a conditional mutant of EphA4 was intercrossed with different Cre-lines to determine the contribution of EphA4 in the

dorsal hindlimb mesenchyme for the dorsal/ventral guidance decision of LMC(l) axons. These studies are currently in progress.

Publication from the work presented in this dissertation

Kramer ER*, Knott L*, Su F, Dessaud E, Krull CE, Helmbacher F#, KleinR#
Cooperation between GDNF/Ret and EphrinA/EphA4 signals for motor axon pathway selection in the limb.
Neuron 2006 Apr 6;50(1):35-47

* and # : These authors contributed equally to this work

Abbreviations

ACSF	artificial cerebrospinal fluid
ACTB	β-actin (human Gen)
ALS	amyotrophic lateral sclerosis
Amp	ampicillin
AP	alkaline phosphatase
APS	Ammoniumpersulfate
ARTN	Artemin
BCIP	5-bromo-4-chloro-3-indolylphosphat
BES	N,N-bis[2-hydroxyethyl]-2-aminoethanesulfonic acid
BDNF	brain-derived neurotrophic factor
BHLH	basic Helix-loop-Helix
Bp	base pair
BPB	bromphenol blue
BSA	bovine serum albumine
°C	degree Celsius
Cad-8	cadherin-8
cDNA	complementary DNA
CHAPS	3-[(3-Cholamidopropyl)dimethylammonio]-1-propanesulfonate
CM	cutaneus maximus
CNS	central nervous system
CVS	cover slip
DAB	diaminobenzidine
DNA	desoxyribonucleic acid
C-terminal	carboxy terminal
D	dorsal
DIG	digoxygenin
DIV	days *in vitro*
DMEM	Dulbecco's modified Eagle's medium
dNTP	deoxyribonucleoside triphosphate
DRG	dorsal root ganglia
DTT	1,4-Dithio-DL-threitol
E	embryonic day
ECL	enhanced chemoluminescence
E. coli	*Escherichia coli*
EDTA	ethylendiamine-tetra acetic acid
Eph	erythropoietin-producing hepatocellular
Ephexin	Eph-interacting exchange protein
Ephrin	Eph-receptor interacting
EtOH	ethanol
ETS	E-twenty-six
FBS	fetal bovine serum
FL	full length
FLPe	flippase
FRT	FLPe recombinase targets
GC	growth cone

GDNF	glial-cell-line-derived neurotrophic factor
GFL	GDNF family ligand
GFP	green fluorescent protein
GFRα	GDNF family receptor α
GPI	glycosylphosphatidylinositol
Grb	growth-factor receptor-bound protein
h	hour
Hb9	homeobox gene 9
HBSS	Hank`s balanced salt solution
HeLa	Henrietta Lacks
HRP	horse radish peroxidase
HGFAP	human glia fibrillary protein
HPSF	High Purity Salt Free
HS	horse serum
HSCR	Hirschsprung`s disease
IF	immunofluorescence
Ig	immunoglobuline
IHC	Immunohistochemistry
IP	immunoprecipitation
Ip3	inositolphosphate 3
ISH	in situ hybridisation
IRES	internal ribosome entry site
ISCS	iron supplemented calf serum
Isl1	insulin-enhancer-binding protein 1
JM	juxtamembrane (region)
JNK	Jun N-terminal kinase
KD	kinase dead
ko	knock out
LB	Luria-Bertani
LD	Latissimus dorsi
LIM	TF of gene products lin11, Isl1 and mec-3
Lmxb1	LIM homeobox transcription factor 1, beta
LMC	lateral motor column
LMC(l)	lateral LMC
LMC(m)	medial LMC
lx	loxP
M	Mol
MAP	mitogen-activated protein
MEN2A	multiple endocrine neoplasia type 2A
MEN2B	multiple endocrine neoplasia type 2B
MetOH	methanol
min	minute
MMC	medial motor column
MN	motor neuron
mRNA	messenger RNA
NBT	nitroblue tetrazolium
NCAM	neural cell adhesion molecule
NCC	neural crest cell
neo	neomycin
Nes	Nestin
NGF	neurotrophic growth factor

Ngn	neogenin
Npn	neuropilin
NRTN	Neutrurin
NS	nervous system
N-terminal	amino terminal
OD	optical density
Olig2	oligodendrocyte lineage transcription factor 2
O/N	over night
P	postnatal day
PAGE	polyacrylamide-gel-electrophoresis
PBM	PDZ binding motif
PBS	phosphate buffered saline
PBST	PBS with Tween
PCD	programmed cell death
PCR	polymerase chain reaction
PDZ	Psd95/DL/ZO1
Pea 3	polyomavirus enhancer activator 3
pen/strep	penicillin/streptomycin
PFA	paraformaldehyde
PGK	phosphoglycerat kinase
PGT	PBS with gelatine and triton
pH	*potentium hydrogenii*
PI3-kinase	phosphatidylinositol 3-kinase
PLAP	placental alkaline phosphatase
PLCγ	Phospholipase γ
PMN	progenitor motor neuron
PNS	peripheral nervous system
PN	peroneal nerve
PSD-95	postsynaptic density protein 95
PSPN	Persephin
PVDF	polyvinylidene fluoride
pY	phospho-tyrosine
R	receptor
RA	retinoic acid
RALDH2	retinoic aldehyde dehydrogenase 2
Ret	rearranged in transformation
RNA	ribonucleic acid
RT	room temperature
RTK	receptor tyrosine kinase
SAM	sterile-α-motif
SC	spinal cord
SDS	sodium dodecyl sulfate
sec	second
Sema 3	semaphorin 3
Shh	sonic hedgehog
sol.	solution
TAE	Tris-acetate EDTA
Tbx4	T-box protein 4
TCL	total cell lysate
TD	transmembrane domain

TE	Tris-EDTA
TEMED	N,N,N´,N´-Tetremethylethylenediamine
TF	transcription factor
TK	tyrosine kinase
TN	tibial nerve
Tris	Tris[hydroxymethyl]aminomethane
TxR	Texas Red
UV	ultra violet
v	ventral
WB	western blot
wt	wild type
X-gal	5-bromo-4-chloro-3-indolyl-β-D-galactopyraniside
Y	Tyrosine
α	anti
βgal	β-galactosidase
μ	micro

List of Figures

1 Introduction

Almost five hundred years ago, Leonardo da Vinci recognized that nerve fibers project throughout the body in a highly stereotyped manner. To establish this amazingly precise pattern, a tremendous amount (~10^{15}) of specific neuronal connections is generated during development (Tessier-Lavigne and Goodman 1996). Thousands and thousands of neurons must selectively project to, and synapse with their appropriate targets, in order to perform coordinated movement and complex behavior (Landmesser 2001). En route to their often distant synaptic targets, neuronal axons migrate in a stepwise manner performing multiple pathfinding decisions as they navigate through the embryonic environment (Schneider and Granato 2003). Studies using surgical displacement of motor neurons or muscle targets revealed the existence of specific guidance cues (reviewed by (Landmesser 2001). To be able to sense and decipher these signals, growing axons are tipped with a specialized structure called a growth cone. Each growth cone is equipped with guidance receptors, which enable the axon to recognize a variety of cues presented by the environment and thereby find the correct target. Growth cone navigation is controlled by short- and long-range, attractive and repulsive cues. These guidance signals can be tethered to a cell surface or an extracellular matrix and thereby repel or attract axons in a contact-dependent manner. In contrast, diffusible signals can set up gradients and influence growth cones over long distances (Goodman 1996) (Figure 1). In the developing organism the distinction between long-range versus short-range is blurred and some signals can act as repulsive or attractive cues making it difficult to assign one molecule to a certain guidance mechanism (Goodman 1996; Dickson 2002). The establishment of topographically organized motor projections in the vertebrate hindlimb offers an easily manipulated model system, which can be used to better understand mechanisms involved in axon guidance decisions such as the interaction of different guidance cues. On the following pages I will give a brief introduction about motor

neuron development. I will also introduce the GDNF/Ret and ephrin/Eph signaling systems and emphasize their importance in motor neurons and axon guidance.

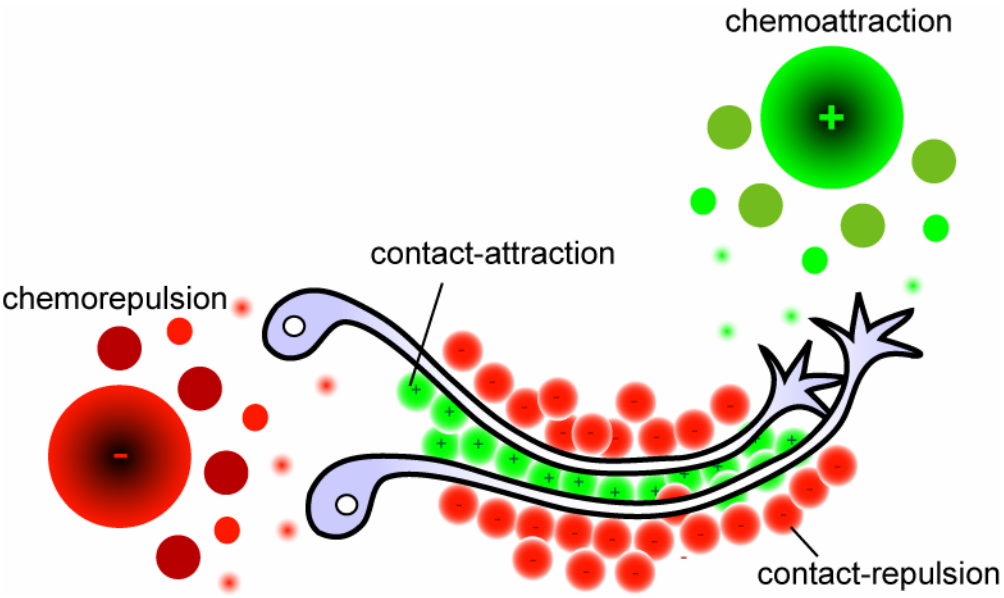

Figure 1 Axon guidance mechanisms

Schematic representation of the four basic guidance mechanisms: contact-attraction, contact-repulsion, chemoattraction and chemorepulsion. The growth cones of the two neurons are roughly directed by an opposing gradient of repulsive and attractive diffusible cues. Cells expressing repulsive or attractive guidance signals at their surface provide short-range cues giveing a more detailed path to grow on. Figure adapted from (Tessier-Lavigne and Goodman 1996).

1.1 Motor neurons

1.1.1 The "birth" of motor neurons

Early patterning events during neural tube closure establish the identity of neuronal progenitors in the spinal cord. In the dorsal spinal cord, bone morphogenic proteins (BMPs), which are secreted from the surface ectoderm and roof plate, control the specification of dorsal cell types such as neural crest cells or dorsal sensory interneurons (Lee and Jessell 1999). In contrast, Sonic hedgehog (Shh), a glycoprotein secreted from the notochord and the floor plate, creates a gradient that is required to specify the pattern of ventral progenitor domains at the ventricular zone including the motor neuron progenitor domain (pMN) (Briscoe and Ericson 1999). In response to the concentration of Shh, a unique combination of transcription factors termed class I (repressed by Shh) and class II (induced by Shh) is expressed in each progenitor domain, specifying five different regions (Figure 2). In addition, cross-repressive interactions between neighboring class I and II transcription factors are believed to sharpen the boundaries of the different domains (Briscoe, Pierani et al. 2000). Transcription factors Nkx6.1 and Nkx6.2 are present in motor neuron progenitors and allow the expression of Olig2 by repressing other cell determinants. Olig2 in turn regulates the expression of transcription factors Ngn2 and Hb9, which are involved in motor neuron differentiation (Shirasaki and Pfaff 2002). The birth of motor neurons is determined as the exit from the cell cycle, which is dependent on the action of Olig2 and Ngn2 (Novitch, Wichterle et al. 2003). Although Hb9 is not required initially for the generation of motor neurons, it is indispensable for the progression of a normal program of motor neuron specification. In the absence of Hb9 function, cells produced as motor neurons upregulate V2 interneuron characteristics (Nornes and Carry 1978; Pfaff, Mendelsohn et al. 1996; Thaler, Harrison et al. 1999). Once the progenitor cells have become motor neurons, they start to migrate laterally towards their final positions in the ventral spinal cord.

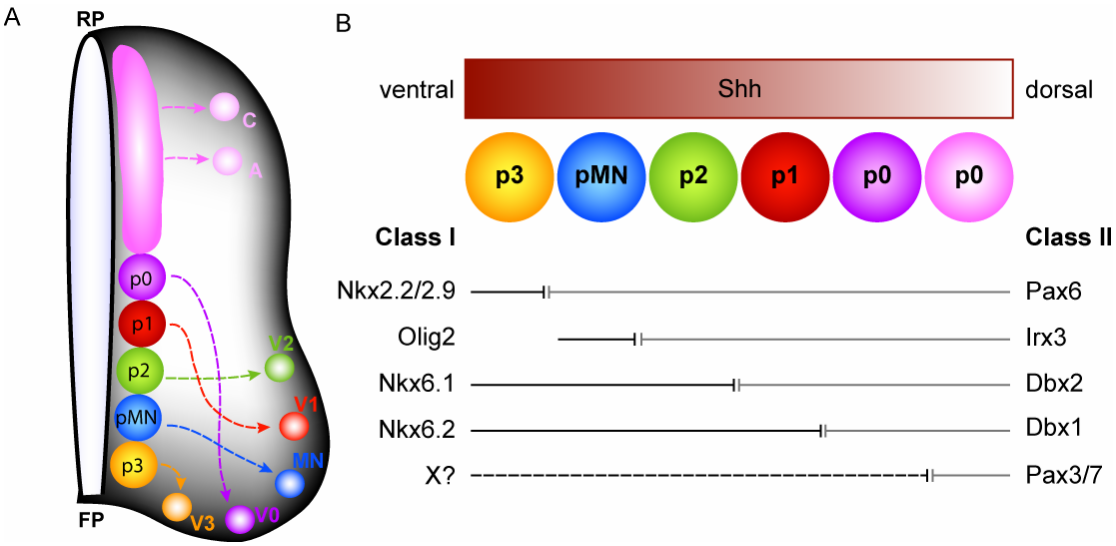

Figure 2 The birth of motor neurons

(A) The ventral spinal cord contains five progenitor domains (p0,p1,p2,pMN and p3) each giving rise to a certain type of interneurons (V0-V3) or motor neurons (MN), which migrate laterally to their stereotypic position. (B) A gradient of Shh leads to the differential expression of several transcription factors, which in turn determine the progenitor regions and the fate of their progeny. RP (roof plate), FP (floor plate), p (progenitor), MN (motor neuron), Shh (sonic hedgehog). Figure adapted from (Lee and Pfaff 2001).

1.1.2 Motor neuron organization – colonization of the ventral spinal cord

In vertebrates, each muscle fiber is contacted by a single motor neuron (MN), which can synapse with several muscle fibers (Kandel, 2000). Motor neurons innervating the same muscle are grouped together and form a MN pool. These pools are in turn organized in longitudinal columns in the ventral half of the spinal cord (Shirasaki and Pfaff 2002). Thereby, the anteroposterior and mediolateral position of a MN cell body correlates with the position of its target in the periphery forming a topographic neuronal map. Neurons within the medial motor column (MMC), which is present throughout the whole spinal cord, project to trunk muscles. In contrast, motor neurons innervating the limbs are located in the discontinuous lateral motor column (LMC), which is only present at limb levels (Lance-Jones and Landmesser 1981; Tsuchida, Ensini et al. 1994). Both MMC and LMC can each be further subdivided into a lateral and a medial part. While neurons of the medial MMC, which innervate axial muscles, are present throughout the whole rostro-caudal axis of the spinal cord, those of the lateral MMC are only found at thoracic levels projecting to

ventral body wall muscles (Figure 3A and B). Medial motor neurons within the LMC project to targets in the ventral limb, whereas cells located in the lateral fraction of the LMC only innervate the dorsal limb muscles (Figure 3A and C). A second column that is only present at thoracic levels connects with sympathetic ganglia and is termed the preganglionic motor column (PMC) (Figure 3A and B) (Landmesser 1978; Tsuchida, Ensini et al. 1994; Shirasaki and Pfaff 2002).

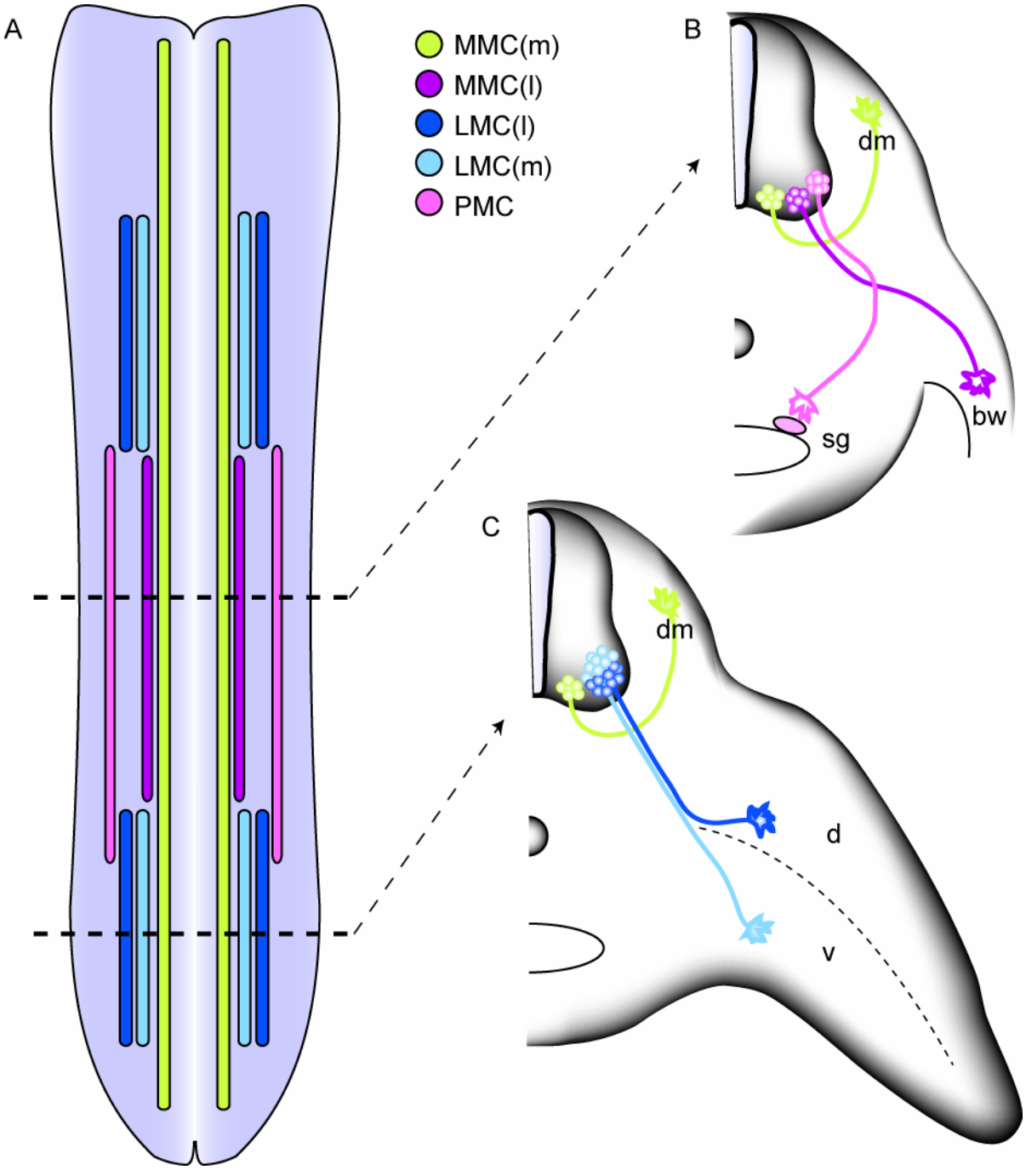

Figure 3 Organization of motor neurons in the spinal cord

(A) Schematic drawing of a spinal cord open-book preparation. Motor neuron cell bodies are organized in longitudinal columns along the rostrocaudal and mediolateral axis. Cross sections at thoracic (B) and lumbar (C) levels indicate the target regions innervated by different motor columns. Axons from the discontinuous LMC(l) and LMC(m) project to dorsal (d) and ventral (v) limb mesenchyme, respectively. MMC(m) neurons innervate the dermomyotome (dm), while neurons of the MMC(l) form connections with body wall muscles (bw). The PMC projects to neurons of the sympathetic ganglia (sg). Figure adapted from (Shirasaki and Pfaff 2002).

1.1.3 The LIM code and motor axon trajectories

As mentioned earlier, motor neurons are born at the ventricular zone of the ventral spinal cord. At that time, their fate is determined by the combinatorial expression of several transcription factors specifying their motor neuron subtype identity. In 1994 Tsuchida et al. identified a family of chick LIM homeodomain (LIM-HD) transcription factors that are expressed in spinal motor neurons in a combinatorial and highly dynamic manner. The differential expression of the four members Isl1, Isl2, Lim1 and Lhx3 (Drosophila Lim3) - the Lim-code – defines subtypes of motor neurons that occupy different columns in the spinal cord and innervate distinct targets. Because future LMC(l) neurons are born after LMC(m) neurons, they have to travel through the population of previously born LMC(m) neurons, which express RALDH2 (Hollyday and Hamburger 1977). This enzyme converts vitamin A into retinoic acid and induces the expression of Lim1 in LMC(l) motor neurons while migrating through the LMC(m) population. At the same time, the expression of Isl1 is extinguished in LMC(l) neurons (Sockanathan and Jessell 1998). Thus, LMC(l) motor neurons express Isl2 and Lim1, while those in the LMC(m) express Isl1 and Isl2 (Figure 4A and D). Lim-HD transcription factors are thought to have key functions in activating axon guidance programs for specific pathway selection and target recognition (Shirasaki and Pfaff 2002).

Each spinal cord segment has a common exit point for the axons of all cell bodies within that segment – the ventral horn. A remarkable feature of axon pathfinding by motor neurons is that after leaving the spinal cord, they initially follow a common ventral trajectory around embryonic day 11 (~E11.0) before they diverge into subtype specific trajectories (Landmesser 1978; Tosney and Landmesser 1985). The unique combination of transcription

factors in each motor neuron subtype allows them to express a particular set of guidance receptors that enables them to decipher specific guidance cues present at exit points from the common pathway (Shirasaki and Pfaff 2002). In the vertebrate hindlimb, LMC axons from lumbar segments L3-5 share a common pathway (sciatic nerve) to the base of the limb (sciatic plexus). Here, axons from the lateral and medial fraction of the LMC diverge into a dorsal and a ventral branch termed peroneal and tibial nerve, respectively (~E11.5) (Figure 4A). In Lim1 deficient mice, LMC(l) axons project into dorsal and ventral mesenchyme, randomizing dorsal/ventral-choice (Kania, Johnson et al. 2000) (Figure 4B). Mice deficient for another LIM-HD transcription factor, Lmx1b, which is expressed in dorsal hindlimb mesenchyme, have the phenotype of Lim1 knockout mice and in addition show a randomized dorsal/ventral–choice of LMC(m) axons (Riddle, Ensini et al. 1995; Kania, Johnson et al. 2000) (Figure 4C). In 2003, Kania et al. showed that LIM homeodomain proteins regulate the expression of the EphA4 receptor on LMC neurons and the level of ephrin-A protein along the dorsoventral axis of the limb mesenchyme.

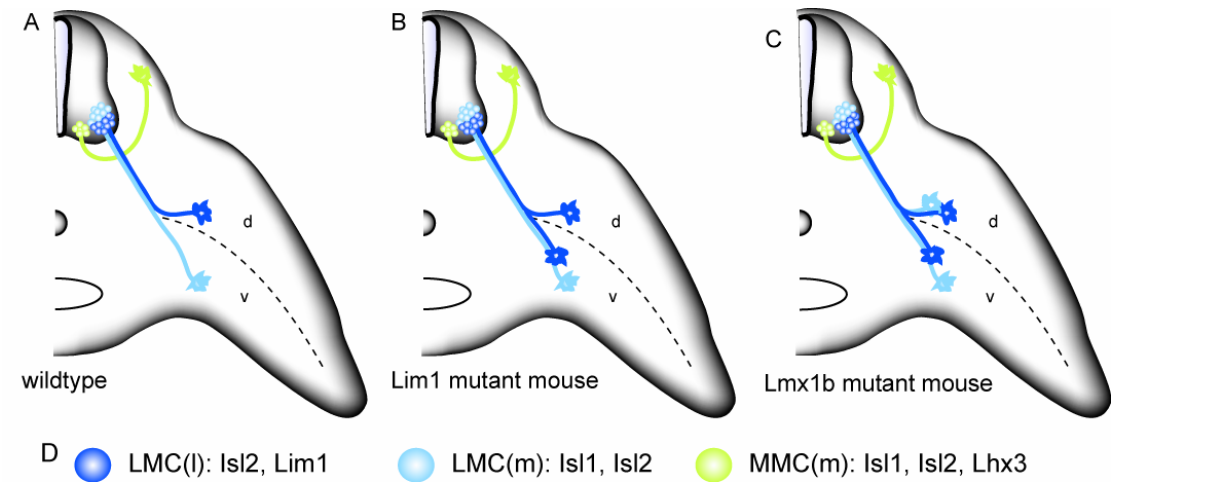

Figure 4 Mouse mutants and the Lim-code

(D) The combinatorial expression of different LIM-HD transcription factors defines motor neuron subclasses (e.g. LMC(l) and LMC(m)) and is important for the establishment of intrinsic axon guidance programs specific for each subclass. (A) In the wildtype situation, LMC(l) neurons express Lim1 and project their axons into the dorsal region of the hindlimb. LMC(m) neurons express Isl1 and innervate the ventral hindlimb. (B) Absence of Lim1 randomizes the dorsal/ventral choice of LMC(l)

axons. (C) Embryos lacking Lmx1b expression show defects in the projection of LMC(l) and LMC(m) motor axons. Figure adapted from (Shirasaki and Pfaff 2002).

However, the LIM-code by itself is insufficient to specify the entire range of motor neuron subtypes and does not alone distinguish the identity of motor pools. The clustering of motor neurons into pools occurs at the time when axons first invade their target muscles (Landmesser 1978). The allocation of neurons to specific motor pools can be revealed by the expression of members of the ETS gene family, notably Er81 and Pea3 (Lin, Saito et al. 1998; Livet, Sigrist et al. 2002). In the absence of Pea3 function, the axons of specific sets of motor neurons fail to branch appropriately within their target muscle, resulting in a marked defect in neuromuscular innervation. In addition, the cell bodies of Pea3-deficient motor neurons fail to cluster or to settle in their characteristic position in the LMC, suggesting that the peripherally regulated induction of ETS gene expression coordinates the terminal arborization and central positioning of specific sets of spinal motor neurons (Livet, Sigrist et al. 2002).

1.1.4 Programmed cell death

During normal development, large numbers of neurons in the central and peripheral nervous system (CNS and PNS) undergo naturally occurring cell death. About half of all spinal motor neurons die over a period of a few days in developing avian, rat and mouse embryos (Oppenheim, Houenou et al. 1995). In mice this period includes embryonic days 13-18 with a peak at E14 (Lance-Jones 1982; Oppenheim 1986). According to the classical neurotrophin hypothesis, neuronal survival is regulated by limited access to target-derived neurotrophic substances (Giehl 2001). Neurons, generated in excess, must compete for a limited amount of neurotrophic factors, such as BDNF (brain-derived neurotrophic factor), GDNF (glial-cell-line-derived-neurotrophic factor) or NGF (nerve growth factor) produced by the target cells (Figure 5). In GDNF deficient mice, the loss of spinal motor neurons is increased, while *in utero* treatment with GDNF leads to increased survival rates (Oppenheim, Houenou et al. 2000). The trophic support of GDNF for spinal motor neurons is mediated by Ret, which was previously known as an orphan oncogenic receptor tyrosine kinase (Durbec, Marcos-Gutierrez et al. 1996).

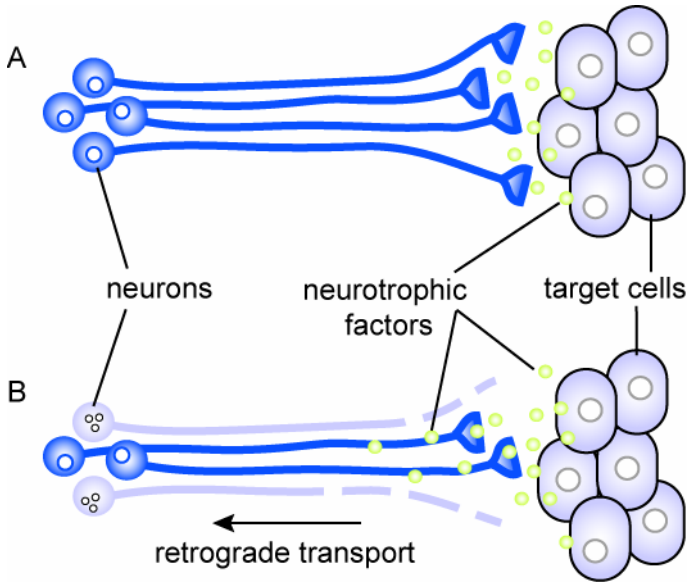

Figure 5 Neurotrophin hypothesis

(A) During development, neurons are produced in excess and compete with each other for target derived trophic support. (B) Limited amounts of neurotrophic factors leads to programmed cell death and to a marked reduction in the cell number. Figure adapted from (Reichardt).

1.2 GDNF and Ret

1.2.1 Receptor tyrosine kinase Ret and its signaling crew

Ret (*rearranged in transformation*) is a member of the receptor tyrosine kinase family and was originally identified as a proto-oncogene (Takahashi, Ritz et al. 1985). The Ret receptor is composed of an extracellular domain, a transmembrane domain and an intracellular kinase domain, which is divided into two parts by a linker region (Iwamoto, Taniguchi et al. 1993). The extracellular part consists of a cadherin-related motif and a cystein-rich domain (Takahashi, Buma et al. 1989) (Figure 6). So far, three isoforms that are generated by alternative splicing in the 3` region have been cloned (Ishizaka, Itoh et al. 1989; Myers, Eng et al. 1995). The short and the long isoform contain 9 and 51 amino acids in the C-terminal tail, respectively, and are the best-characterized isoforms *in vivo*. The third isoform has 43 amino acids. Monoisoformic Ret9 mice are viable and normal, whereas monoisoformic Ret51 mice display kidney hypoplasia and lack enteric ganglia from the colon, suggesting that

these isoforms have different tissue-specific effects during development (de Graaff, Srinivas et al. 2001).

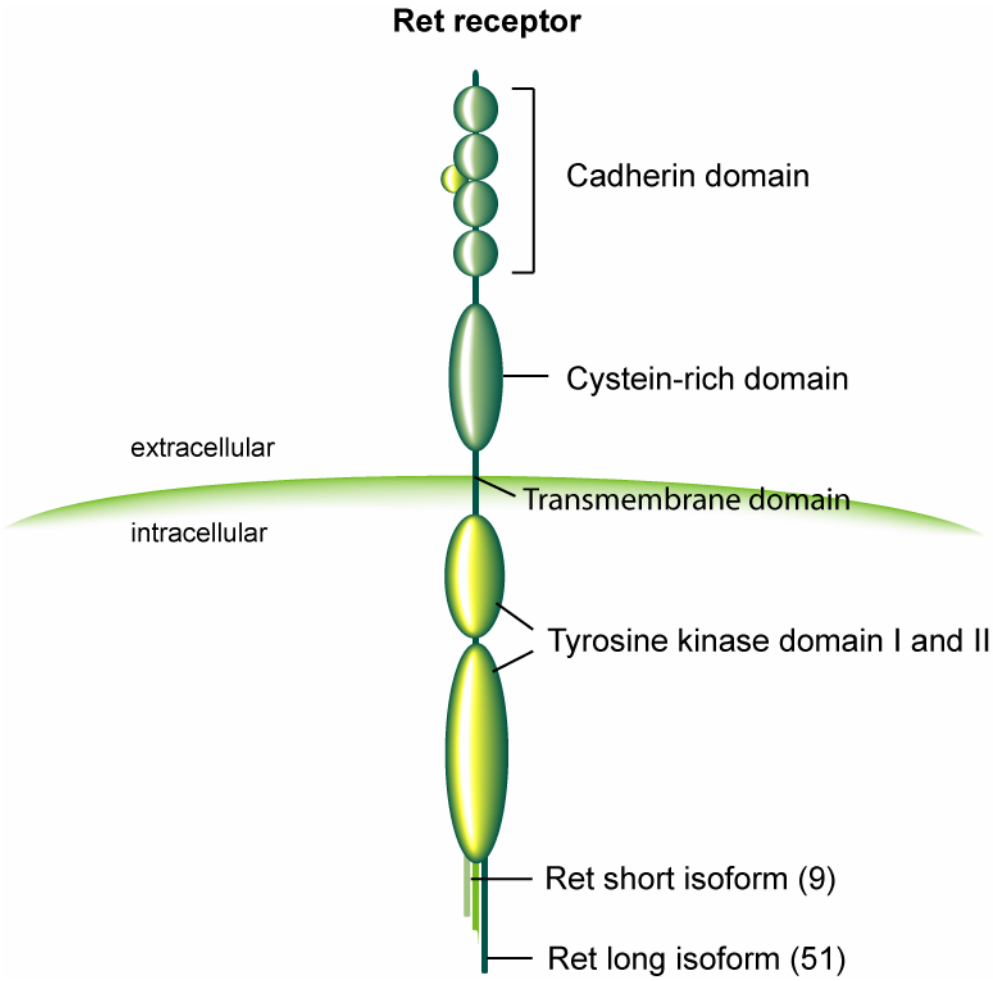

Figure 6 Structure of the Ret receptor

Schematic drawing of receptor tyrosine kinase Ret. The extracellular part is comprised of a cystein-rich domain and a cadherin domain, which binds $Ca2^{+}$. The cytoplasmic domain contains a tyrosine kinase domain, which is divided into two parts by a linker region. The short, medium and long isoforms have 9, 43 or 51 amino acids, respectively, and are generated by alternative splicing.

Ret is the receptor for the members of the glial-cell-line-derived neurotrophic factor (GDNF) family of ligands (GFLs) (Baloh, Enomoto et al. 2000). This family includes GDNF, Neurturin (NTRN), Artemin (ARTN) and Persephin (PSPN), which are structurally related to transforming growth factor (TGF)-β and contain seven conserved, similarly spaced cystein residues (Takahashi 2001). GFLs signal through a unique multicomponent receptor complex

consisting of glycosyl-phosphatidylinositol (GPI) -anchored coreceptor (Gfrα1-4) as a ligand-binding component and Ret as a signaling component (Airaksinen, Titievsky et al. 1999). GDNF, NTRN, ARTN and PSPN use Gfrα1, Gfrα2, Gfrα3 and Gfrα4 as the preferred ligand-binding receptors, respectively, although alternative ligand-coreceptor interactions are possible (Airaksinen, Titievsky et al. 1999; Sariola and Saarma 2003; Plaza-Menacho, Burzynski et al. 2006) (Figure 7).

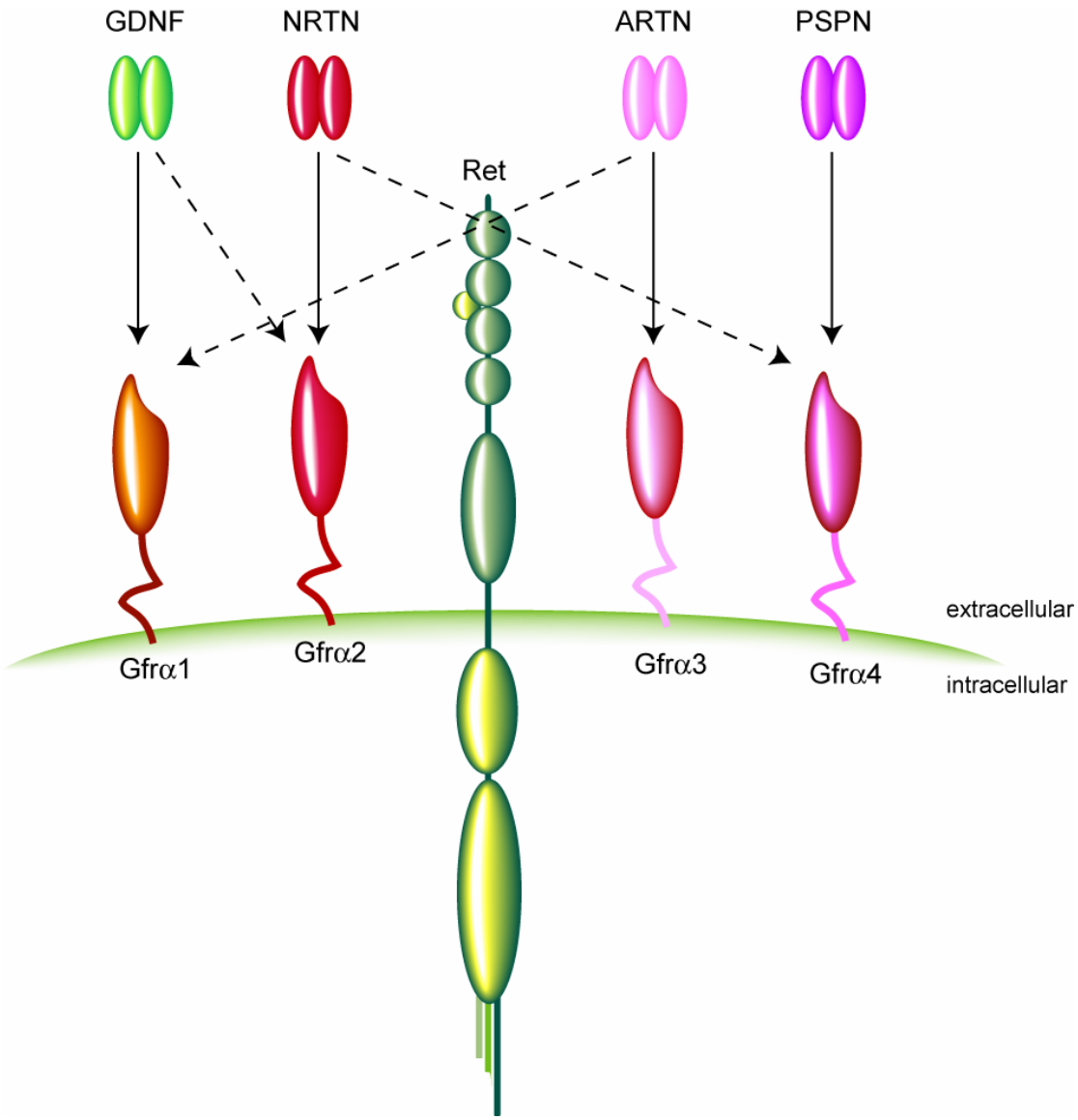

Figure 7 Ret and its signaling crew

Ret is the signaling receptor for ligands of the GDNF-family. GDNF, Neurturin (NTRN), Artemin (ARTN) and Persephin (PSPN) bind to the coreceptors Gfrα1, Gfrα2, Gfrα3 and Gfrα4, respectively, but alternative ligand-coreceptor interactions are possible. Figure adapted from (Airaksinen, Titievsky et al. 1999)

A dimeric GDNF binds to Gfrα1 or 2 and this complex in turn interacts with Ret inducing homodimerization and subsequent auto-phosphorylation of its 12 tyrosine residues (Jing, Wen et al. 1996; Kawamoto, Takeda et al. 2004) (Figure 8).

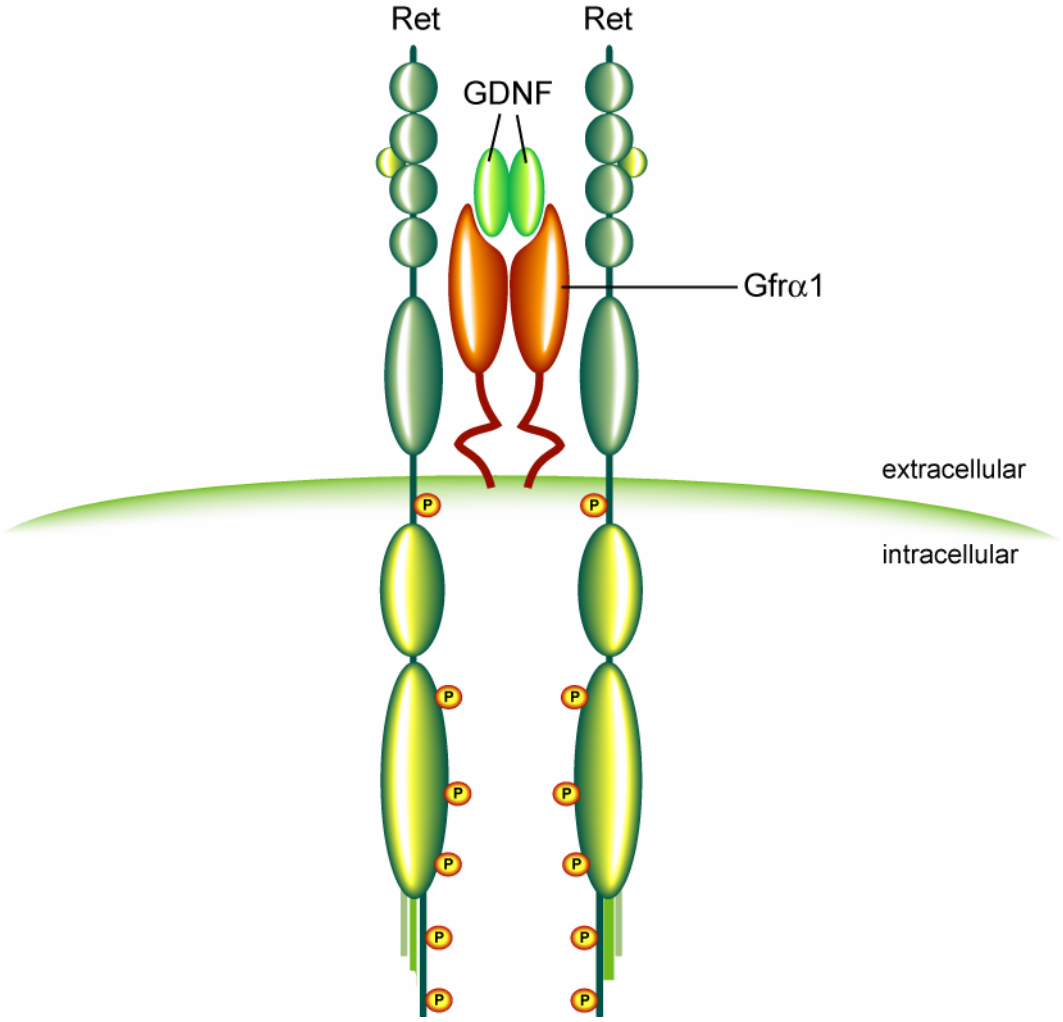

Figure 8 GDNF/Gfrα1/Ret signaling complex

A GDNF dimer binds to Gfrα1 or 2 and this complex in turn interacts with Ret inducing homodimerization and subsequent auto-phosphorylation of its 12 tyrosine residues (only 6 phosphotyrosines are indicated with P on orange background).

1.2.2. Expression pattern of Ret, Gfrα1 and GDNF

During development, receptor tyrosine kinase Ret is present in the nervous and excretory systems of the mouse. While its expression is maintained during adulthood in CNS and PNS, it is down-regulated in the excretory system (Pachnis, Mankoo et al. 1993). Ret mRNA can be detected in peripheral enteric, parasympathetic, sympathetic and sensory neurons (Enomoto, Heuckeroth et al. 2000). In addition, Ret is found in central motor neurons, noradrenergic and dopaminergic neurons (Miyazaki, Asai et al. 1993; Trupp, Arenas et al. 1996). In contrast to GDNF, which is mainly expressed in the target regions of Ret-positive neurons, Gfrαs are usually coexpressed with Ret (Trupp, Belluardo et al. 1997). However, Gfrα receptors are also present in neurons of the basal fore-brain, which lack Ret expression, suggesting a Ret-independent function possibly involving other transmembrane molecules (Trupp, Belluardo et al. 1997). Neural cell adhesion molecule (NCAM) has been shown to function as a signaling receptor for members of the GDNF ligand family in association with GFRα1 (Paratcha, Ledda et al. 2003). Conversely, there are also GDNF sensitive neurons, which express Ret but no Gfrα receptors. These neurons either use another co-receptor, or they can interact with soluble Gfrα receptor presented *in trans* (Trupp, Belluardo et al. 1997).

1.2.3 Biological functions of GDNF and Ret

As mentioned in the section on programmed cell death, GDNF, which was originally identified as a survival factor for embryonic dopaminergic neurons (Lin, Doherty et al. 1993), promotes survival of Ret/Gfrα1-expressing motor neurons. Subsequently, GDNF has been shown to be a physiological survival signal and axon outgrowth promoting factor (Henderson, Phillips et al. 1994; Oppenheim, Houenou et al. 1995; Oppenheim, Houenou et al. 2000; Markus, Patel et al. 2002). Ectopic expression of GDNF in muscle of mouse models leads to local hyperinnervation (Nguyen, Parsadanian et al. 1998). In addition, GDNF was found to specify motor neuron identity by inducing expression of ETS transcription factor

Pea3, thereby modulating axon growth toward specific muscle targets (Haase, Dessaud et al. 2002).

Loss of Ret, GDNF or the coreceptor GFRα1 results in renal agenesis in mice, due to inhibition of ureteric bud growth and branching (Schuchardt, D'Agati et al. 1994; Treanor, Goodman et al. 1996). In the developing kidney, the ureteric bud diverticulum grows out of the nephric duct and invades a group of adjacent cells, the metanephric mesenchyme. This outgrowth is stimulated by GDNF, which is expressed in the mesenchyme and activates the Ret receptor tyrosine kinase on the ureteric bud epithelia through co-receptor GFRα1 (Kim and Dressler 2007). In cell culture, GDNF is a chemoattractant for Ret-expressing epithelial cells (Tang, Worley et al. 1998). Similarly, the GDNF/Ret pathway is required for migration of enteric neuron precursor cells into the gut, also through a chemotactic mechanism (Natarajan, Marcos-Gutierrez et al. 2002). Later, GDNF promotes proliferation and differentiation of these enteric precursor cells (Natarajan, Grigoriou et al. 1999). Thus, inactivating mutations of Ret, GDNF and Grfα1 result in the absence of innervation from enteric neurons below the stomach (Enomoto, Araki et al. 1998; Airaksinen, Titievsky et al. 1999). In contrast, activating mutations of Ret are associated with multiple endocrine neoplasia type 2 (MEN2A and MEN2B) and several endocrine and neural-crest-derived tumors. In MEN2A, the replacement of a crucial cystein residue facilitates an inter-molecular instead of an intra-molecular disulfide bond resulting in a permanently dimerized, and thus activated, receptor. In MEN2B and familial medullary thyroid carcinoma (FMTC), patients have mutations located in the cytoplasmic part of Ret, resulting in altered catalytic activity and substrate specificity (Plaza-Menacho, Burzynski et al. 2006).

1.3 Eph receptors and ephrin ligands

Eph receptors constitute the largest family among receptor tyrosine kinases (RTKs) including 14 vertebrate members (1997; Orioli and Klein 1997). In contrast, there are only one Eph receptor and four ephrin ligands found in *C.elegans*, while Drosophila has a single Eph receptor and ephrin ligand (George, Simokat et al. 1998; Scully, McKeown et al. 1999). The family of Eph receptors has several unique features in comparison to other RTKs. First, Eph receptors and ephrin ligands are both membrane-bound and therefore cell-cell contact is required for receptor-ligand binding. Second, following activation upon binding, both Eph

receptors and ephrin ligands, can transduce signals into their host cells via forward and reverse signaling, respectively (Zimmer, Palmer et al. 2003; Poliakov, Cotrina et al. 2004). Third, Ephs and ephrins are able to form higher order clusters, which have been shown to be important for cellular responses (Stein, Lane et al. 1998; Egea, Nissen et al. 2005). In molecular terms, many of the signaling pathways that are downstream of Ephs and ephrins converge to regulate the cytoskeleton. The Rho family of small GTPases, including Cdc42, Rac and Rho, has a central role in the control of dynamic reorganization of the actin cytoskeleton (Hall and Nobes 2000). The activity of Rho family GTPases in turn is controlled by guanine nucleotide exchange factors (GEFs) that facilitate the exchange of GDP to GTP (Schmidt and Hall 2002). The ability of Eph receptors and ephrins to bind and/or activate such GEFs enables them to regulate the actin cytoskeleton in an extremely localized manner resulting in a directional response to attractive or repulsive cues (Noren and Pasquale 2004). Eph/ephrin modulation of Rho family GTPases in neuronal cells regulates growth cone dynamics, in which a shift of signaling towards RhoA results in growth cone retraction, while prevalence of Rac1 and Cdc42 activity stimulates neurite extension (Shamah, Lin et al. 2001; Gallo, Yee et al. 2002; Gallo and Letourneau 2004).

1.3.1 Eph receptor family

Eph receptors are single-pass transmembrane molecules including a globular (ligand-binding) domain, a cystein-rich domain and two fibronectin type-III motifs in the extracellular part. They can be grouped into two subclasses (A-type and B-type) on the basis of extracelluar domain homology (1997; Orioli and Klein 1997). The intracellular part is comprised of a juxtamembrane region, a kinase domain, a sterile-α-motif (SAM domain) and a PDZ-interaction motif at the very c-terminus (Kullander and Klein 2002) (Figure 9). The two latter ones appear to be involved in the dimerization and tetramerization of the receptor (Stapleton, Balan et al. 1999; Thanos, Goodwill et al. 1999). Interaction with ephrin ligands leads to auto-phosphorylation of the two juxtamembrane tyrosines, which induces the release of auto-inhibition ultimately resulting in “forward signaling” (Kalo and Pasquale 1999; Himanen and Nikolov 2003).

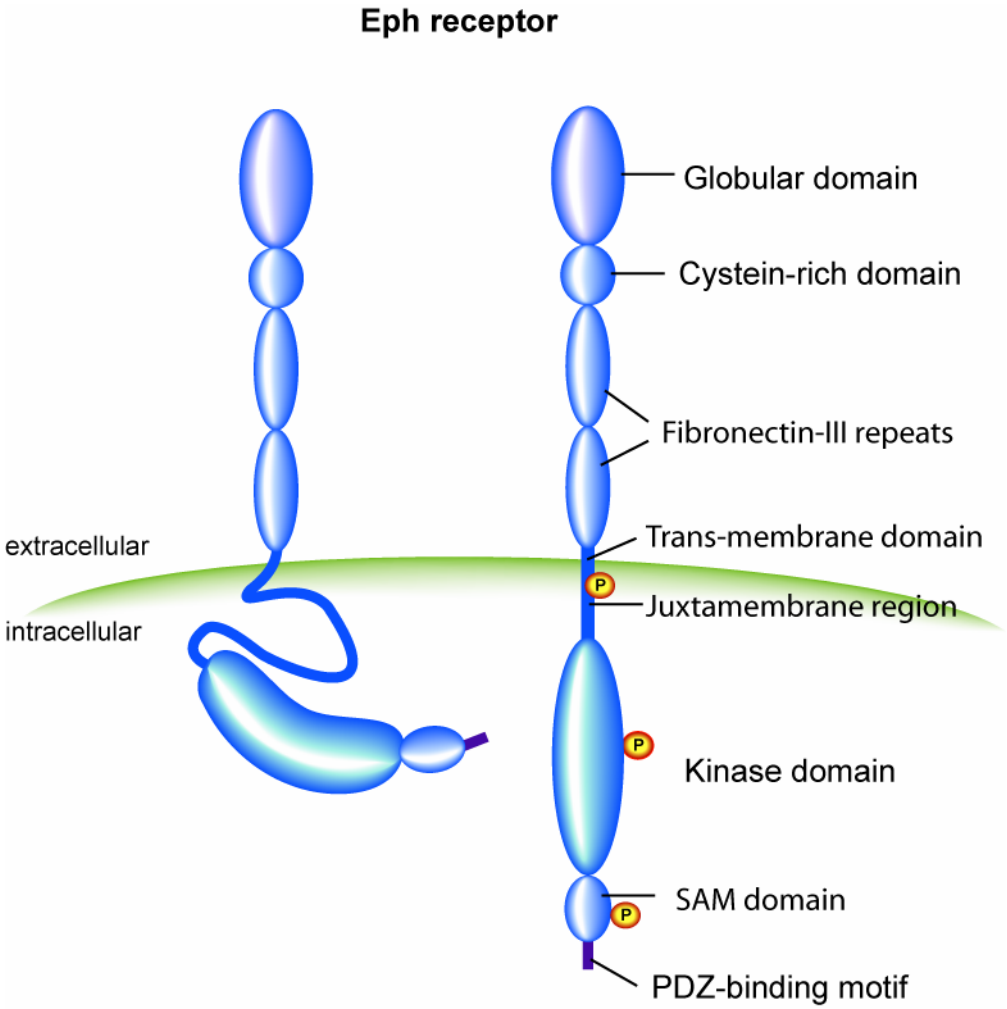

Figure 9 Structure of Eph receptors

The structure of the Eph receptor is shown in its inactive conformation on the left, with an auto-inhibited kinase domain resulting from interaction with the juxtamembrane region. On the right side the Eph receptor structure is shown in its active conformation caused by oligomerisation with ephrin ligand (not depicted). The phosphorylated tyrosine residues are indicated with orange balls. SAM (sterile-α-motif), PDZ (PSD-95Disc large and ZO [Zona Occludens]-1/2) binding motif are also indicated. Figure adapted from (Himanen and Nikolov 2003).

1.3.2 Ephrin ligands

Eph receptor-binding proteins, the ephrins, are also classified into A-type or B-type depending on sequence conservation and their binding preferences to EphA and EphB receptors (1997; Orioli and Klein 1997). Typically, ephrinAs interact with EphA receptors and ephrinBs with EphB receptors. However, ephrinB2 and B3 can also bind to EphA4 and ephrinA5, which can bind to EphB2. Within each subclass binding is rather promiscuous

(Brambilla, Bruckner et al. 1996; Himanen and Nikolov 2003). The mammalian genome encodes five ephrinA and three ephrinB ligands. EphrinAs are linked to the membrane via a glycosylphosphatidylinositol (GPI) anchor, while ephrinBs contain a transmembrane domain and a short cytoplasmic tail, which includes a PDZ-binding motif and five highly conserved tyrosine residues (Bergemann, Zhang et al. 1998) (Figure 10). Although lacking an intrinsic kinase activity, ephrins can transduce signals via interactions with PDZ-binding proteins. Furthermore, ephrinBs become tyrosine phosphorylated upon EphB receptor binding (Holland, Gale et al. 1997; Bruckner and Klein 1998). Despite the absence of a cytoplasmic tail, ephrinAs have been shown to mediate integrin-dependent adhesion to laminin upon Eph receptor stimulation (Huai and Drescher 2001), presumably by recruiting other signaling molecules into microdomain complexes in rafts (Gauthier and Robbins 2003; Holmberg, Armulik et al. 2005).

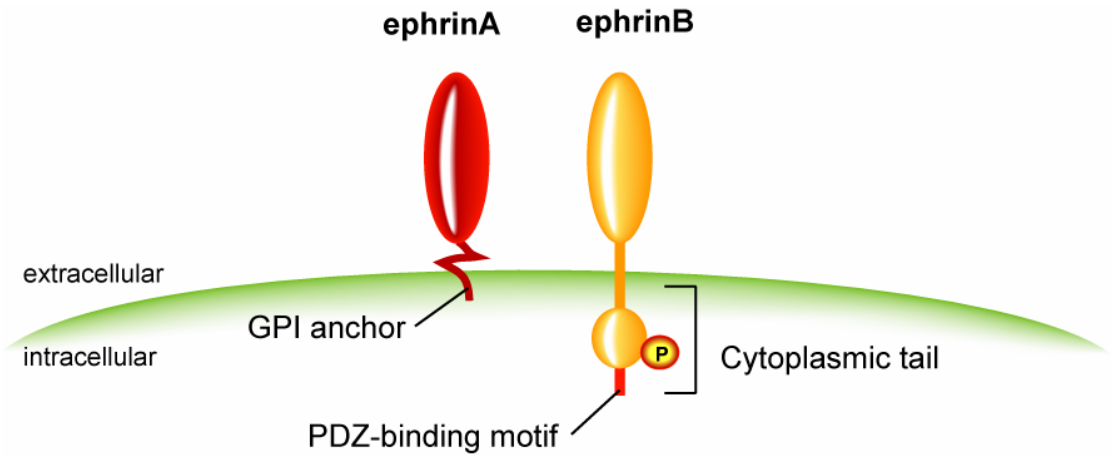

Figure 10 Structure of ephrin ligands

EphrinAs are tethered to the membrane via a GPI anchor, while ephrinBs have a single transmembrane domain. Both ligands have a conserved extracellular Eph receptor binding domain. EphrinBs have a short cytoplasmic tail including a PDZ binding motif and five highly conserved tyrosine residues, which are phosphorylated upon interaction with Eph receptor (indicated as orange ball).

1.3.3 Roles of Ephs and ephrins in axon guidance

Eph receptors and ephrin ligands are expressed in many tissues during development and adulthood in a sometimes overlapping, or sometimes reciprocal fashion and are therefore important for a vast array of different biological functions. Due to their membrane attachment, Ephs and ephrins are predestined for functions that require cell-cell contact such as tissue-border formation, cell migration, angiogenesis, segmentation or axon guidance (Wang and Anderson 1997; Zhang and Hughes 2006). The influence of Eph/ephrin activation on cell behavior depends on the cell-type, but can typically be attributed to repulsion, such as in preventing migrating cells or neuronal growth cones from crossing into ligand-expressing territory (Flanagan and Vanderhaeghen 1998; Wilkinson 2001). However, in a few cases, Eph/ephrin activation can lead to increased attraction or adhesion (Eberhart, Barr et al. 2004). While it is naturally easy to understand how membrane-bound molecules mediate adhesion between cells, disengagement of high affinity binding molecules such as Eph receptors and ephrin ligands, which is a prerequisite for repulsion, was puzzling until two mechanisms were discovered: (i) proteolytic cleavage of the ephrinA ectodomain by Kuzbanian metalloproteases, allowing the receptor expressing cell to retract (Hattori, Osterfield et al. 2000) and (ii) bi-directional endocytosis of the intact receptor-ligand-complex into EphB or ephrinB-expressing cells (Zimmer, Palmer et al. 2003).

1.3.3.1 Topographic mapping – navigating along gradients

In topographic maps, axons from a field of neuronal cell bodies establish connections with a target tissue thereby maintaining nearest-neighbor relationships. Complementary expression of Eph receptors on navigating axons and ephrin gradients in their target areas is consistent with a role for these in the formation of topographic projections (Tessier-Lavigne 1995). Indeed, the first functional evidence of a role for Eph receptors in axon guidance came from the purification and cloning of ephrinA5 as a tectal protein with the ability to collapse retinal axon growth cones (Drescher, Kremoser et al. 1995). The retinotectal projection is the prototypic model system for studying the development of topographic maps. Axons from the nasal retina project to the posterior tectum and those from the temporal retina innervate the anterior tectum. (Mey and Thanos 2000; Thanos and Mey 2001). In a simplified model,

axons expressing EphA receptors at a high density project to a region of the tectum with low ephrinA expression and conversely, axons with a low EphA receptor density innervate a region of the tectum with high ephrinA expression. In recent years this situation has become more complicated, because both EphA receptors and ephrinA ligands were found to be expressed on retinal axons and in the tectum (Knoll and Drescher 2002) (Figure 11). The response of retinal axons expressing high levels of EphA receptors to the tectal ephrinA gradient has been found to be less sensitive with increasing coexpression of ephrinAs. Carvalho and colleagues (2006) discovered that EphA3 and ephrinA5 can interact *in cis*, which inhibits the receptor signaling, thus resulting in a loss of sensitivity of retinal axons to ephrinAs *in trans* (Yin, Yamashita et al. 2004; Carvalho, Beutler et al. 2006). In contrast, the vomeronasal system (accessory olfactory system), which is involved in mating and aggression behavior provides a more simple model, because the expression of ephrinA ligand and EphA receptor is restricted to axons emerging from the vomeronasal organ (VNO) or the accessory olfactory bulb (AOB), respectively. Axons coming from the apical VNO express ephrinA6 at high density and project to the anterior AOB, which has high levels of EphA6, while axons from the basal VNO with low levels of ephrinA ligand connect to the posterior part of the AOB, which has low levels of EphA6. These results suggested a role for ephrinAs as receptors mediating attraction for navigation vomeronasal axons to their target zones (Knoll, Zarbalis et al. 2001).

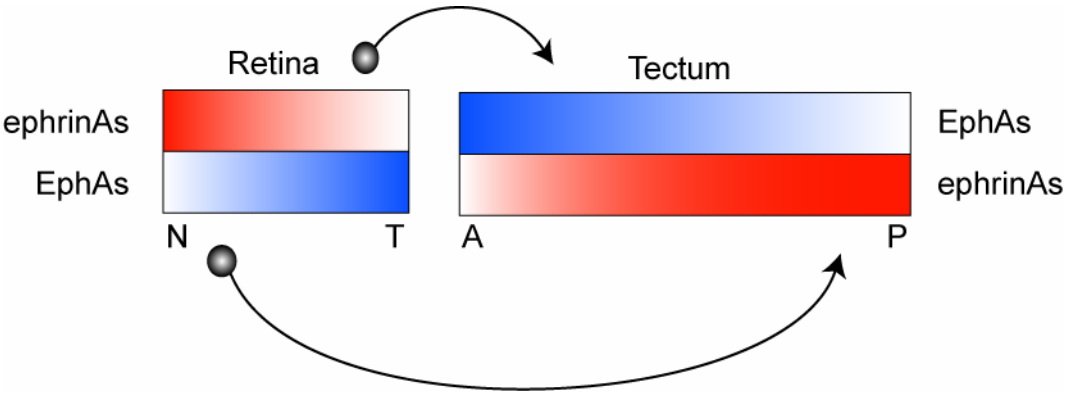

Figure 11 The retinotectal system

Schematic representation of Eph and ephrin gradients in mouse retina and tectum. Temporal (T) retinal ganglion cells (RGCs) expressing low amounts of ephrin, but high amounts of Eph receptor, project to anterior regions of the tectum, which has high levels of Eph receptor and low levels of

ephrin ligand. The opposite is true for nasal (N) RGCs, which innervate posterior regions of the tectum.

1.3.3.2 Ephs and ephrins – motor axon scouts in the vertebrate hindlimb

A number of studies in mice and chick have implicated the ephrinA/EphA4 signaling system in repulsive guidance of LMC(l) axons to the dorsal compartment of the limb. LMC(l) axons express EphA4 at high density, whereas LMC(m) axons express it at low density, and ephrinA protein levels are higher in ventral than dorsal limb mesenchyme (Eberhart, Swartz et al. 2000; Helmbacher, Schneider-Maunoury et al. 2000) (Figure 12A). Inactivation of the *ephA4* gene (ephA4^{lacZ} allele) causes misprojection of dorsal axons towards a ventral trajectory, which can lead to hindlimb stiffness (club foot phenotype) (Helmbacher, Schneider-Maunoury et al. 2000) (Figure 12B). Moreover, ectopic expression of EphA4 in chick LMC(m) neurons causes dorsal rerouting of their ventrally fated axons indicating that EphA4 is sufficient to guide motor axons (Eberhart, Swartz et al. 2002; Kania and Jessell 2003) (Figure 12C). Thus, it is believed that axons expressing high levels of EphA4 are repelled by ventral mesenchyme expressing high levels of ephrinA. Interestingly, LMC(l) axons coexpressing ephrinA ligands with EphA4 receptor, and EphA4 mRNA and protein are expressed by dorsal limb mesenchyme (Eberhart, Swartz et al. 2000; Helmbacher, Schneider-Maunoury et al. 2000; Kania and Jessell 2003). A recent study showed that ephrinA ligands are functionally uncoupled from coexpressed EphA receptors in chick motor axon growth cones. Ephs and ephrins segregate laterally into distinct membrane domains and signal opposing effects on the growth cone: EphAs direct growth cone collapse/repulsion and ephrinA signaling leads to motor axon growth/attraction (Marquardt, Shirasaki et al. 2005). These results are contradictory to the findings in the retinotectal system and so far it is unknown if axonal ephrinAs on LMC(l) neurons and mesenchymal EphA4 in the dorsal hindlimb play a role for the guidance of those motor axons.

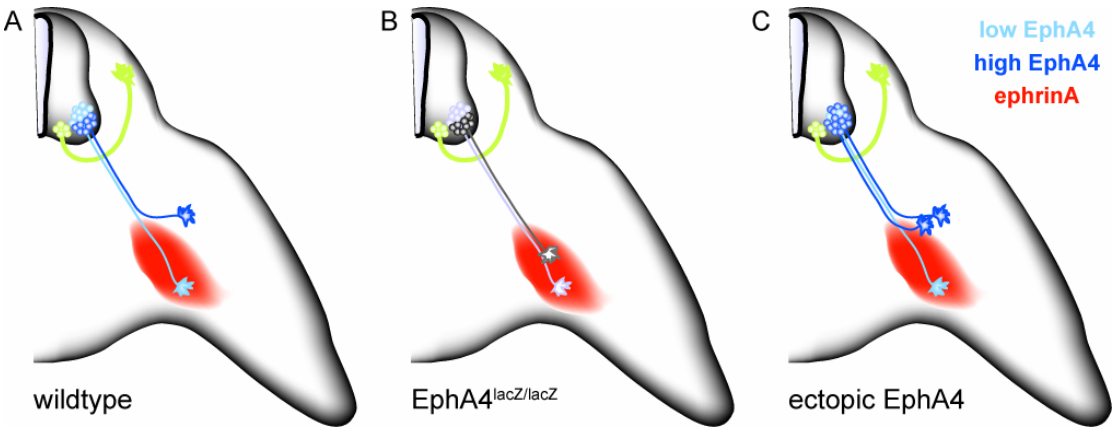

Figure 12 EphrinAs and EphA4: motor axon guidance in the limb

(A) In the wildtype situation, axons from the LMC(l), which express high levels of EphA4 are repelled by ventrally expressed ephrinA ligands into the dorsal compartment of the limb. (B) In the absence of EphA4 receptor, LMC(l) axons are insensitive to the repulsive signals and grow into ephrinA expressing territory. (C) In contrast, ectopic expression of EphA4 in LMC(m) neurons redirects their ventrally fated axons into the dorsal hindlimb mesenchyme.

1.4 The thesis project

As outlined in the previous chapters, genetic and biochemical studies have revealed important principles of axon guidance, especially using the motor neuron system. In the early 1990s, several conserved families of axon guidance molecules were discovered, including Slits, semaphorins and ephrins (Dickson 2002). Despite these major advances, many questions remain unanswered. For example, it is not understood, how repulsive ephrinAs in the ventral hindlimb mesenchyme instruct EphA4-positive axons to extend dorsally in the limb. Also, the severity of the *ephA4* loss-of–function phenotype is somewhat variable depending on which *ephA4* allele is studied and does not always result in stiff hindlimbs (Dottori, Hartley et al. 1998; Helmbacher, Schneider-Maunoury et al. 2000; Kullander, Croll et al. 2001; Leighton, Mitchell et al. 2001). These unsolved issues suggest the existence of yet unknown guidance cues that act in parallel to the established EphA4 pathway.

Here, I provide evidence that Ret and GDNF mediate the dorsoventral choice of limb-innervating motor neurons. This requirement becomes evident before the period of programmed cell death and appears to be a true guidance decision rather than an outgrowth

promoting effect. In the absence of Ret or GDNF, a significant proportion of dorsally fated LMC(l) axons is misguided into the ventral compartment of the hindlimb. Moreover, this phenotype is enhanced in EphA4/Ret double mutants, suggesting that both signaling systems act simultaneously and in a cooperative manner to enforce the same binary choice in motor axon guidance. The hypothesis of cooperation between GDNF/Ret and ephrinA/EphA4 signaling systems is supported by the fact that Ret and EphA4 receptor do not interfere with the expression of each other in motor axons. In addition, preliminary experiments using a biochemical approach give an indication for an activity-dependent interaction of the two receptors.

Interestingly, EphA4 is also expressed in dorsal hindlimb mesenchyme, and ephrinAs are present in lumbar motor neurons. Contradicting studies provide evidence for both an interaction of axonal EphA receptor and ephrinA ligand in cis, resulting in a silenced receptor signaling (Yin, Yamashita et al. 2004; Carvalho, Beutler et al. 2006), and independent mediation of repulsion by EphA receptor and attraction through ephrinA ligand signaling in the same axon (Marquardt, Shirasaki et al. 2005). To better understand and dissect out the function of coexpressed EphA4 and ephrinAs in the dorsoventral choice of LMC(l) axons, I started to use a conditional allele of EphA4 in order to remove the protein selectively from motor axons or hindlimb mesenchyme.

2 Results

2.1 Differential expression of Ret and GDNF in motor neurons and hindlimb mesenchyme

For a signaling system to be able to coordinate topographic pathway selection of motor axons into the limb, differential expression of the receptors in motor axons and of the ligand in limb mesenchyme would be expected.

2.1.1 Ret resembles EphA4 expression pattern on hindlimb innervating motor axons

Previous studies have shown that differential expression of the EphA4 receptor on dorsal versus ventral nerve tracts is required to guide LMC(l) axons to the dorsal hindlimb mesenchyme (Helmbacher, Schneider-Maunoury et al. 2000; Eberhart, Swartz et al. 2002; Kania and Jessell 2003). Immunostainings on E11.5 mouse embryos with antibodies against Ret revealed a similar expression pattern as described for the EphA4 receptor (Fig.13 B, E, C and I). Cross sections at the level of the sciatic plexus showed high immunoreactivity for Ret in axons growing into the dorsal hindlimb mesenchyme (peroneal nerve) and lower expression of Ret in axons growing into the ventral hindlimb mesenchyme (tibial nerve) (Fig.13 E and I). Peroneal and tibial nerves contain motor and sensory axons coming from the lateral motor column (LMC) or the dorsal root ganglia (DRGs), respectively. To distinguish between the two types of axons, Ret expression was examined at the ventral roots proximal to the point where motor and sensory axons join a common pathway towards the base of the limb. Motor axons emerging from the spinal cord showed intense staining for Ret, whereas axons from the DRG neurons were labeled weakly at this stage of development (Fig.13 D). The cell bodies of LMC neurons showed a uniformly high immunoreactivity for Ret. To assess information about Ret protein levels before and during the occurrence of the dorsal/ventral (d/v) choice of hindlimb innervating axons, Ret immunoreactivity was monitored at early stages of

development, before axons choose between the two trajectories. In 40–41 somite-stage embryos (~E10.5), when axons of LMC neurons have just reached the d/v-choice point in the limb, Ret protein was clearly detectable on distal axons (Figure 13G). In older embryos (45–46 somites [~E11.0]), in which two nerve bundles emerge from the plexus, the ventral LMC(m)- derived fraction showed lower levels of Ret than seen on proximal or on dorsally projecting LMC(l) axons (Figure 13H). At ~E11.5 (~52 somites), differential Ret expression was even more pronounced (Fig. 13I). In contrast to Ret, GFRα1 immunoreactivity was equal on both peroneal and tibial nerves (Figure 13F). The very strong levels on dorsal root ganglia neurons precluded a comparison of GFRα1 levels on motor axons versus sensory axons (data not shown).

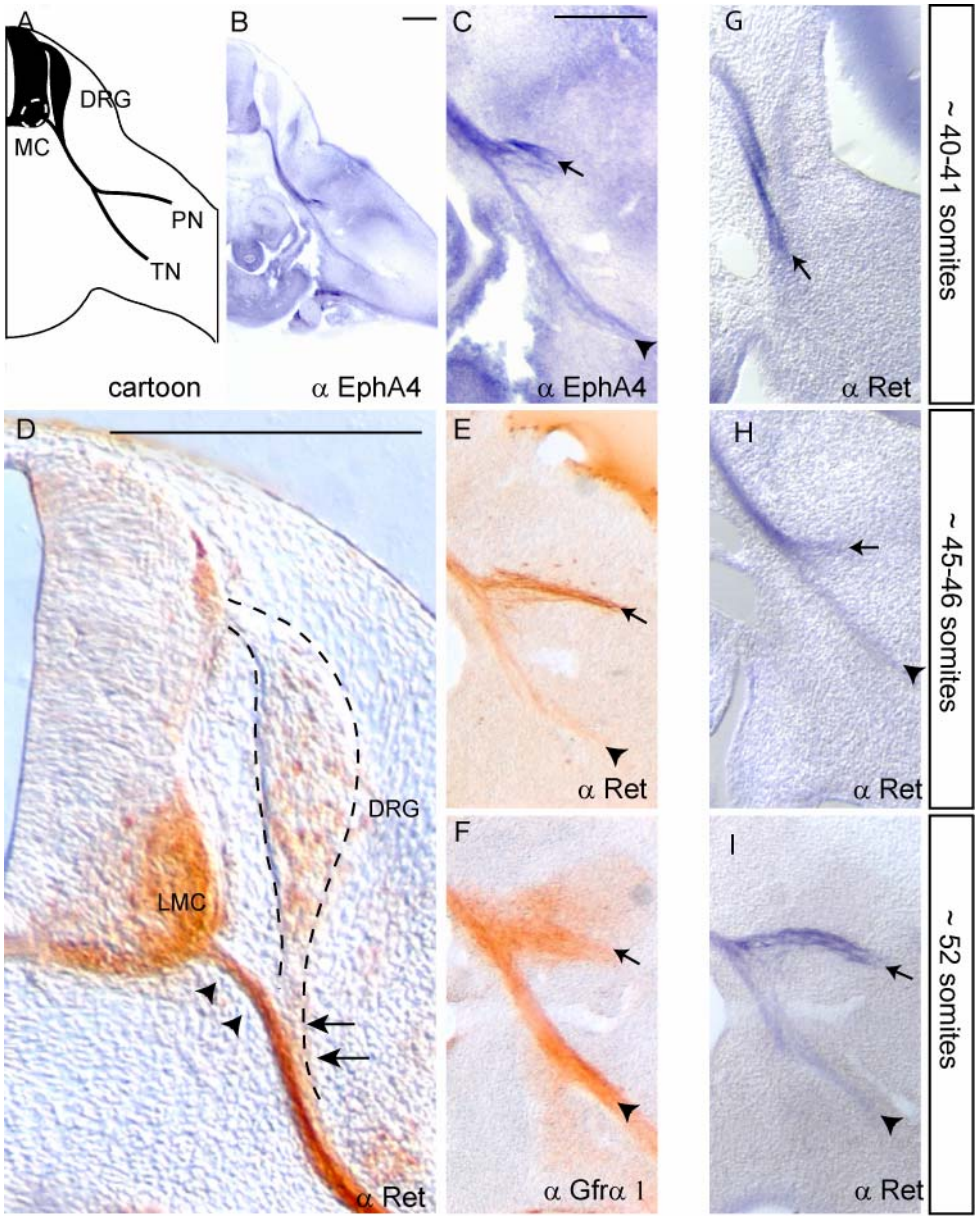

Figure 13 Differential levels of Ret protein in hindlimb-innervating axons

(A) Schematic drawing of limb-innervating peroneal (peroneal, PN) and tibial nerves (tibial, TN) in transverse sections of E11.5 mouse embryos. Spinal cord (SC), dorsal root ganglion (DRG), motor column (MC). (B–F) Immunohistochemical analyses on transverse vibratome sections of wild-type mouse embryos at the level of the sciatic plexus with antibodies against EphA4 (B and C), Ret (D, E, G, H and I), and GFRα1 (F) with either alkaline phosphatase (B, C, G, H and I) or peroxidase (D–F) substrates for stainings. In E11.5 embryos, high levels of EphA4 (B and C) and Ret (E and I) were detected in peroneal nerve axons innervating the dorsal part of the limb (arrow), whereas ventral tibial axons were weakly labeled (arrowhead). High levels of Ret were detected in cell bodies of LMC motor neurons and their ventral roots (arrows in [D]), whereas cell bodies and peripheral axons of DRG sensory neurons were weakly labeled (arrowhead in [D]). In a time course of Ret expression (G-I), the difference in protein levels on the axons appeared at ~45 somite stage. Antibodies against neurofilament (see Figure 17) and GFRα1 labeled dorsal and ventral axons equally well (F). All panels except (B) were taken at the same magnification as (C). Scale bars are 250 μm.

2.1.2 Ret mRNA expression in lumbar motor neurons before and during the period of dorsoventral pathway selection

In situ hybridisation analysis of Ret, RALDH2 and Lim1 was used to examine the expression pattern of Ret mRNA on transverse sections of mouse embryos at the level of the sciatic plexus with respect to the other motor neuron markers. RALDH2 and Lim1 were used as markers for all LMC and LMC(l) neurons, respectively (Tsuchida, Ensini et al. 1994; Sockanathan and Jessell 1998). Ret mRNA was detected in all motor neurons with consistently higher levels in LMC(l) versus LMC(m) neurons, based on the comparison with RALDH2 and Lim1. In agreement with the immunhistochemical results, Ret mRNA expression was observed in all neurons of the LMC at E11.0 (Fig. 14A, D and G encircled area) matching expression of RALDH2 (Fig. 14B, E and H). At E11.5 and E12.5, highest levels of Ret expression were found in subsets of LMC neurons that co-localize with expression of Lim1, a marker of LMC(l) neurons (Fig. 14C, F and I).

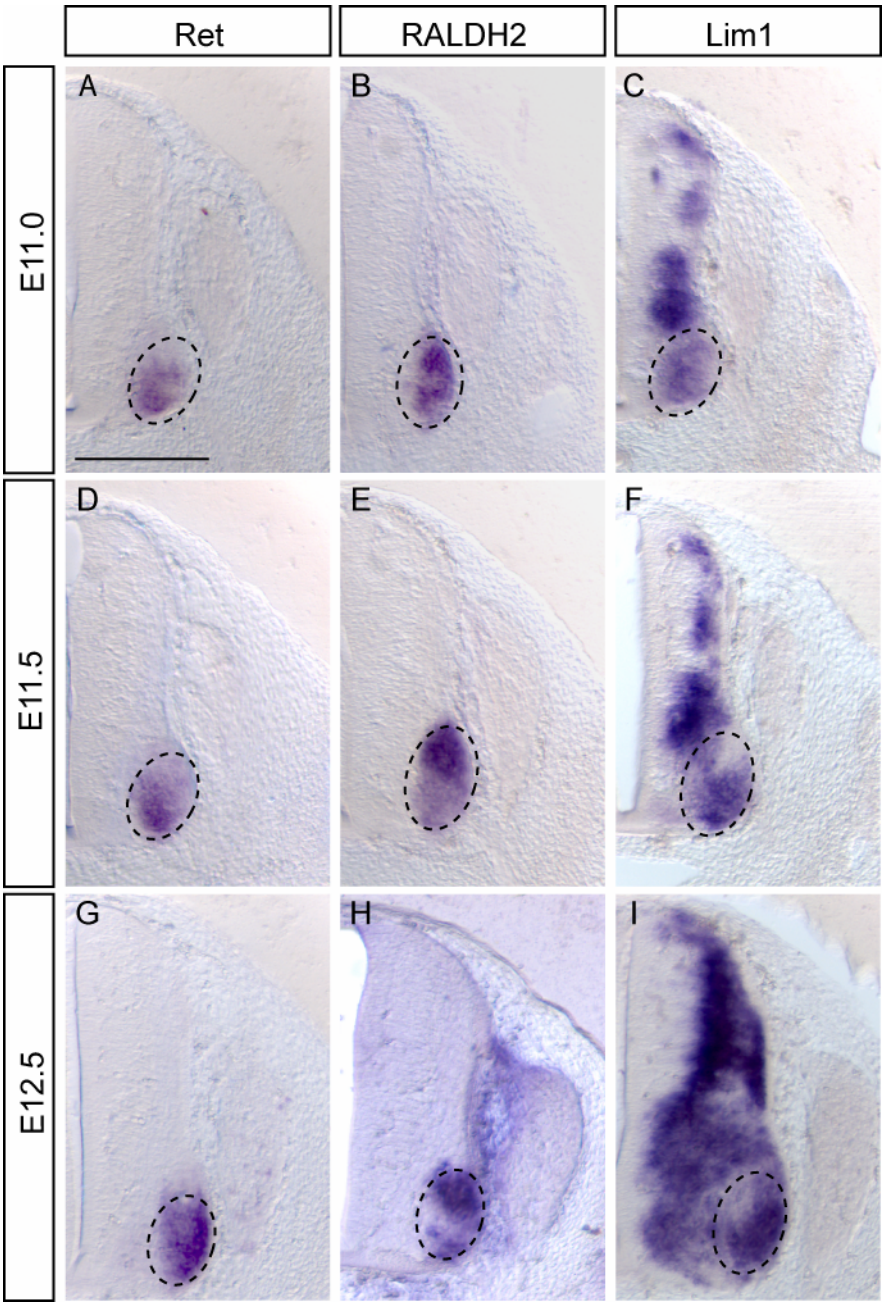

Figure 14 Expression of Ret mRNA in lumbar LMC neurons

(A-I) In situ hybridization analyses on transverse vibratome sections of wildtype mouse embryos at the level of the sciatic plexus using probes against Ret (A,D,G), RALDH2 (B,E,H), and Lim1 (C,F,I). At E11.0, Ret mRNA expression was observed in neurons of the LMC (encircled area) matching expression of RALDH2, a marker of all LMC neurons (Sockanathan and Jessell 1998). At E11.5 and E12.5, the highest levels of Ret expression were found in subsets of LMC neurons that co-localize with expression of Lim1, a marker of LMC(l) neurons (C,F,I). This pattern is maintained at later stages (E12.5). Scale bar is 250 μm.

2.1.3 GDNF expression at the pathway selection point

The interesting expression pattern of Ret and one of its coreceptors Gfrα1, in hindlimb innervating axons during the phase of dorsoventral pathway selection raised the question of the expression pattern of a possible ligand, GDNF. Expression of GDNF was analyzed using specific anti-GDNF antibodies and monitoring β-galactosidase activity in $GDNF^{lacZ/+}$ embryos (Moore, Klein et al. 1996). On E11.5 mouse embryo sections, strong immunoreactivity for GDNF was detected in a region just dorsal to the pathway selection point and another more ventral source where axons branch off from the tibial nerve (Figure 15B encircled area). Anti-GDNF immunoreactivity was also detected in limb innervating axons (Figure 15A-C) possibly representing retrogradely transported GDNF.

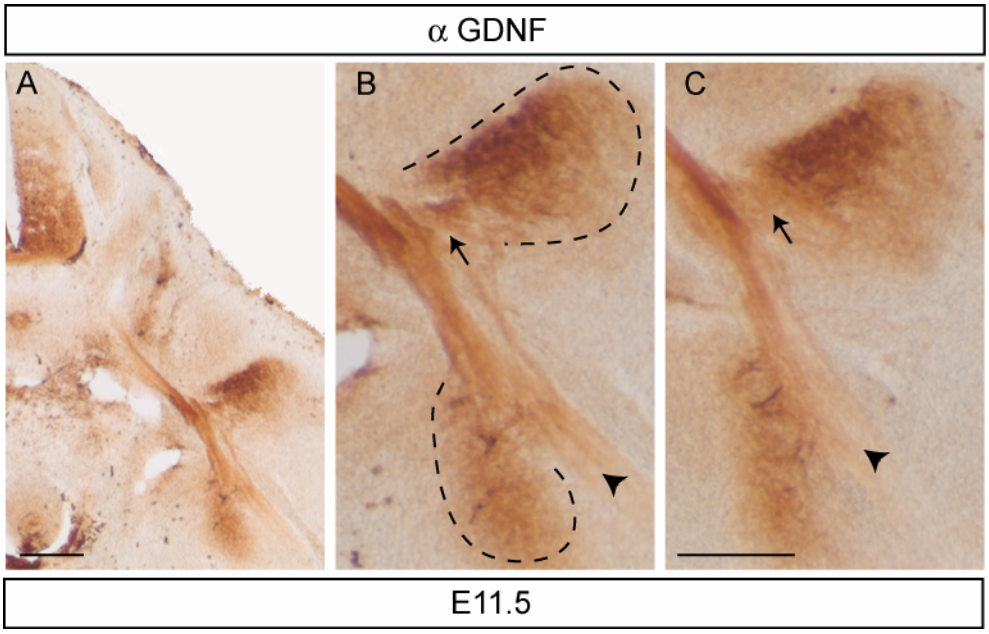

Figure 15 GDNF expression at the dorsoventral pathway selection point

(A–C) Immunohistochemical analyses on transverse vibratome sections of wild-type E11.5 (52 somites) embryos at the level of the sciatic plexus with antibodies against GDNF. GDNF immunoreactivity (stippled line) was highest in the vicinity of dorsal axons and lower near ventral axons (arrowhead). Some labeling of the axons was also observed (arrow in [A] and [B]) possibly because of uptake of GDNF. An additional ventral source of GDNF can be seen, where small side branches of the tibial nerve develop (stippled line in C). Scale bars are 250 μm.

To determine the exact timing and spatial distribution of GDNF expression with respect to axon outgrowth, a combination of neurofilament and β-gal staining was performed using $GDNF^{lacZ/+}$ mice, which express lacZ under the GDNF promoter. In 39–40 somite-stage embryos, no GDNF was present at the base of the limb before the arrival of axons (Figure 16A, E and I). In 41–42 somite-stage embryos, a highly localized source of GDNF was seen around and slightly dorsal to the point of nerve defasciculation (Figure 16 B, F and J). In older embryos (45–46 somites), both nerve branches had extended along their dorsal and ventral trajectories, and GDNF expression was increased. The bulk of GDNF expression was seen just dorsal to the branch point of the two nerves (Figure 16 C-L). At E11.5 (52 somites), GDNF expression was maintained and somewhat enlarged adjacent to the dorsal branch (Figure 16D, H and L). Similar to the results of GDNF immunoreactivity, an additional source of GDNF was detected just ventral to the tibial nerve and may be the source of attraction for some axon branches emerging from the tibial nerve (Figure 16 D, H and L and Fig. 15A-C). Together, the expression pattern raised the possibility that GDNF acts as a guidance signal for Ret-positive motor axons.

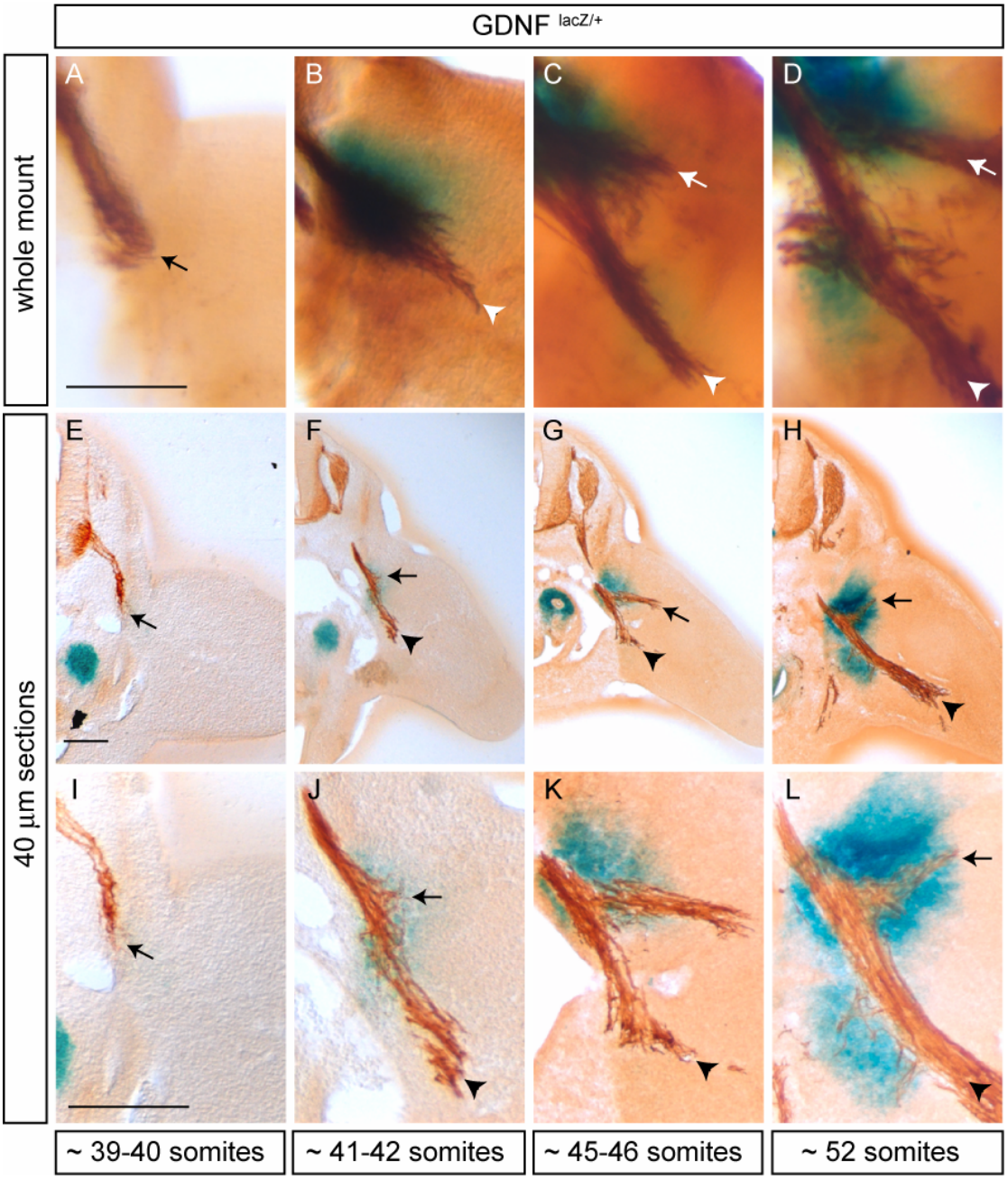

Figure 16 GDNF expression at the dorsoventral pathway selection point

(A–L) Anti-neurofilament 160 antibody staining on whole-mount (A-D) and vibratome sectioned (E-L) GDNF$^{lacZ/+}$ embryos at the indicated somite stages (ranging from E10.5 to E11.5). β-galactosidase activity (blue) reflects GDNF-producing cells. No GDNF-lacZ was detected in the future sciatic plexus, which the axons of lumbar motor neurons are about to reach (arrow in A, E and I). The only nearby source of GDNF detected was from the developing kidney. β-galactosidase activity was first detected at the plexus (41–42 somites [B, F and J]), when tibial axons (arrowhead) have already extended ventrally past the plexus, while few axons are seen taking a dorsal turn (arrow), just where GDNF-expressing cells are located. In older embryos (45–46 somites), the peroneal nerve branch splits away from the

tibial branch at the point of highest GDNF concentration (C, G and K), while peroneal growth cones have already exited the stained area. In 52 somite embryos, GDNF expression continues to increase as the nerves elongate (J, D, H and L). An additional ventral source of GDNF can be seen, where small side branches of the tibial nerve develop (H and L). Scale bars are 250 μm.

2.2 Defective dorsal hindlimb innervation in Ret and GDNF mutant embryos

2.2.1. Ret *null* embryos display a reduction of the peroneal nerve

To test if Ret signaling was required for guidance of hindlimb innervating axons during development, hindlimb innervation was analyzed in Ret *null* mutant embryos (Kramer, Knott et al. 2006). The analysis was focused on the branches of the sciatic nerve, which innervate the distal hindlimb, since these axons showed the differential expression of Ret during the time of pathway selection. At E11.5, the dorsal and ventral hindlimb innervating axons of wild type controls have diverged from the sciatic plexus and formed two branches of approximately the same length (Fig. 17A). In stage-matched Ret *null* mutants, the developing tibial nerve appeared somewhat thicker and the peroneal nerve was reduced in length (Fig. 17C, E and G). Because the severity of the phenotype varied between different stage-matched mutants, embryos were classified into three categories (Cat I: mild, Cat II: intermediate and Cat III: strong [for detailed definitions see material and methods section]) according to the strength of peroneal nerve reduction. Most Ret *null* embryos fell into the intermediate category (Figure 17I). At E12.5, both nerves have grown considerably in length and became subdivided into smaller branches. In wild type mice the peroneal nerve developed a prominent fork-like branch at the distal end (arrow in Fig. 17B, B`), which was slightly reduced in diameter in Cat I mutants (Figure 17D, D`) or even completely absent in Cat III mutant embryos (Figure 17H, H`). At the same time, the tibial nerve appeared to be thicker in stage-matched Ret *null* embryos with a strength that could be correlated to the loss of thickness of the dorsal branch. Most Ret *null* embryos could be assigned to Cat II at E12.5 (Figure 17I). These results indicate that the expression of Ret protein is required for the topographic projection of hindlimb-innervating axons.

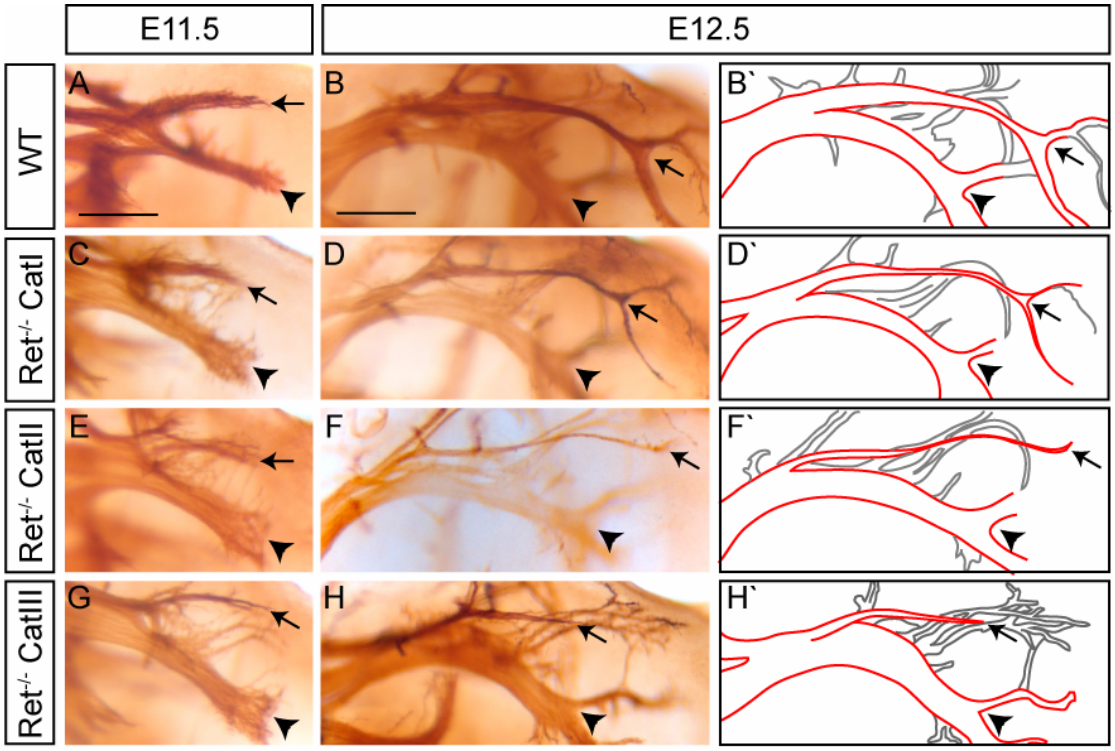

I	stage	n	WT	Cat I	Cat II	Cat III
Ret -/-	E11.5	14	0	1	8	5
	E12.5	26	1	3	16	6

Figure 17 Reduction of dorsal hindlimb innervation in Ret$^{-/-}$ mice

Anti-neurofilament 160 whole-mount-stained hindlimbs from wildtype (wt) (A and B) and Ret$^{-/-}$ embryos (C–H) at the indicated embryonic stages. Ret$^{-/-}$ embryos were classified into different categories (I = mild, II = intermediate, or III = severe) as specified in the material and methods section. The images show the hindlimb with distal to the right and dorsal at the top. In E11.5 wt embryos, the distal extensions of dorsal and ventral axons had approximately the same length (A). In contrast, dorsal axons (arrows) of Ret$^{-/-}$ embryos showed limited extension compared to stage-matched controls and were reduced in numbers and diameter (C, E, and G). At E12.5, limb nerves of wt embryos had grown in length and extended side branches in a stereotyped pattern (B). The corresponding schematic drawing depicts the relevant nerves in red, whereas other axons are drawn in grey (B`, D`, F`, and H`). Peroneal nerves of stage-matched Ret$^{-/-}$ embryos were much reduced in length and complexity (arrows in [D], [F], and [H]). The sciatic plexus is indicated with an asterisk and the ventral axons with an arrowhead. Scale bars are 250 μm. (I) Distribution of different categories of phenotypes in Ret$^{-/-}$ mutants at E11.5 and E12.5 (n = number of legs).

2.2.2 Conditional inactivation of Ret reveals a cell-autonomous function of Ret in motor neurons

To answer the question whether the hindlimb innervation phenotype reflected a cell-autonomous function of Ret in motor neurons or is a secondary consequence of defects in other Ret-expressing cell types, such as sensory neurons and somite derivatives (Pachnis, Mankoo et al. 1993; Golden, DeMaro et al. 1999), a conditional allele of the Ret locus was used to delete the Ret gene in specific cell populations with the Cre-loxP recombination system (Kramer, Knott et al. 2006).

2.2.2.1 Recombination of Ret using Hb9-Cre

An Hb9-GFP promoter-driven Cre (Hb9-Cre mice) (Arber, Han et al. 1999; Yang, Arber et al. 2001) was used to remove Ret specifically from spinal motor neurons. Hb9-Ret$^{lx/lx}$ mice were viable and fertile, but did not show a detectable peroneal nerve reduction at E12.5 compared to stage-matched wild type controls (Figure 18A-C; also presented in my diploma thesis).

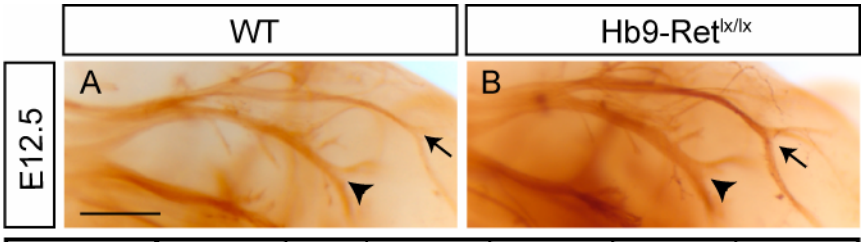

C Hb9-Ret$^{lx/lx}$	stage	n	WT	Cat I	Cat II	Cat III
	E12.5	3	3	0	0	0

Figure 18 Normal hindlimb innervation in Hb9-Ret$^{lx/lx}$ mice

Anti-neurofilament 160 whole-mount-stained hindlimbs from wildtype (A) and Hb9-Ret$^{lx/lx}$ embryos (B) at E12.5. Peroneal (arrow) and tibial (arrowhead) nerves of mutant embryos show no difference to stage matched wildtype controls. Thus, all embryos fall into the wildtype category (C). Scale bar is 250 μm (n=number of embryos).

The absence of the peroneal nerve reduction in Hb9-Ret$^{lx/lx}$ embryos could be due to a non-cell-autonomous function of Ret for this phenotype or be a result of ithe ncomplete excision of Ret in the lumbar motor column. To overhaul the recombination efficiency of Hb9-cre recombinase, mice were intercrossed with a lacZ reporter line (Rosa26R (Soriano 1999)). In Hb9-Rosa embryos, Cre recombination can be monitored by activity of β-galactosidase. Although Hb9-Rosa mice showed specific and robust recombination in motor neurons of the brachial region (Figure 19B), recombination in the lumbar region was more widespread and included other neuronal populations, but was incomplete with respect to the LMC(l) subpopulation at L3-L5 levels (Figure 19C-E). This result suggested that a sufficient amount of Ret remained in the lumbar motor column, which allowed their axons to perform a correct pathway selection. Since the Hb9-Cre turned out to be a suboptimal tool for motor neuron specific deletion of Ret, a nervous system-specific recombinase (Nestin-Cre (Tronche, Kellendonk et al. 1999)) was used instead.

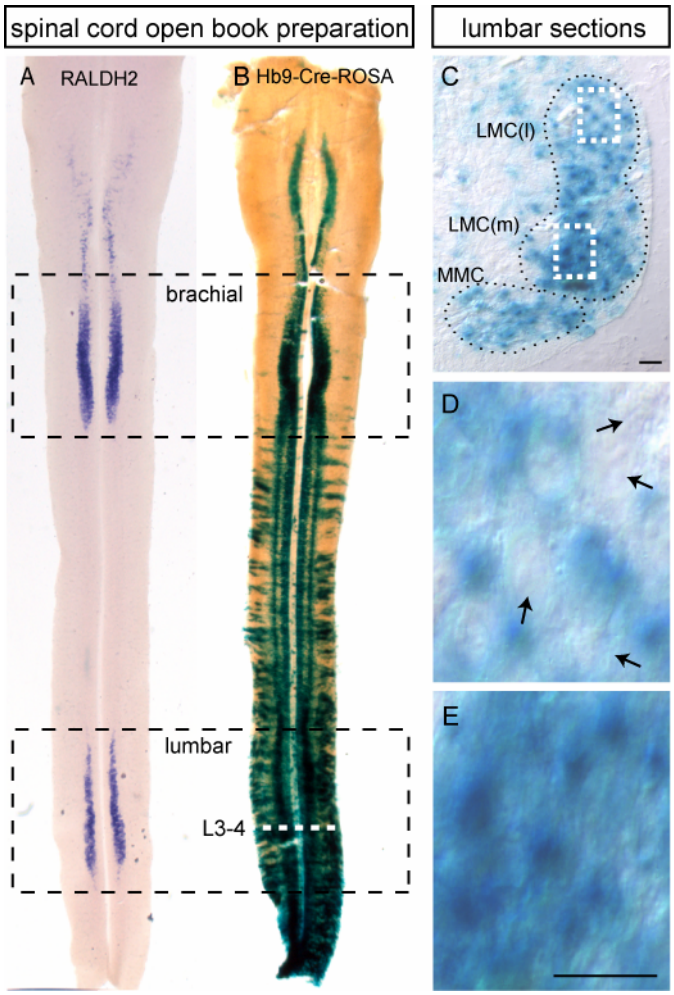

Figure 19 Recombination activity of HB9-cre in lumbar spinal cord

(A) In situ hybridization analysis of the LMC-specific marker RALDH2 to visualize the position of motor neurons in an open book preparation of an entire E12.5 spinal cord.
(B-E) β-gal-stained E12.5 spinal cord from a double transgenic HB9-cre/Rosa26R embryo. Note the specific recombination in motor columns at brachial level (stippled box in panel B). At lumbar levels, many interneurons in dorsal spinal cord are labeled (B, lower stippled box). (C-E) Cross sections of β-gal stained E12.5 spinal cord at L3-L4 levels. HB9-cre-mediated recombination is widespread throughout the spinal cord (not shown) including most motor pools and many interneurons. Recombination appears incomplete in LMC(l), since not all motor neuron profiles appear stained (arrowheads point to unstained motor neurons in D). Scale bars are 10 μm.

2.2.2.2 Recombination of Ret using Nestin-Cre

Timing and efficiency of Nestin-Cre-mediated recombination was tested using the Rosa reporter line. LacZ stainings of whole Nes-Rosa embryos showed strong β-galactosidase activity at E10.5 throughout the entire nervous system (Figure 20B). For a more detailed analysis of the recombination, sections of the lumbar spinal cord were examined. Robust recombination was detected in most cells of the spinal cord. Importantly, in early stage embryos (E10.5 and E11.5), Nestin-Cre mediated recombination was absent from lumbar level DRG neurons (Figure 20C and D). At E12.5 initiation of Nestin-Cre activity could be detected in some cells of the dorsal root ganglia (DRGs). Hence, in homozygous $Ret^{lx/lx}$ mutants carrying one copy of Nestin-Cre (Nes-$Ret^{lx/lx}$ mice), only limb innervating motor axons would be deficient for Ret protein before E12.5.

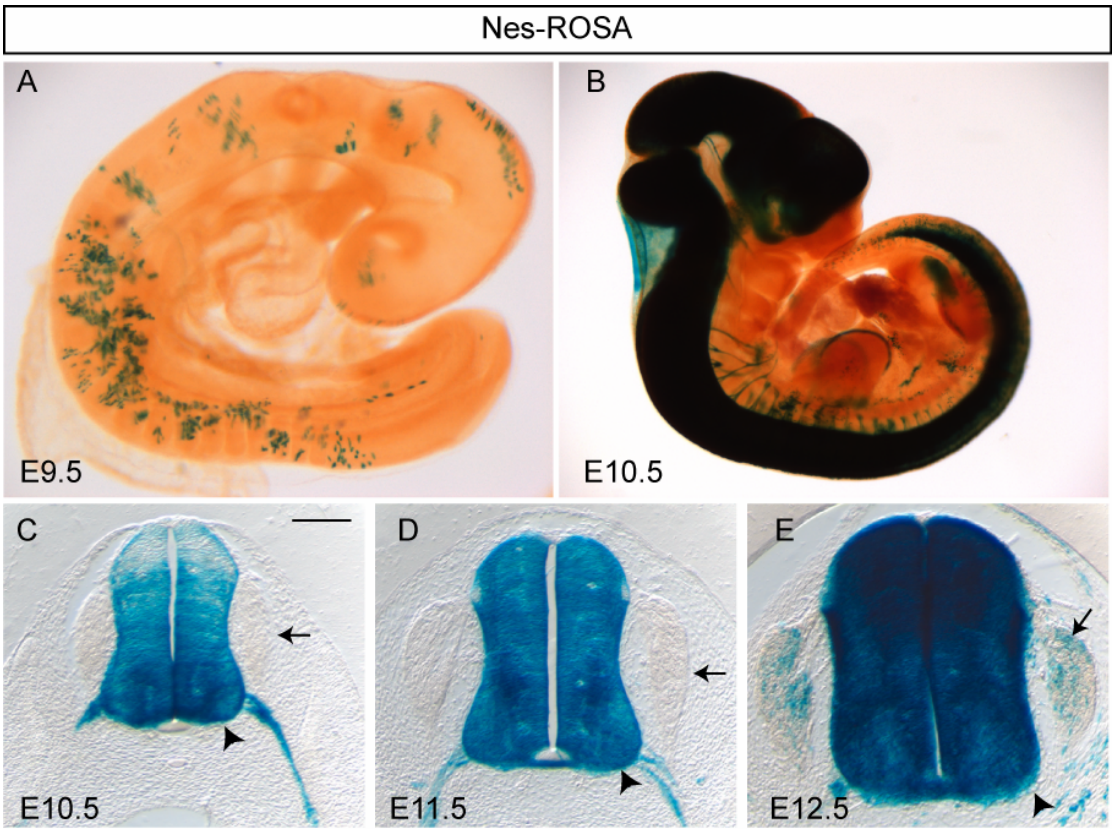

Figure 20 β-galactosidase activity in Nes-Rosa embryos

β-galactosidase activity in whole mounts and sections of nestin-Cre;Rosa26R (Nes-Rosa) transgenic spinal cords of the indicated embryonic stages at lumbar level. Specific expression of Nestin-cre is detectable from E10.5 onwards (A and B). Note that in E10.5 and E11.5 embryos, Nestin-cre-mediated recombination is very strong in spinal cord including LMC neurons but absent from DRGs (C and D). At E12.5, recombination starts in DRG neurons (E). Scale bar is 100 μm.

Western blot analysis and immunostainings were used to test the excision of Ret in Nes-Ret$^{lx/lx}$ spinal cords. Protein levels in Nes-Ret$^{lx/lx}$ spinal cords were reduced strongly but not entirely compared to control and Ret knockout samples (Figure 21 A). Antibody stainings against Ret revealed a certain degree of recombination variability, with some animals showing complete excision and others with considerable Ret immunoreactivity in the motor columns (Figure 21B). In contrast to Ret null mutants, which die at birth due to kidney agenesis (Schuchardt, D'Agati et al. 1994), Nes-Ret$^{lx/lx}$ mice were viable and fertile. Interestingly, they displayed a similar abnormal hindlimb position (club-foot) phenotype as the EphA4$^{lacZ/lacZ}$ mutants (Helmbacher, Schneider-Maunoury et al. 2000) (Figure 21C). Although this phenotype may be quite complex due to the known requirement of GDNF/Ret for

motor neuron survival during late embryonic development (Oppenheim, Houenou et al. 2000), the limb position was most consistent with misbalanced innervation of distal hindlimb muscles.

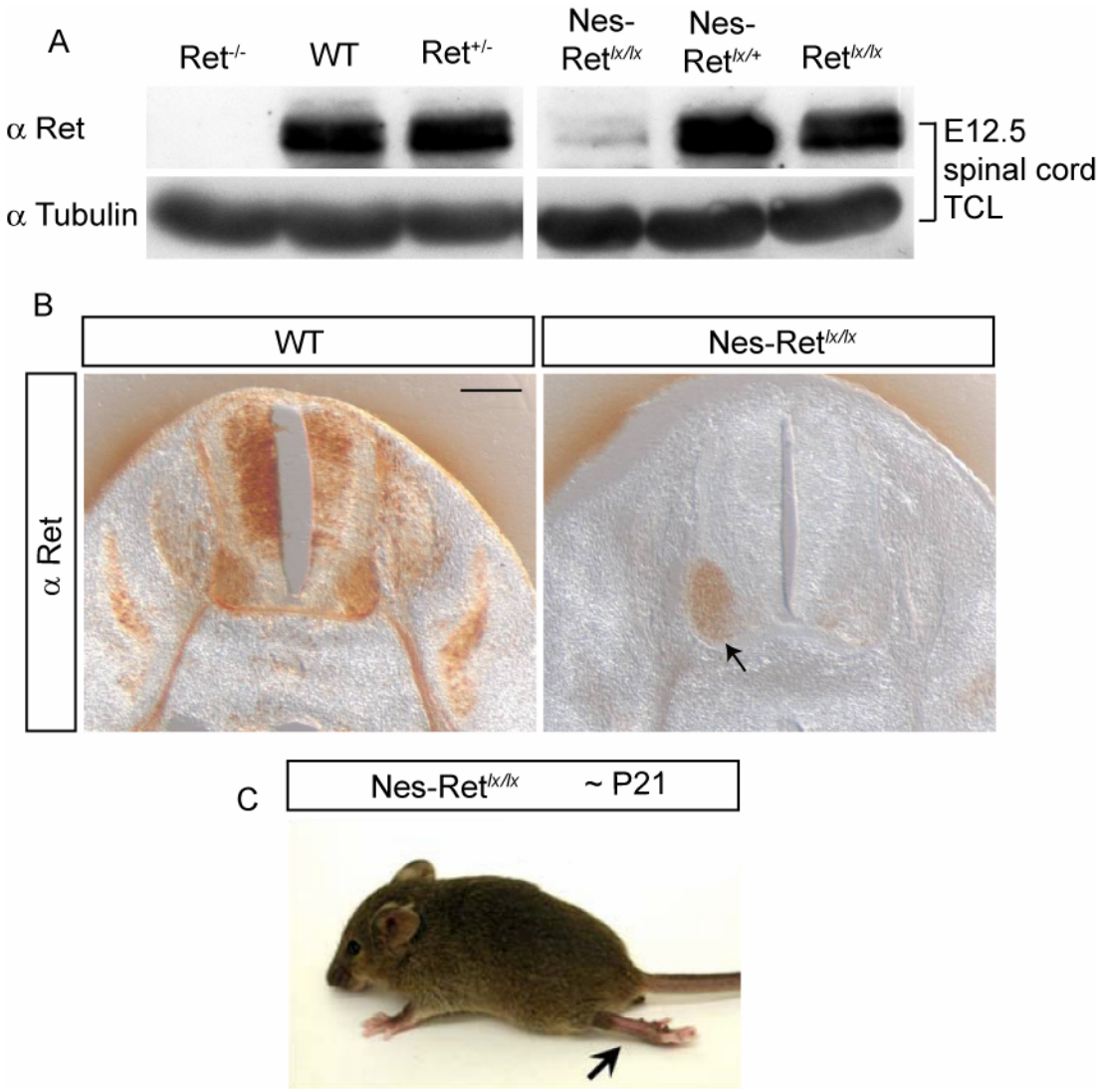

Figure 21 Excision of Ret using Nestin-Cre recombinase

(A) Western blot analysis of Ret protein levels in lysates from E12.5 spinal cords derived from $Ret^{+/-}$ and $Ret^{-/-}$ and from control ($Ret^{lx/+}$ and Nes-$Ret^{lx/+}$) and Nestin-cre;$Ret^{lx/lx}$ mutants (Nes-$Ret^{lx/lx}$). No signal for Ret can be detected in the $Ret^{-/-}$ spinal cords (lane 1). A small amount of protein remains in Nes-$Ret^{lx/lx}$ spinal cords (lane 4). Immunoblots were reprobed with α-tubulin antibody as a loading controls. (B) Immunohistochemical analyses on transverse vibratome sections of wild-type and Nes-$Ret^{lx/lx}$ E11.5 embryos at the level of the sciatic plexus with antibodies against Ret. Ret immunoreactivity is removed to a large extent, but some staining can be detected in the left motor column (arrow). Scale bar is 100 μm. (E) Picture of a postnatal day-21 Nes-$Ret^{lx/lx}$ mutant with stiff hindlimb (arrow).

To verify the hindlimb innervation before the period of programmed cell death, whole-mount neurofilament stainings of Nes-Ret$^{lx/lx}$ mutants were compared to stage-matched Ret$^{lx/lx}$ controls at early embryonic stages. Control embryos displayed normal peroneal and tibial nerves (Figure 22A and B), while Nes-Ret$^{lx/lx}$ mutants showed a reduction of the peroneal nerve in length at E11.5 and complexity at E12.5 (Figure 22C and D). The majority of Nes-Ret$^{lx/lx}$ mutants at E12.5 showed mild phenotypes, somewhat less severe than Ret *null* mutants, possibly because of the variability in Nestin-Cre recombination (Figure 23). These results demonstrate that removing Ret in the spinal cord is sufficient to alter the formation of the peroneal nerve, indicating that this phenotype reflects a cell-autonomous function of Ret in motor neurons.

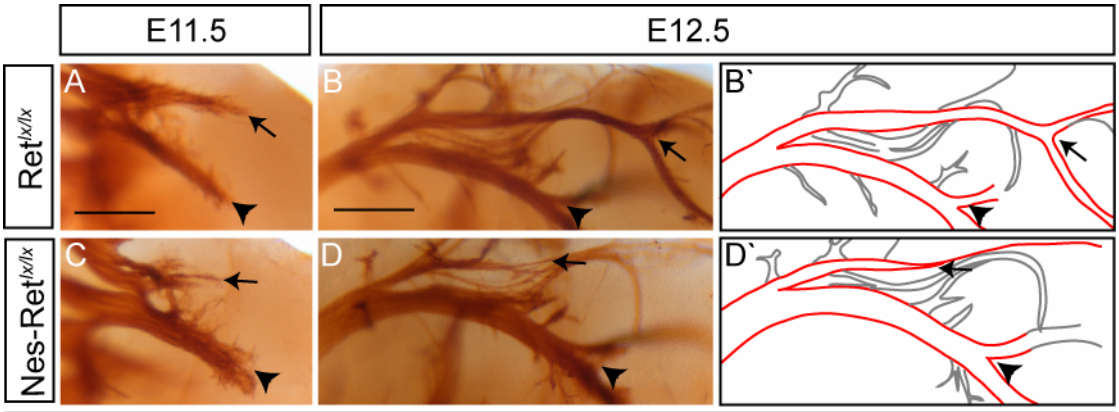

E Nes-Ret$^{lx/lx}$	stage	n	WT	Cat I	Cat II	Cat III
	E11.5	24	2	5	12	5
	E12.5	30	8	15	5	2

Figure 22 Reduction of dorsal hindlimb innervation in Nes-Ret$^{lx/lx}$ mice

(A-D) Anti-neurofilament 160 staining of hindlimbs from stage-matched control (Ret$^{lx/lx}$) (A and B) and Nes-Ret$^{lx/lx}$ mutant (C and D) embryos of the indicated embryonic stages. B` and D` show schematic representations. Control embryos show normal peroneal and tibial nerves (A and B), while Nes-Ret$^{lx/lx}$ mutants display a reduction of the peroneal nerve in length at E11.5 and complexity at E12.5 (C and D). (E) Distribution of different categories of phenotypes in Nes- Ret$^{lx/lx}$ mutants at E11.5 and E12.5. (n = number of legs) Scale bars are 250 μm.

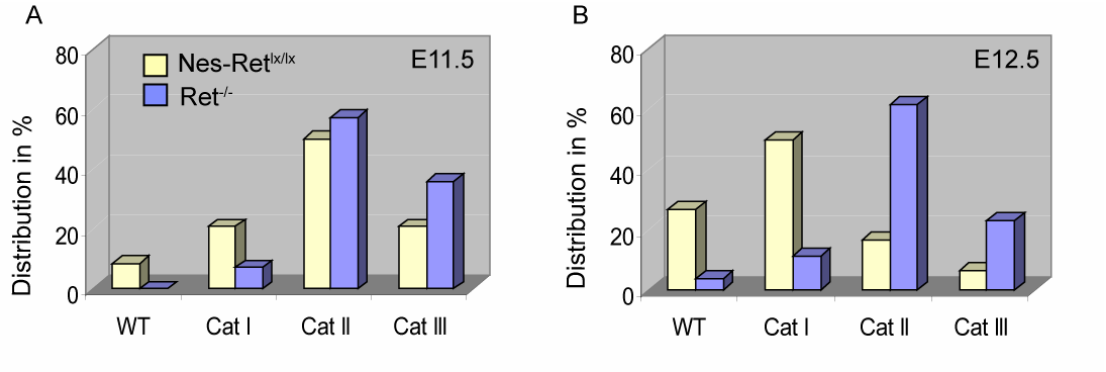

Figure 23 Distribution of Ret *null* and Nes-Ret$^{lx/lx}$ mutants into categories

(A) At E11.5, both Ret *null* and Nes-Ret$^{lx/lx}$ mutants show a very similar distribution. Most embryos display an intermediate reduction of the peroneal nerve and are assigned to category II. (B) The majority of Nes-Ret$^{lx/lx}$ mutants at E12.5 show mild phenotypes, somewhat less severe than Ret *null* mutants.

2.2.3 The hindlimb phenotype analysis

2.2.3.1 Quantification of neurofilament stainings

The observed peroneal nerve reduction could be a result of motor neuron death, disordered axonal outgrowth or redirected axon projections. Although GDNF, Gfrα1 and Ret have been shown to be required for motor neuron survival, analyses of the respective mouse mutants failed to detect increased motor neuron death before the onset of naturally occurring cell death at E13 (lumbar levels) (Oppenheim, Houenou et al. 2000). Increased motor neuron cell death was therefore discarded as a possible reason for the phenotype at E11.5 and E12.5. To get an initial clue about the true cause of the hindlimb phenotype, a detailed analysis of whole-mount neurofilament stainings at both stages was done measuring length and thickness of the affected nerves (Figure 24B and C). In E11.5 embryos, the average length of the peroneal nerve was reduced by approximately 40% in both Nes-Ret$^{lx/lx}$ and Ret *null* mutants (Figure 24A). In E12.5 embryos, the average thickness of the peroneal nerve was reduced, and the thickness of the tibial nerve was increased, in both Ret *null* and Nes-Ret$^{lx/lx}$ mutants (Figure 24D and E). This suggested that LMC(l) axons, which normally project to the dorsal hindlimb mesenchyme were rerouted to a ventral pathway.

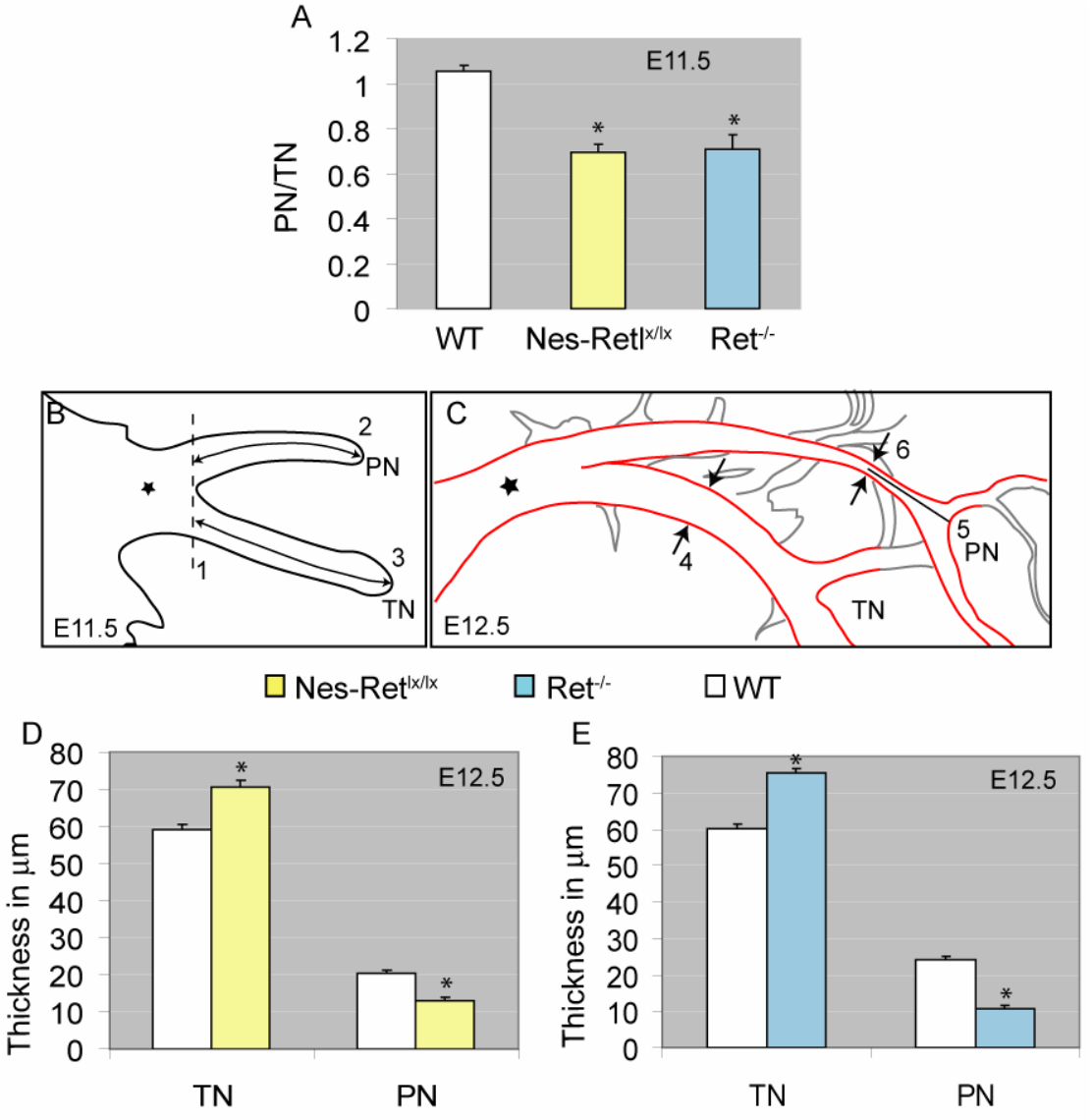

Figure 24 Quantification of neurofilament stainings

(B and C) Schematic drawings of the peroneal (PN) and tibial nerves (TN) growing out of the sciatic plexus (asterisk) in E11.5 (B) and E12.5 embryos (C). (B) Reference lines (1–3) used for measuring the lengths of PN and TN are indicated. (A) Quantification of the nerve lengths in E11.5 embryos (pooling all categories) indicated as the ratio PN/TN. The average reductions in Nes-Ret$^{lx/lx}$ and Ret$^{-/-}$ mutants were significant ($p < 0.00001$; Student's t test). (C) The thickness of the tibial nerve was determined at reference point 4, which was located just distal to a characteristic dorsal branchpoint where some axons (gray) take a trajectory toward the posterior limb mesenchyme. To measure the thickness of the peroneal nerve, reference point 5 was first placed at the major distal branchpoint of the nerve, and the thickness of the nerve was determined at reference point 6, which was placed proximal to point 5. (D and E) Average thickness of TN and PN in the indicated E12.5 mutants compared to their stage-matched wild-type controls (asterisk indicates $p < 0.00001$; Student's t test). Note the

correlation between the increase in TN thickness and the decrease in PN thickness in all mutants compared to stage-matched controls. Error bars represent SEM.

2.2.3.2 Tracing motor axons using different marker lines reveals an axon guidance defect of LMC(l) neurons

The simultaneous decrease of peroneal and increase of tibial nerve thickness suggested a rerouting of peroneal nerve axons onto the tibial nerve trajectory. To test this hypothesis, mice carrying a marker for all motor axons (EphA4^{PLAP} mice (Leighton, Mitchell et al. 2001)) or for LMC(l) axons only (Lim1^{tlacZ} mice (Kania, Johnson et al. 2000)), were crossed with control and mutant mice. In EphA4$^{PLAP/+}$ embryos, alkaline phosphatase staining labeled all EphA4 positive axons and revealed a wild type pattern for dorsal and ventral branches of the sciatic nerve (Figure 25A and B). Due to the absence of EphA4 from DRG neurons, nerves visualized with this marker exclusively contained motor axons. Serial sections from E11.5 Nes-Ret$^{lx/lx}$ embryos carrying one copy of EphA4^{PLAP} allele showed a reduction of the dorsal axons and an increase of the ventral axons (Figure 25C and D).

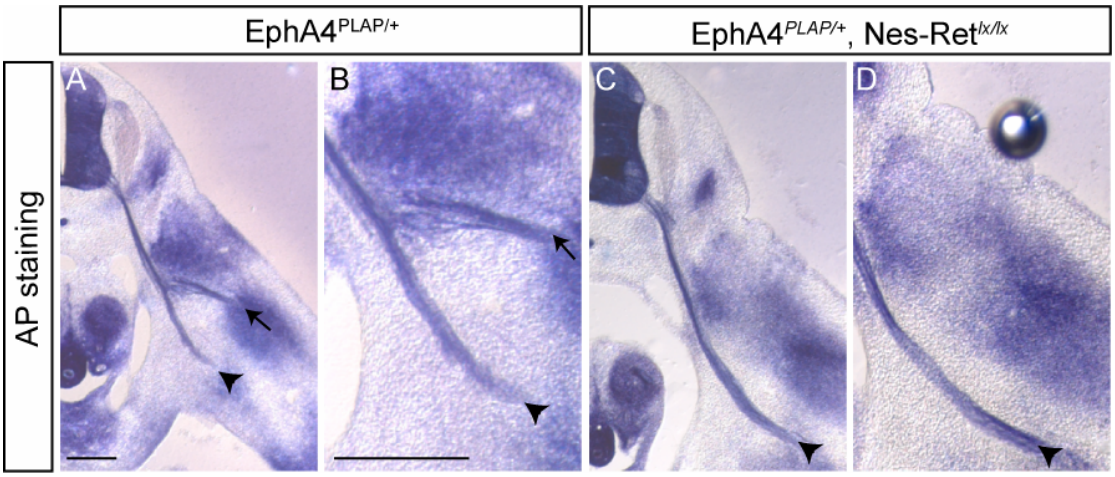

Figure 25 Tracing motor axons using EphA4^{PLAP} mice

(A-D) Alkaline phosphatase staining of E11.5 control and mutant embryo sections at the level of the sciatic plexus. (A and B) In EphA4$^{PLAP/+}$ embryos, hindlimb innervating motor axons show the typical wildtype situation with two nerve bundles diverging from the sciatic plexus (arrow for PN and arrowhead for TN). (C and D) In the mutant background, the peroneal nerve axons are much reduced, but some are still present in other sections (not shown). Scale bars are 250μm.

Although quantification of nerve thickness with this method was not possible due to the variation in the amount of fibers in each section, and because staining in whole-mount preparation was impossible; this result supports the idea of misrouted motor axons.

To circumvent these problems, another marker line (Lim1τlacZ) was used to specifically label LMC(l) axon projections. The expression of β-galactosidase in Lim1τlacZ/+ whole-mount embryos specifically labeled LMC(l) axons projecting to the dorsal limb (Figure 26A and C). Lim1τlacZ/+ mice were crossed with both the Ret null and Nes-Retlx/lx mutants and projections of β-gal-positive hindlimb axons were analyzed and compared to stage-matched anti-neurofilament-stained embryos of the same genotype. Analysis of Lim1τlacZ/+; Nes-Retlx/lx embryos at E12.5 (Cat III; n = 4 embryos) revealed that most detectable β-gal positive axons followed an aberrant ventral trajectory matching that of the tibial nerve (Figure 26B and D).

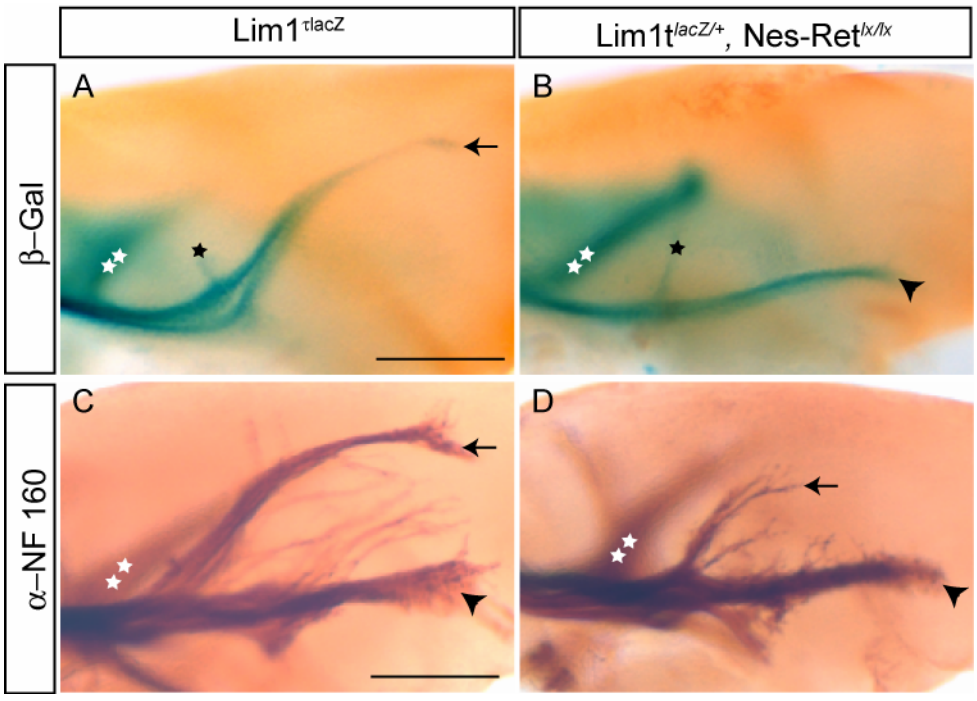

Figure 26 Rerouting of Lim1-positive LMC(l) axons to a ventral pathway

(A and B) β-galactosidase staining of E12.5 Lim1t$^{lacZ/+}$ control and Lim1$^{\tau lacZ/+}$;Nes-Ret$^{lx/lx}$ embryonic hindlimbs (dorsal top, distal right) depicting the path of peroneal axons. (C and D) Anti-neurofilament 160 staining of genetically identical age-matched controls depicting peroneal and tibial nerves. The positions of peroneal (blue in [A] and [B]) and tibial

(unstained) axons are indicated by arrows and arrowheads, respectively. Note that the peroneal nerve in Lim1$^{\tau lacZ/+}$;Nes-Ret$^{lx/lx}$ embryos (stained blue) is rerouted to the path of the tibial nerve. The remaining peroneal axons in the neurofilament-stained Lim1$^{\tau lacZ/+}$;Nes-Ret$^{lx/lx}$ embryo (D) are not β-galactosidase positive and may contain mostly sensory axons. β-galactosidase positive axons emerging from the femoral plexus are out of focus (indicated by two asterisks). The small branch emerging from the rerouted Lim1-positive axons (black asterisk in [B]) does not match the very stereotyped trajectory of dorsally growing PN axons but matches the branch that exits the PN in the wild-type at this level (black asterisk in [A]). The branches appear different in length because the pictures are taken from whole-mount legs, which can have a slightly different position. Scale bars are 250 μm.

Similar results were obtained with Lim1$^{\tau lacZ/+}$; Ret$^{-/-}$ embryos (n = 3 embryos, data not shown). Despite the variability in strength of the phenotype observed by anti-neurofilament staining, dorsally projecting β-gal positive axons were not detected, most likely because of the low level of lacZ expression. Because the bundle of ventrally projecting β-gal positive axons was comparable in length and diameter to those that project dorsally in control embryos, these results suggest that the absence of Ret protein redirects LMC(l) axons from a dorsal to a ventral trajectory without affecting axonal growth.

2.2.4 GDNF *null* embryos resemble Ret knockout and conditional mutants

To find out if GDNF is the ligand required for the correct selection of this specific motor axon pathway, whole-mount neurofilament stainings of E12.5 GDNF$^{-/-}$ and stage-matched control embryos were analyzed. GDNF$^{-/-}$ embryos resemble the hindlimb phenotype of Nes-Ret$^{lx/lx}$ and Ret *null* mutants, showing a reduced complexity of the peroneal nerve compared to controls (Figure 27A and B). Similar to Ret mutants, quantification of the sciatic nerve branches revealed an increase in ventral and a consistent decrease of dorsal nerve thickness (Figure 27D). The majority of mutants fell into the most strongly affected category III when classified according to peroneal nerve reduction (Figure 27C). These results indicate that GDNF is required as a ligand for Ret in the correct pathfinding of hindlimb innervating axons.

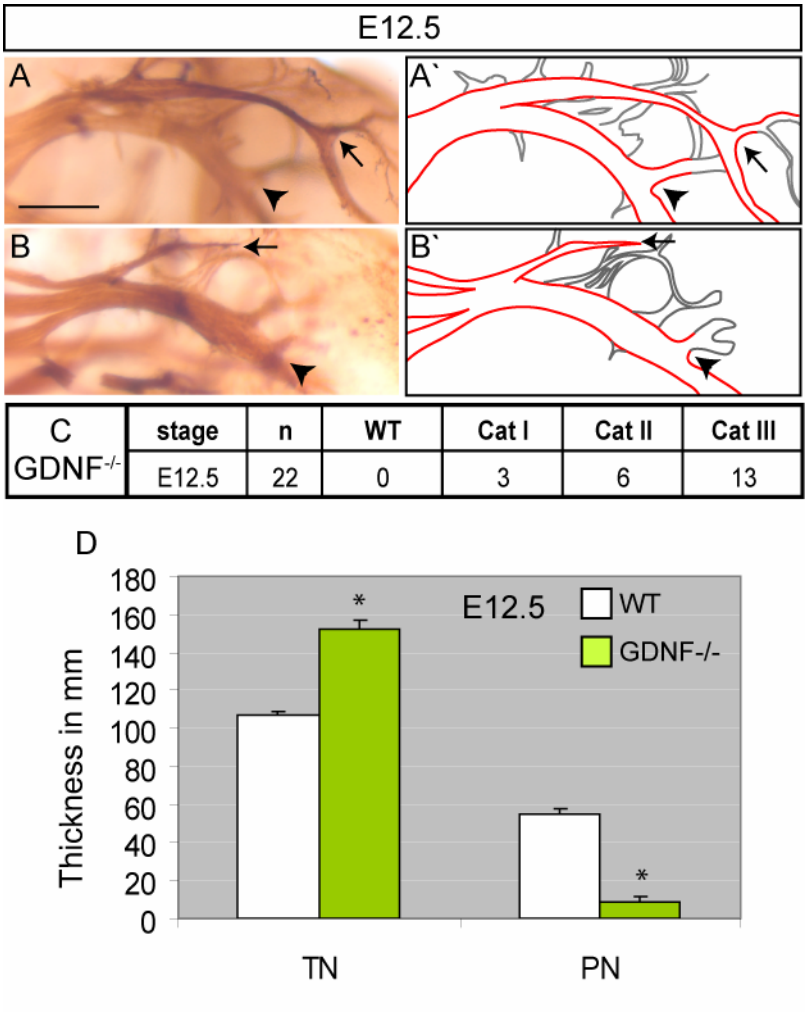

C GDNF$^{-/-}$	stage	n	WT	Cat I	Cat II	Cat III
	E12.5	22	0	3	6	13

Figure 27 GDNF is required for dorsal hindlimb innervation *in vivo*

(A and B) Anti-neurofilament 160 staining of hindlimbs from stage-matched controls (wt and GDNF$^{lacz/+)}$ (A) and GDNF null mutant (B) embryos at E12.5 (Cat III, severe). Schematic representations in (A`) and (B`). Scale bar is 250 μm. (C) Distribution of different categories of phenotypes in GDNF *null* mutants. (D) Average thickness of tibial (TN) and peroneal (PN) nerves in E12.5 GDNF$^{-/-}$ mutants compared to their stage-matched wildtype and heterozygous controls (asterisk indicates $p < 0.00001$; Student's t test). (E) Thickness of the nerves indicated as the ratio PN/TN (asterisk indicates $p < 0.00001$; Student's t test). Error bars represent SEM.

2.3 Teamwork between GDNF/Ret and ephrinA/EphA4 signals for the guidance hindlimb innervating axons

So far, the described results have provided strong evidence for a requirement of GDNF/Ret signaling in the establishment of the dorsal trajectory of LMC(l) axons in addition to the known EphA4/ephrinA guidance system. Maintenance of RALDH2, Lim1 and EphA4 mRNA expression (data not shown) in Ret mutant motor neurons suggests that, like EphA4, Ret acts downstream of Lim1 in the LMC(l) population. It would therefore, be interesting to investigate a possible cooperation between the two signaling systems in the guidance of LMC(l) axons into the limb. For such a partnership between the Ret and EphA4 receptors, several conditions would need to be fulfilled: (i) Ret could not regulate EphA4 protein expression on LMC motor axons, (ii) EphA4 could not regulate Ret protein expression on LMC axons, and (iii) the hindlimb phenotype (peroneal nerve reduction) would be enhanced in double mutant embryos.

2.3.1 Protein expression of EphA4 and Ret receptors remains at high levels in misguided axons

Anti-EphA4 immunostainings of E11.5 wild type embryos showed high levels of EphA4 in dorsal and lower levels in ventral axons (Figures 28A, also see 13B and C). In stage-matched Ret *null* mutant embryos, strongly EphA4-positive dorsal axons chose the same ventral trajectory as weakly EphA4-positive ventral axons (Figure 28B). The level of EphA4 expression on these ectopic ventral axons was similar to the high level of EphA4 expression observed on the remaining dorsal axons in adjacent sections (data not shown), suggesting that LMC(l) axons that failed to project dorsally maintained the level of EphA4 expression characteristic of their LMC(l) identity. Because the nerve bundles did not mix with each other, these strongly EphA4-positive ''dorsal'' axons clearly stood out from the weakly labeled LMC(m) axons (Figure 28B and B`). Similar results were obtained with GDNF *null* mutants (Figure 28C and C`). These results indicate that GDNF/Ret signaling is not required to induce high levels of EphA4 expression. Moreover, they show that in the absence of GDNF/Ret, EphA4 is not sufficient to mediate the repulsive action of ventral ephrinAs.

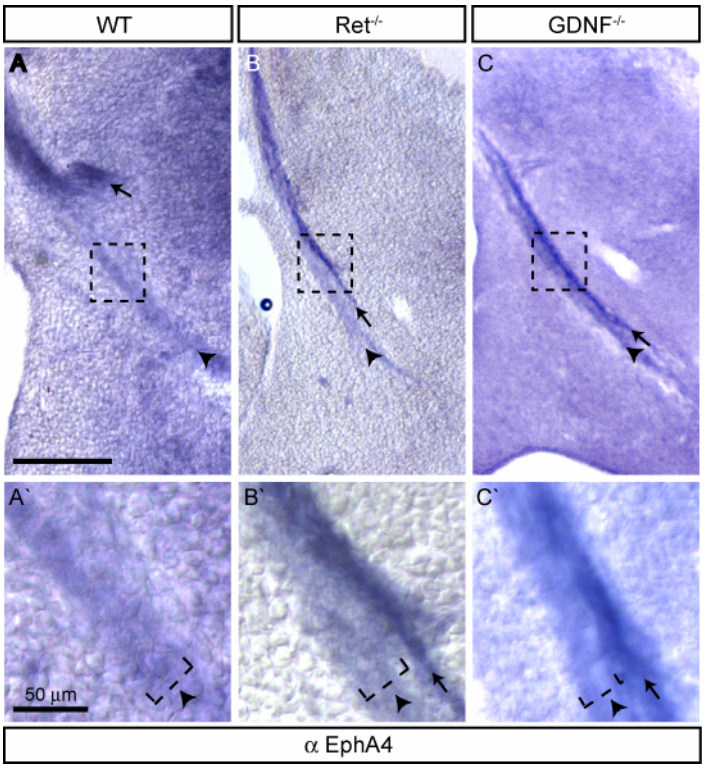

Figure 28 EphA4 protein expression is not regulated by GDNF/Ret

(A–C) Immunohistochemical analyses on E11.5 transverse vibratome sections of stage-matched wild-type (A) of Ret$^{-/-}$ (B) and of GDNF$^{-/-}$ (C) mutant embryos with anti-EphA4 antibodies. In this particular wt example (A), both dorsal and ventral nerve branches are visible on a single section. In many cases however, the sectioning angle is slightly oblique, so that dorsal and ventral branches are visible on adjacent sections (data not shown). The example shown in (C) is from a Cat III GDNF$^{-/-}$ embryo, in which there was no longer an EphA4-positive dorsal branch visible. Arrowheads: ventral (tibial) nerve; arrows: ectopic axons. (A`–C`) Higher magnification views of the ventral nerves of the respective boxed area in A-C. Note the different intensities of anti-EphA4 staining in the ventral nerves of Ret$^{-/-}$ (B`) and GDNF$^{-/-}$ embryos (C`). Although wt ventral nerves contained only axons expressing low levels of EphA4 (stippled area with arrowhead), mutant nerves contained axons bundles with high EphA4-staining intensity (arrow in [B`] and [C`]), similar to dorsal axons. This indicates rerouting of dorsal axons to a ventral pathway. Scale bar in (A) is 250µm.

Since Ret protein expression resembles that of EphA4, and EphA4 knockout embryos also show a defective hindlimb innervation (Helmbacher, Schneider-Maunoury et al. 2000), anti-Ret immunostainings were performed on sections of E11.5 EphA4$^{-/-}$ embryos. As previously shown, strongly Ret-positive axons chose a dorsal trajectory, and weakly Ret-positive axons chose a ventral trajectory in wild type control embryos (Figure 29A). In EphA4 *null* mutant embryos, a small population of strongly

Ret-positive axons was detected in the ventral hindlimb together with weakly Ret-positive axons (Figure 29B and B`). The remaining dorsal nerve, seen on neighboring sections, still expressed high levels of Ret (Figure 29C). These results showed that EphA4 is not required to maintain high levels of Ret in LMC(l) axons and suggested that in the absence of EphA4, the subpopulation of LMC(l) axons that was rerouted to the ventral compartment failed to respond to GDNF, despite high levels of Ret. Taken together, these data show that Ret and EphA4 are dispensable for each other's expression, and that one receptor per se is not sufficient to mediate the correct dorsoventral choice.

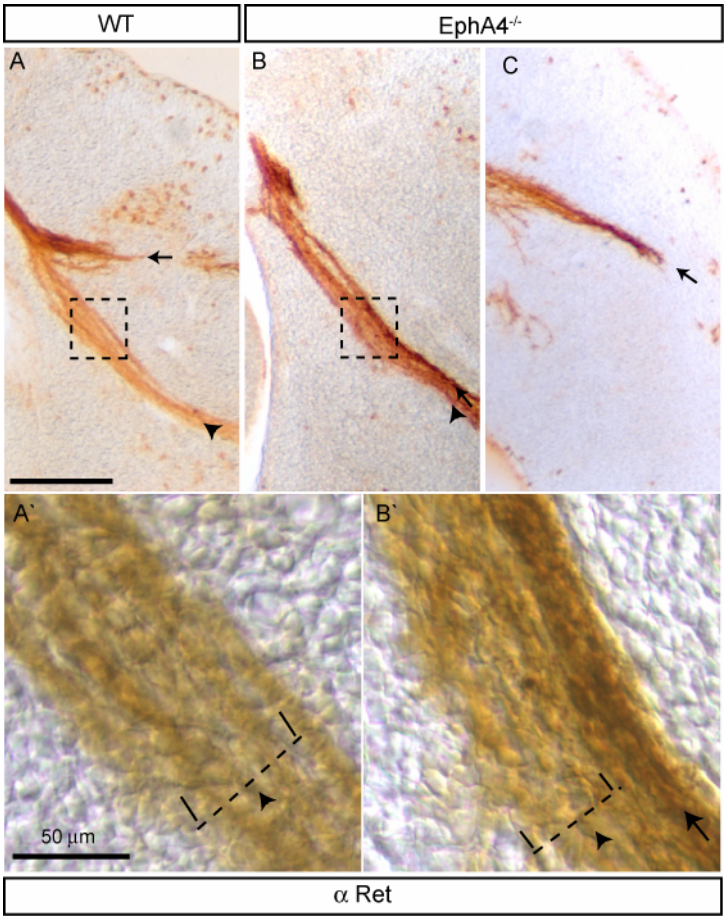

Figure 29 Ret protein expression is not regulated by ephrinA/EphA4

(A-C) Immunohistochemical analyses on E11.5 transverse vibratome sections of stage-matched wildtype (A) and of EphA4$^{-/-}$ (B and C) embryos with anti-Ret antibodies. In the wt embryo, both dorsal and ventral branches are visible on a single section, whereas in the EphA4$^{-/-}$ embryo, ventral (arrowhead) and dorsal branches (arrow) are on adjacent sections (C). The mutant ventral branch contains axon bundles with high Ret staining intensity (arrow in [B`]), similar to the dorsal axons (C). Scale bar in (A) is 250 µm.

2.3.2 EphA4-Ret double mutants display an enhanced hindlimb phenotype

The imperfect response of misguided axons to ephrinA or GDNF ligands despite their high receptor levels implies a parallel action of both receptors to mediate the choice of a dorsal trajectory by LMC(l) axons. To directly test for the presence of a parallel pathway in hindlimb motor axon guidance, $Ret^{-/-}$ mice were intercrossed with $EphA4^{PLAP}$ mice, which display all of the known loss-of-function phenotypes including a mild defect in hindlimb innervation (Kullander, Mather et al. 2001; Leighton, Mitchell et al. 2001). Similar to Ret *null* mutants, the majority of E11.5 $EphA4^{PLAP/PLAP}$ embryos showed an intermediate (Cat II) phenotype characterized by a significantly shorter peroneal nerve (Figure 30E and I). Double homozygous $Ret^{-/-}$; $EphA4^{PLAP/PLAP}$ neurofilament-stained embryos were all severely affected (Cat III) with a severely shortened and often defasciculated peroneal nerve (Figure 30G and I). At E12.5, $EphA4^{PLAP/PLAP}$ embryos showed a rather mild reduction of peroneal axons, whereas the phenotype of the majority of Ret *null* mutants was intermediate (Figure 30D, F, and J). The most severe guidance defects were displayed by $Ret^{-/-}$; $EphA4^{PLAP/PLAP}$ embryos (Figure 30H and J). Based on their characteristic trajectories, the few remaining axons appear to be primarily of a sensory nature. These results suggest that Ret and EphA4 are both required for dorsal pathway selection of limb-innervating axons in what appear to be parallel signaling pathways.

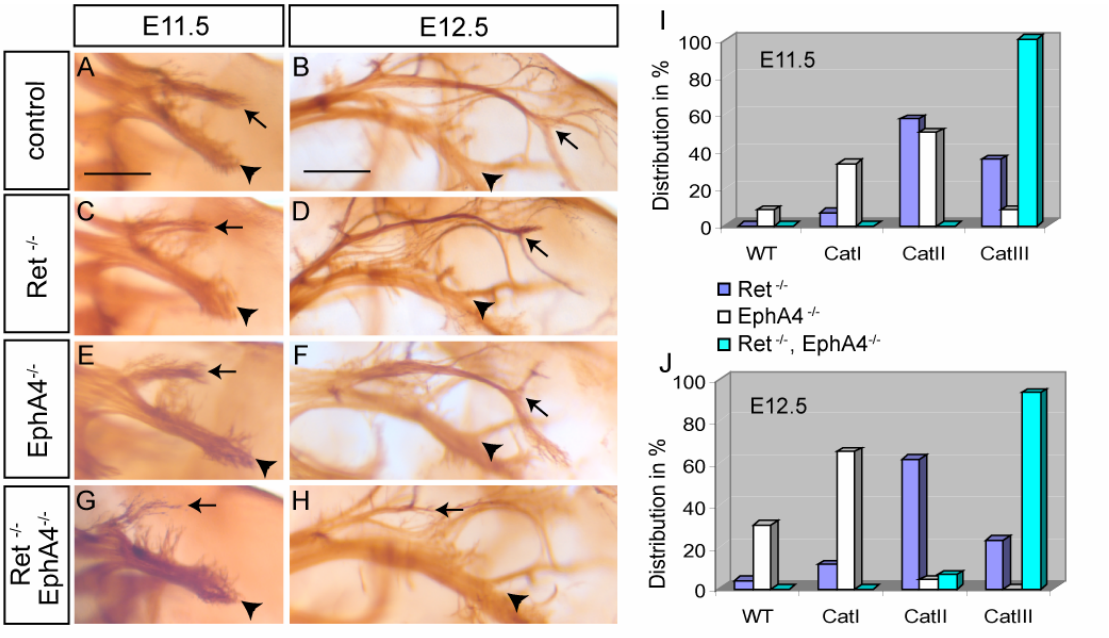

Figure 30 Functional cooperation between Ret and EphA4 *in vivo*

Representative anti-neurofilament 160 stained hindlimbs from wildtype (wt) (A and B), $Ret^{-/-}$ (C and D), $EphA4^{PLAP/PLAP}$ (E and F), and $Ret^{-/-}$;$EphA4^{PLAP/PLAP}$ mutant embryos (G and H) of the indicated embryonic stages. For details see Figure 18. Note the severe reduction of the peroneal nerve in double $Ret^{-/-}$;$EphA4^{PLAP/PLAP}$ mutant embryos (G and H). (I and J) Distribution (in percent) of different categories of phenotypes in single and double mutants at E11.5 (I) and E12.5 (J) Scale bars are 250 μm.

2.3.3 Activity-dependent interaction of Ret and EphA4

A biochemical approach was used to determine whether Ret and EphA4 can physically interact in mammalian cells. Both receptors were transiently expressed in HeLa cells and co-immunoprecipitations were performed. As a result of the over-expression, unstimulated Ret and EphA4 receptors showed a degree of kinase activity (data not shown). However, to fully activate the receptors, formation of dimers or higher order clusters needed to be triggered by ligand stimulation. To stimulate EphA4 receptor, soluble preclustered ephrinA-Fc or control Fc were applied. Activation of Ret was mimicked using a mutated form of Ret (Ret-M2A), which is constitutively dimerized and therefore permanently phosphorylated. $EphA4^{DSP}$ (this EphA4 construct lacks the Sam domain and the PDZ-binding motif) was detected in anti-Ret co-immunoprecipitation (co-IP) when both receptors were fully active (Figure 31). In the case of a mock stimulation using Fc fragment or unstimulated wild type Ret, no signal was detected when probed for EphA4. This result suggests that the interaction of Ret and EphA4 is dependent on full activation of both receptors including phosphorylation of both receptors, and formation of dimers or higher order clusters of Ret and EphA4, respectively.

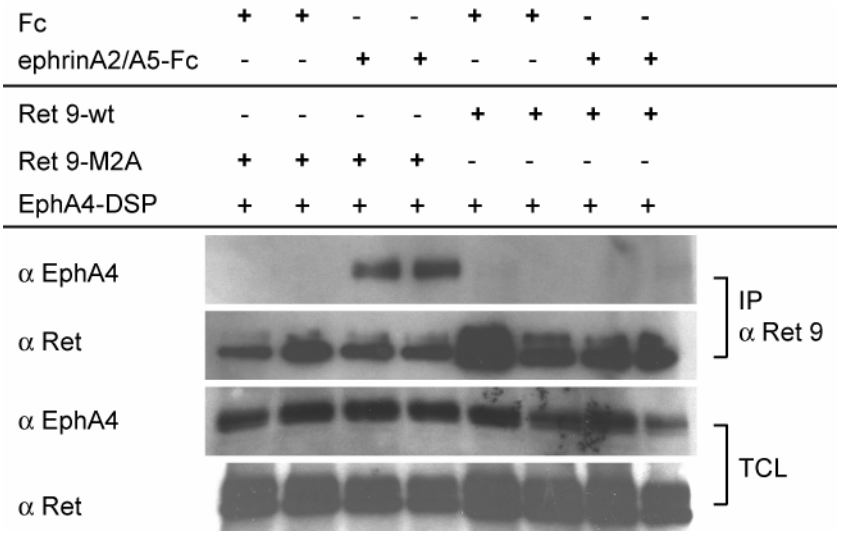

Figure 31 Interaction of Ret and EphA4

Ret 9-wt (lanes 1-4) or Ret 9-M2A (lanes 5-8) constructs were transiently expressed in Hela cells together with EphA4^{DSP}. Both conditions were either stimulated using Fc fragment or ephrinA2- and ephrinA5-Fc. TCLs (50μg protein) show equal expression levels of Ret and EphA4 constructs in all samples. In immunoprecipitations (IPs) of Ret, EphA4 signal can be detected, when both Ret (stimulation is mimicked by the constitutive active from M2A) and EphA4 are active (lanes 2 and 3).

2.3.4 Trans-phosphorylation between Ret and EphA4

Convincing evidence for a true cooperation between the GDNF/Ret and ephrinA/EphA4 signaling systems would be a reciprocal enhancement of their downstream signaling pathways. To test for a positive influence on one-another, trans-phosphorylation between the receptors was tested in transfected cells. A full-length, but kinase-dead version of the EphA4 receptor (EphA4-KD) was transiently expressed in Hela cells together with overactive, wildtype or kinase-dead Ret constructs (long = Ret 51 and short = Ret 9) and empty vectors as controls. EphA4-KD was immunoprecipitated using an antibody directed against the very c-terminal part of EphA4, and tyrosine phosphorylation was detected using anti-pY antibodies. EphA4^{DSP}, which lacks the C-terminal part of the receptor and thus could not be pulled down in the IP, was used as a positive control for trans-phosphorylation of kinase-dead EphA4. Both the long and short isoforms of the Ret receptor trans-phosphorylated kinase-dead EphA4, whereas wildtype or kinase-dead versions of Ret induced only mild or no trans-phosphorylation, respectively (Figure 32A and B).

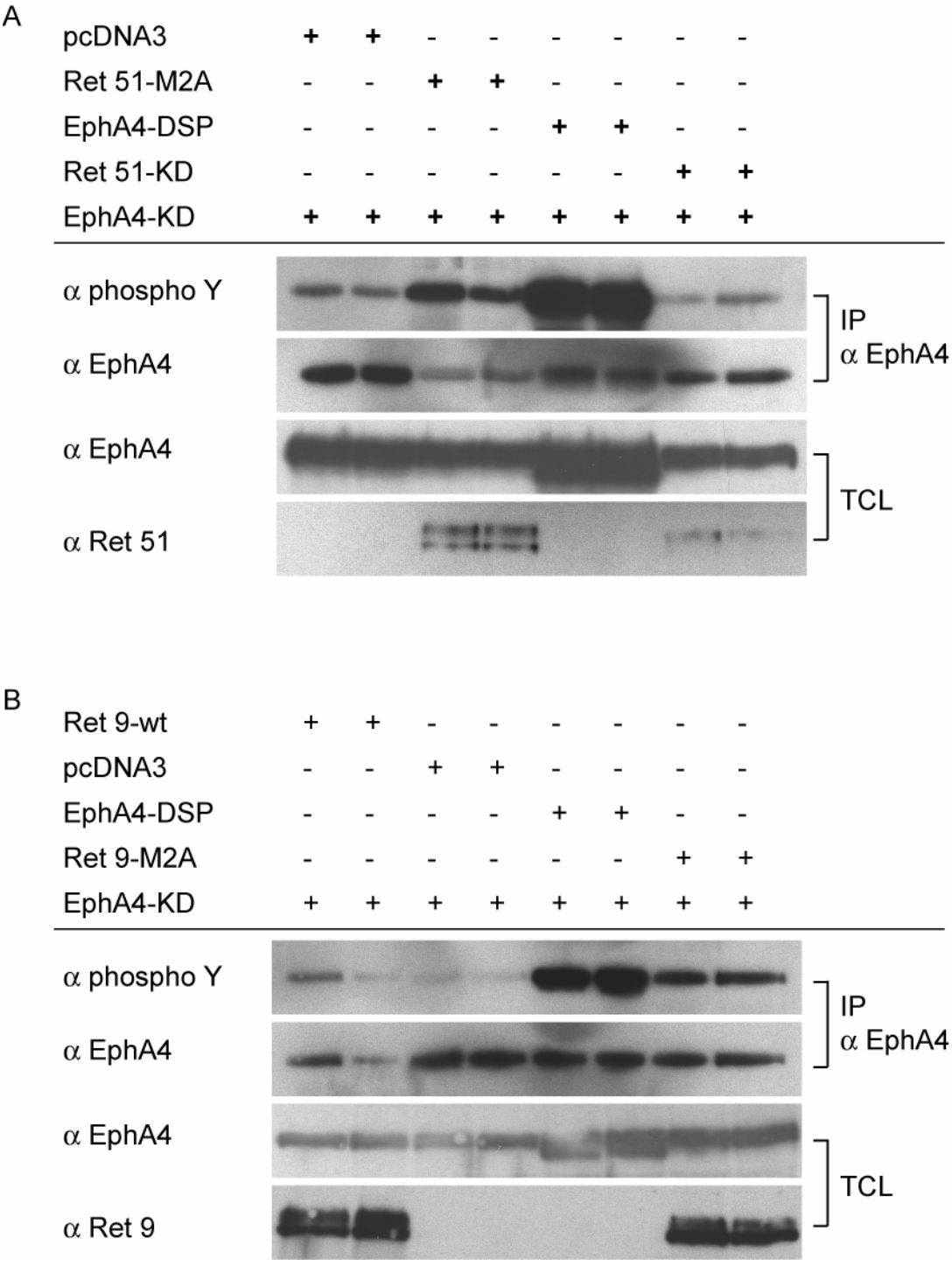

Figure 32 Trans-phosphorylation between Ret and EphA4

Kinase dead EphA4 (EphA4-KD) was transiently expressed in Hela cells with empty vectors (pcDNA3), constitutive active (M2A), kinase dead (KD) or wildtype (wt) Ret 51 (A) and Ret 9 (B) constructs. Expression of the proteins was checked in 50μg of total cell lysate (TCL). IPs for EphA4 were probed with anti-phospho-tyrosine (pY) antibodies. Ret9-M2A (B) and Ret 51-M2A (A) can trans-phosphorylate EphA4-KD, while Ret 9-wt (B) and Ret 51-KD (A) lead to mild or no phosphorylation of EphA4-KD, respectively. Two separate lysates for each condition were loaded.

Next, the opposing situation was tested. Kinase-dead Ret receptors (Ret 51-KD and Ret 9-M2A-KD) were co-expressed together with EphA4^{DSP} or EphA4-KD and a constitutively active form of Ret as a positive control. Ret was immunoprecipitated and phosphorylation was detected with anti-pY antibodies. No signal for tyrosine phosphorylation was seen except in the positive control (Figure 33A).

In another experiment, cells expressing kinase dead Ret and EphA4^{DSP} were stimulated with ephrinA-Fc or Fc as control stimulation. To verify the functioning of ligand and mock stimulations, Hela cells growing on coverslips in the respective culture dishes were stained using EphA4 and anti-Fc antibodies. Diffuse expression of EphA4 but no cluster formation could be seen in Fc control stimulations (Figure 34A). In contrast, signals from anti-Fc antibodies, which detected the Fc fragment of ephrinA-Fc fusion proteins binding to EphA4 receptor, co-localized nicely in clusters detected with the EphA4 antibody (Figure 34B). When cells expressing kinase dead Ret and EphA4^{DSP} were stimulated with the ephrinA ligand, a weak trans-phosphorylation of kinase-dead Ret could be detected (Figure 33B). These results are preliminary and will be repeated, but provide an initial evidence for a liaison between Ret and EphA4 signaling.

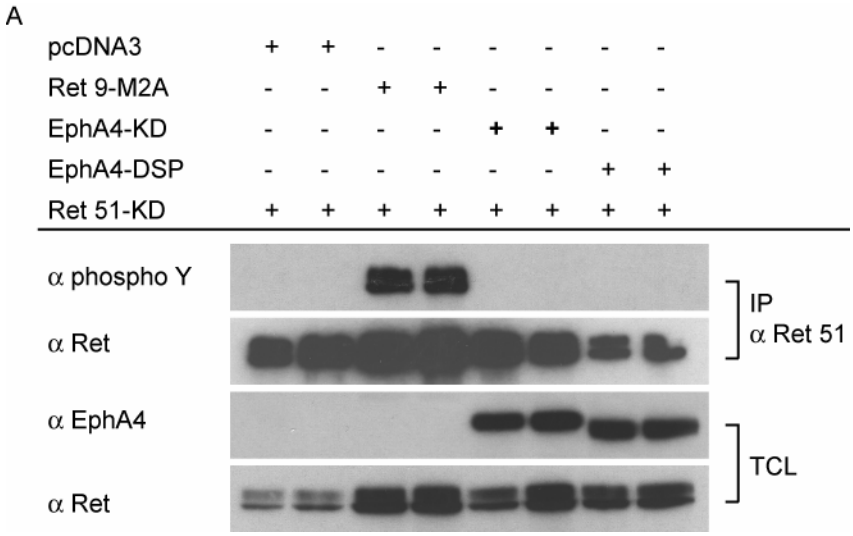

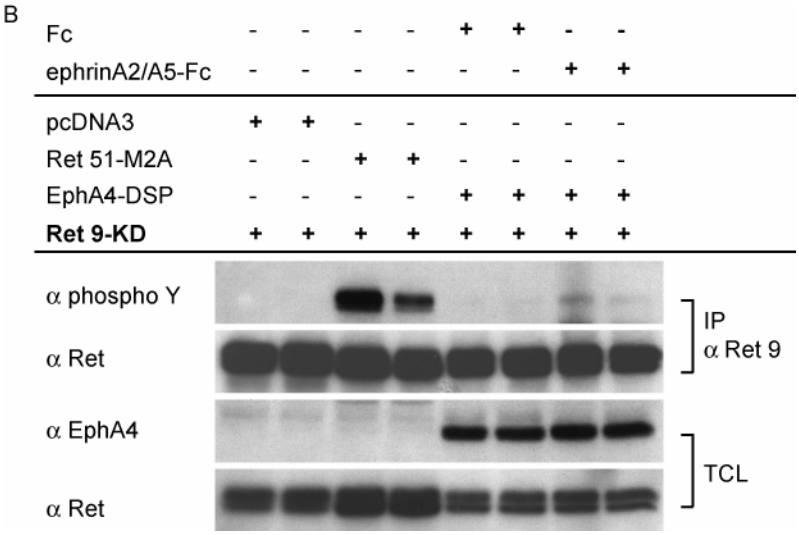

Figure 33 Trans-phosphorylation between EphA4 and Ret

(A) Kinase dead Ret 51 was transiently expressed in Hela together with EphA4^{DSP}, Ret 9-M2A or empty vectors. (B) Kinase dead Ret 9 was transiently expressed in Hela together with EphA4^{DSP}, Ret 51-M2A or empty vectors. Samples expressing Ret and EphA4 were either stimulated with Fc-fragment or ephrinA2/A5-Fc. Mild phosphorylation of kinase dead Ret was only detected in the ephrinA stimulated condition.

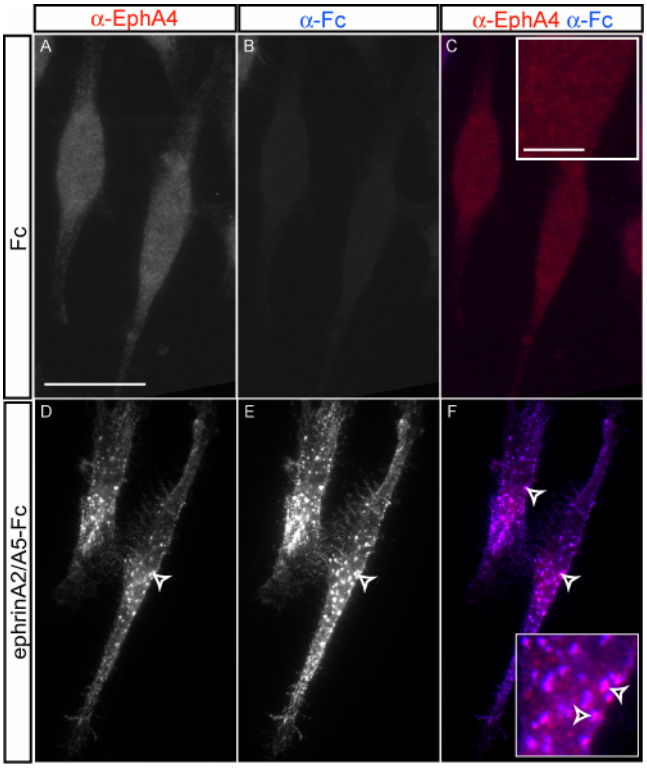

Figure 34 Testing cluster formation in transiently transfected Hela cells

In all co-IP experiments involving stimulation with ephrinA-Fc or Fc-fragment, a round cover slip (CVS) was applied to each condition. The cells were stained using anti-Fc and anti-EphA4 antibodies to test for proper cluster formation and protein expression. (A) In a mock stimulation with Fc-fragment, EphA4 (in red) was detected in many cells showing a diffuse distribution throughout the cells. No signal was detected with the anti-Fc (in blue) antibody. (B) In the ephrinA2/A5-Fc stimulation, EphA4 and Fc-signal overlap completely and show a typical punctuated pattern with many clusters (arrowheads). Scale bar in (A) and inlet in (C) is 25 μm and 5 μm, respectively.

To circumvent the disadvantage of massive overexpression in cells which are transiently transfected with the receptors, cell lines were screened for endogenous expression of Ret and EphA4. Total cell lysates of an immortal motor neuron cell line (MN1) were probed for both receptors. Surprisingly, a promising expression for Ret, but no signal for EphA4 was detected (Figure 35A). A neuroblastoma cell line (SK-N-2BE) also expressed only Ret (data not shown), but could be transfected more easily than MN1 cells. This cell line could be used in future experiments to transfect kinase-dead EphA4 to thoroughly analyze trans-phosphorylation upon stimulation with GDNF using different concentrations and incubation times. Figure 35B shows an initial experiment for the induction of Ret phosphorylation. SK-N-2BE cells were stimulated with GDNF, immunoprecipitated and phosphorylation was detected using anti-pY antibodies. Basal phosphorylation was detected in the unstimulated case, and was enhanced strongly after stimulation with 10 ng GDNF of 30 min or 50 ng of GDNF for 10 min.

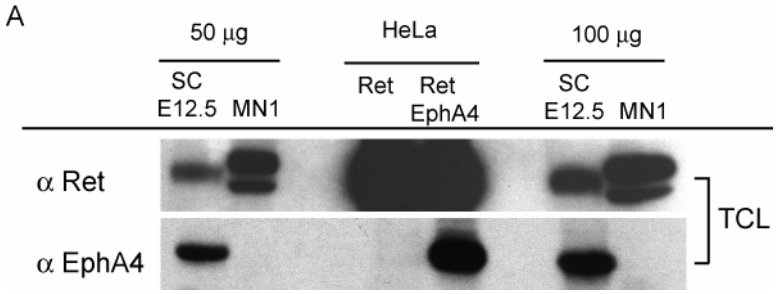

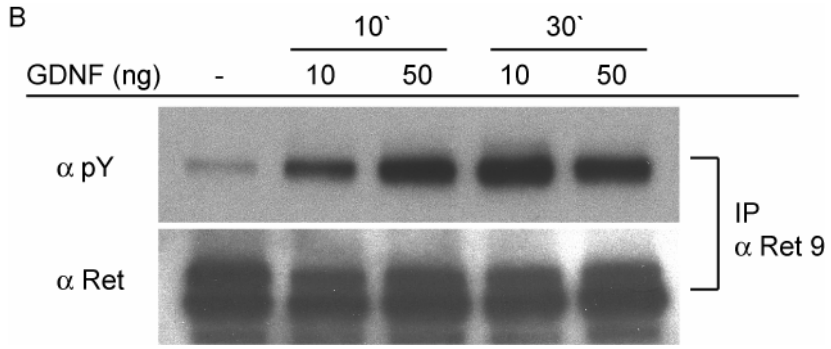

Figure 35 Endogenous expression of Ret and EphA4

(A) An immortalized motor neuron cell line (MN1) was tested for endogenous expression of Ret and EphA4. For positive controls, lysates from E12.5 spinal cords (SC) or transiently transfected Hela cells were used. Expression of Ret, but not EphA4 was seen in MN1 cells. (B) Ret-IP was tested for tyrosine phosphorylation upon stimulation with GDNF in SKN-2BE cells. No GDNF stimulation showed a low basal phosphorylation. Stimulation for 10 and 30 min, using 10 or 50 ng of GDNF induced robust phosphorylation of endogenous Ret.

2.3.5 Motor neuron culture system set up

To obtain information about the subcellular localization of Ret and EphA4 in motor neurons, a cell culture system of dissociated motor neurons was set up following a protocol established by Francoise Helmbacher. Motor neurons were isolated from whole E12.5 spinal cords or limb innervating segments using gradient centrifugation and were seeded on coated cover slips. After 16-36 hrs in culture, the neurons had grown considerably long axons and could be used for different stainings or *in vitro* assays. Although the amount of other cell types was minimized during the motor neuron isolation, other neuronal cell types were growing in the culture dish, too. To visualize motor neurons and not other cells, Hb9-GFP mice, which express GFP under the motor neuron-specific promoter Hb9, were used for the culture (Figure 36). Antibody stainings will be performed to study the subcellular localization of EphA4 and Ret in response to different stimulations using ephrinA ligands or GDNF or combinations of both. Previous studies have demonstrated that EphA4 expressing neurons respond with a growth cone collapse upon ephrinA stimulation (Drescher, Kremoser et al. 1995). These observations were also confirmed in my experiments. Examples of well developed growth cones can be seen in panel B, C and D in Figure 36. The axon in Panel E has a collapsed growth cone as expected after ephrinA stimulation. Figure 36D and E also shows the formation of clusters using anti-Fc

antibodies upon ephrinA2 and A5-Fc stimulation. It will be very exciting to see how growth cones of co-stimulated motor neurons behave in a collapse assay, and if cluster formation is altered upon stimulation with ephrinAs in presence or absence of GDNF.

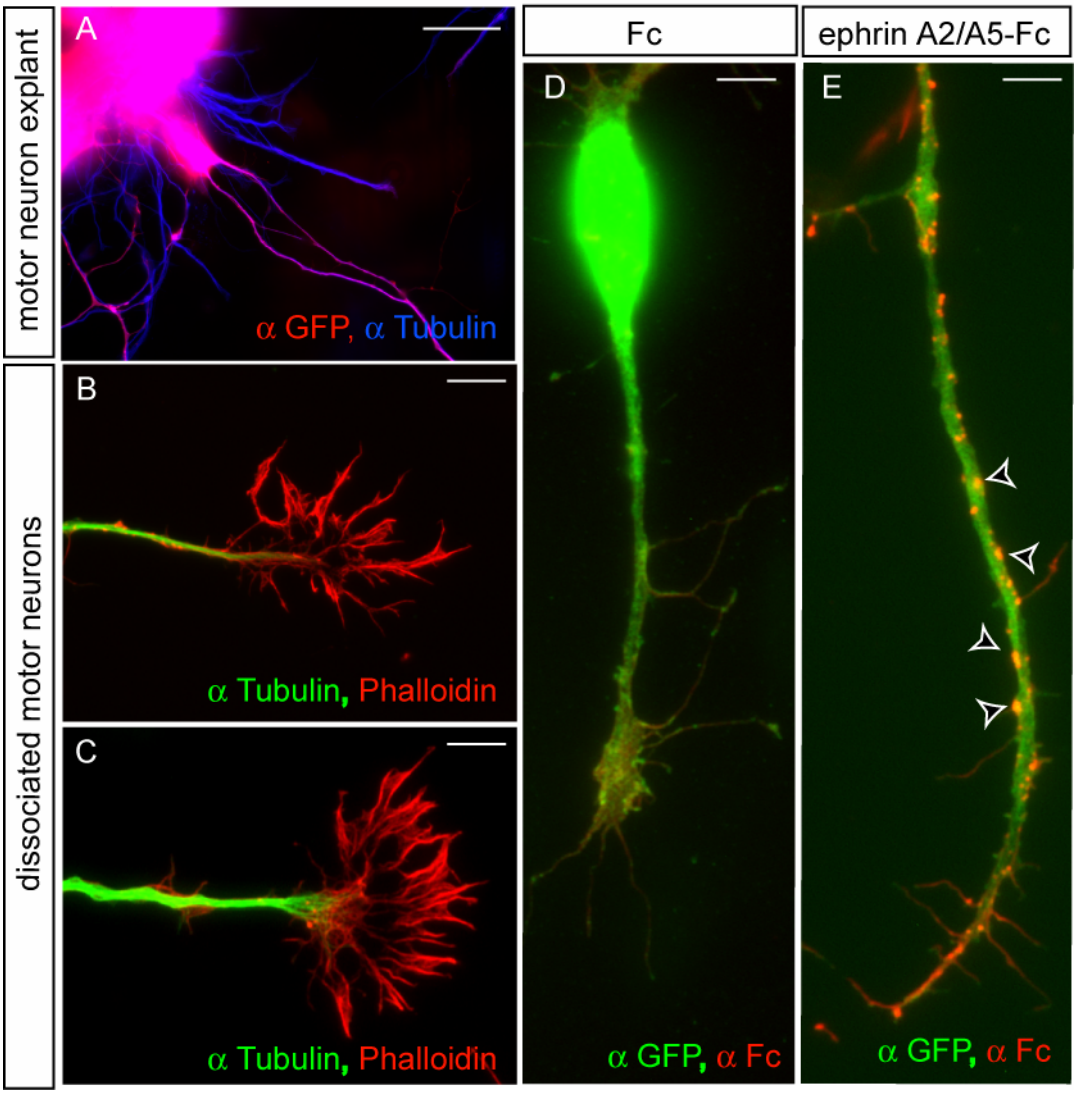

Figure 36 Primary cell culture of motor neurons

Culture of dissociated motor neurons (B-E) or explants form the LMC (A) from E12.5-E13.5 Hb9-GFP embryos. (A) Low magnification image (20x) of an explant. All axons were visualized with anti-tubulin (in blue), among which motor neuron axons, labeled with anti-GFP (in red), appear pink. (B and C) Highe magnification image (100x) of well developed growth cones. Actin filaments were stained with Phalloidin-TexasRed (TxR) and microtubules are labeled with anti-tubulin antibodies (in green). Stimulation of MNs with either Fc-fragment (D) or ephrinA2/A5-Fc (E) (1μg/ml for 30 min) induced robust cluster formation (arrowheads) in the ephrin-stimulated neuron and growth cone collapse.

To be able to closely follow a collapse response, live cell imaging was established using dissociated cultures. Figure 37 shows a motor neuron observed for about 30 min without stimulation. The arrow points to the growth cone. After approximately 10 min the growth cone starts to collapse but at the same time new filopodia more proximal to the cell body begin to explore the environment (Figure 37E arrowhead). Seven minutes later this spot was the origin the outgrowth of two new processes (Figure 37G).

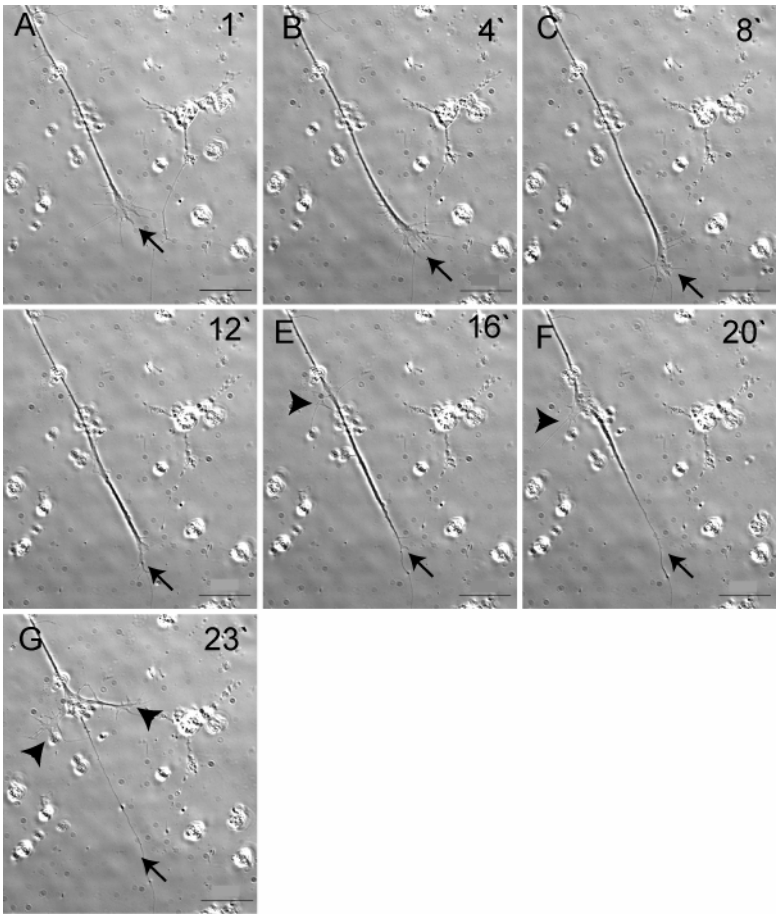

Figure 37 Time lapse imaging of dissociated motor neurons

A low-density culture of dissociated motor neurons (one day in culture) was imaged using time lapse microscopy at one frame/min (supplementary information on the CD-Rom, movie 1). The growth cone of an axon explored the environment quite actively (A-C). After 12 min, a collapse was observed (arrow in D–F) followed by the establishment of two new growth cones at a more proximal position of the axon (arrowhead in E-G). Scale bars are 30 μm.

Dissociated motor neurons behave quite variably in culture. Figure 38 showes one cell, labeled with an arrow, and another, labeled with an arrowhead, displaying fast growth and stationary behavior, respectively. Therefore it can be quite difficult to decide which neuron to image.

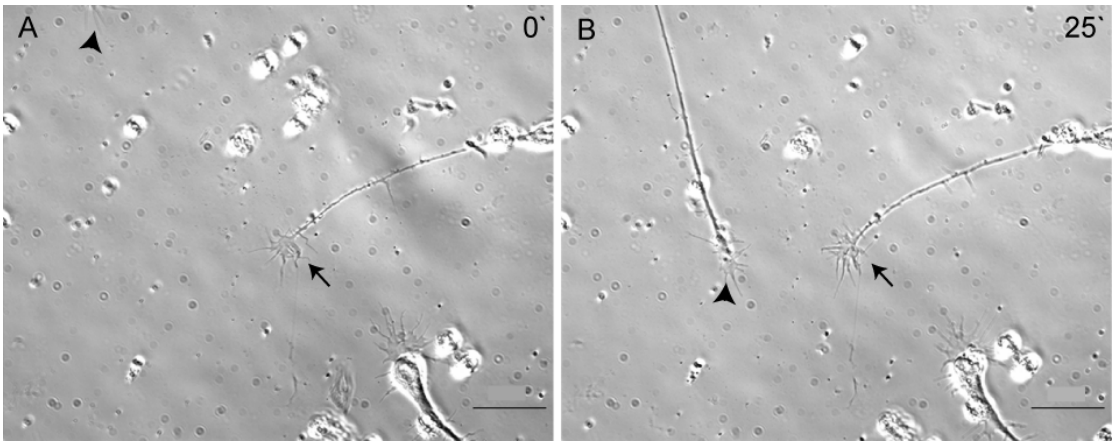

Figure 38 Time lapse imaging of dissociated motor neurons

A low-density culture of dissociated motor neurons (one day in culture) was imaged using time lapse microscopy at one frame/min (supplementary information on the CD-Rom, movie 2). Within 25 min, one axon (arrowhead) covered a distance of 120μm (~4.5μm/min), while the other one displayed stationary behavior (arrow). Scale bars are 30 μm.

As mentioned before, dissociated cultures were obtained from whole spinal cords or limb innervating segments and therefore contained motor neurons from LMC and MMC. The fraction of "interesting" motor neurons belonging to the lumbar LMC(l) is rather small with respect to all spinal motor neurons. To restrict the culture to the important population of motor neurons, an explant culture following a protocol established by Till Marquardt was set up. Hb9-GFP mice were used to visualize the motor columns and allowed precise dissection of the lumbar LMC (see also Figure 46). Small pieces of LMC(l) tissue were seeded onto coated coverslips and cultured for 2 days. Panel A in Figure 36 shows an example of a motor neuron explant stained for tubulin and GFP. Because the axons from the explants were in close contact with each other and grow in a radial fashion, it was easier to find a good spot for a movie. To test conditions for future stimulations, an explant culture was imaged before and after stimulation with soluble pre-clustered ephrinA2/A5-Fc. Before application of the ligand the observed growth cone was very actively producing and retracting filopodia at high frequency (Figure 39A-C). Five minutes after stimulation, the

monitored growth cones were still growing normal, but five more minutes later the growth cones started to display a less complex structure (Figure 39F). During the next 15 min a full growth cone collapse was observed (Figure 39G-I). *In vivo* this collapse happens upon cell-cell contact since receptor and ligand are membrane bound (Orioli and Klein 1997). To better mimic this situation in future experiments the ephrinA ligands will be presented to the growth cones from a located source (e.g. transiently transfected Hela cells or coated beads). In addition, antibody stainings for Ret and EphA4, cluster formation and growth cone behavior assays will be carried out.

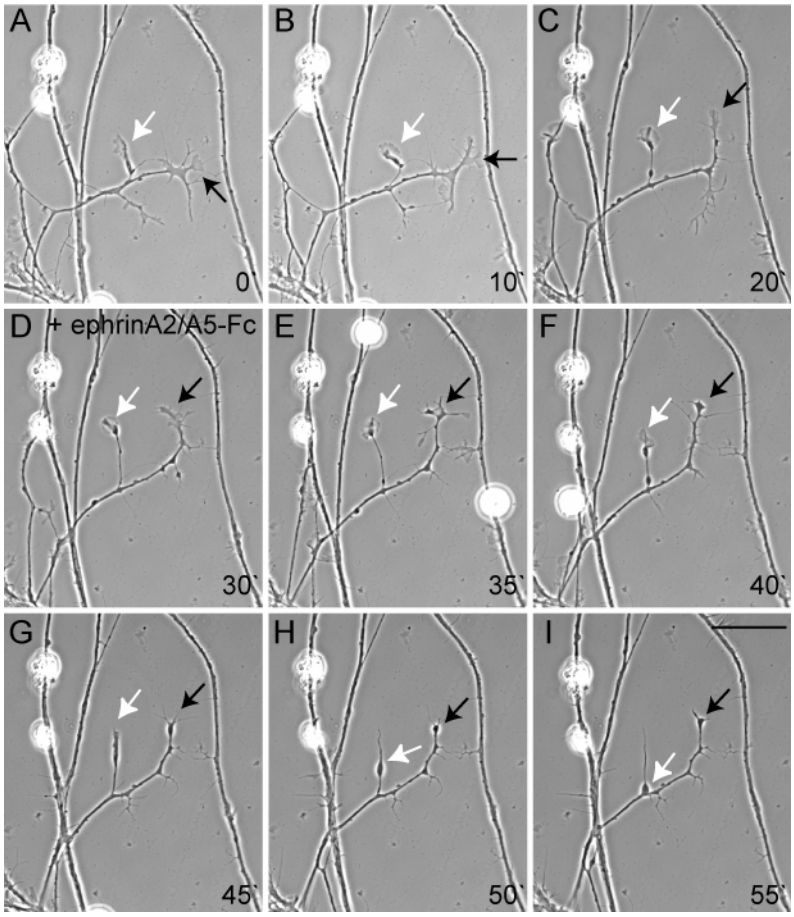

Figure 39 Live-cell imaging of a stimulated motor neuron explant culture

An explant from the LMC (two days in culture) was imaged using time lapse microscopy at one frame/min (supplementary information on the CD-Rom, movie 3). Before stimulation, several growth cones (arrows) and other processes were observed (A-C). Shortly after stimulation with preclustered ephrinA2/A5-Fc (1 μg/ml) normal growth can be observed (D and E). About 10 min after the stimulation, the growth cones became simpler (F) and after 25 min a full growth cone collapse was observed (G-I). Scale bar is 30 μm.

2.4 The requirement of axonal and mesenchymal EphA4 for pathway selection in the hindlimb

As already mentioned in the introduction, inactivation of the mouse *ephA4* gene can cause misprojection of peroneal nerve axons onto the tibial nerve pathway (Helmbacher, Schneider-Maunoury et al. 2000). Conversely, ectopic expression of EphA4 in chick LMC(m) neurons leads to misprojection of their ventrally fated axon onto the dorsal trajectory (Eberhart, Swartz et al. 2002; Kania and Jessell 2003). The current simple model holds that LMC(l) axons expressing high levels of EphA4 are repelled by ventral hindlimb mesenchyme expressing ephrinA ligands. Interestingly, ephrinA ligand is co-expressed on hindlimb innervating motor axons (Eberhart, Swartz et al. 2000) and EphA4 protein is found in the dorsal hindlimb mesenchyme (Eberhart, Swartz et al. 2000; Helmbacher, Schneider-Maunoury et al. 2000; Kania and Jessell 2003) (see also Figure 13B and C, 25A-D). A recent study suggested that axonal ephrinAs act independently from EphA4 and mediate attraction toward EphA4-positive dorsal mesenchyme (Marquardt, Shirasaki et al. 2005). To investigate the contribution of axonal and mesenchymal EphA4 to the pathfinding of LMC(l) axons, a conditional inactivation strategy was developed to remove EphA4 selectively from the motor axons using Nestin-Cre or from hindlimb mesenchyme using Tbx4-Cre (Artur Kania, unpublished).

2.4.1. Specific and robust recombination activity of Tbx4-Cre

Before intercrossing Tbx4-Cre and EphA4$^{lx/lx}$ mice, lacZ reporter mice (Rosa26R) were used to visualize the onset and distribution of Tbx4-Cre activity. Robust β-galactosidase activity was detected in the hindlimbs of E9.5 embryos (Figure 40A and B). The signal was even more intense at E11.5 and was maintained at later stages (E12.5) (Figure 40C, E and F). Nervous system tissue was completely devoid of signal (Figure 40D). Due to the complete and specific expression, Tbx4-Cre will be used as a tool to remove EphA4 from hindlimb mesenchyme tissue. To verify excision in Tbx4-EphA4$^{lx/lx}$ embryos, EphA4 protein levels will be evaluated in total cell lysates of legs compared to lysates from spinal cords.

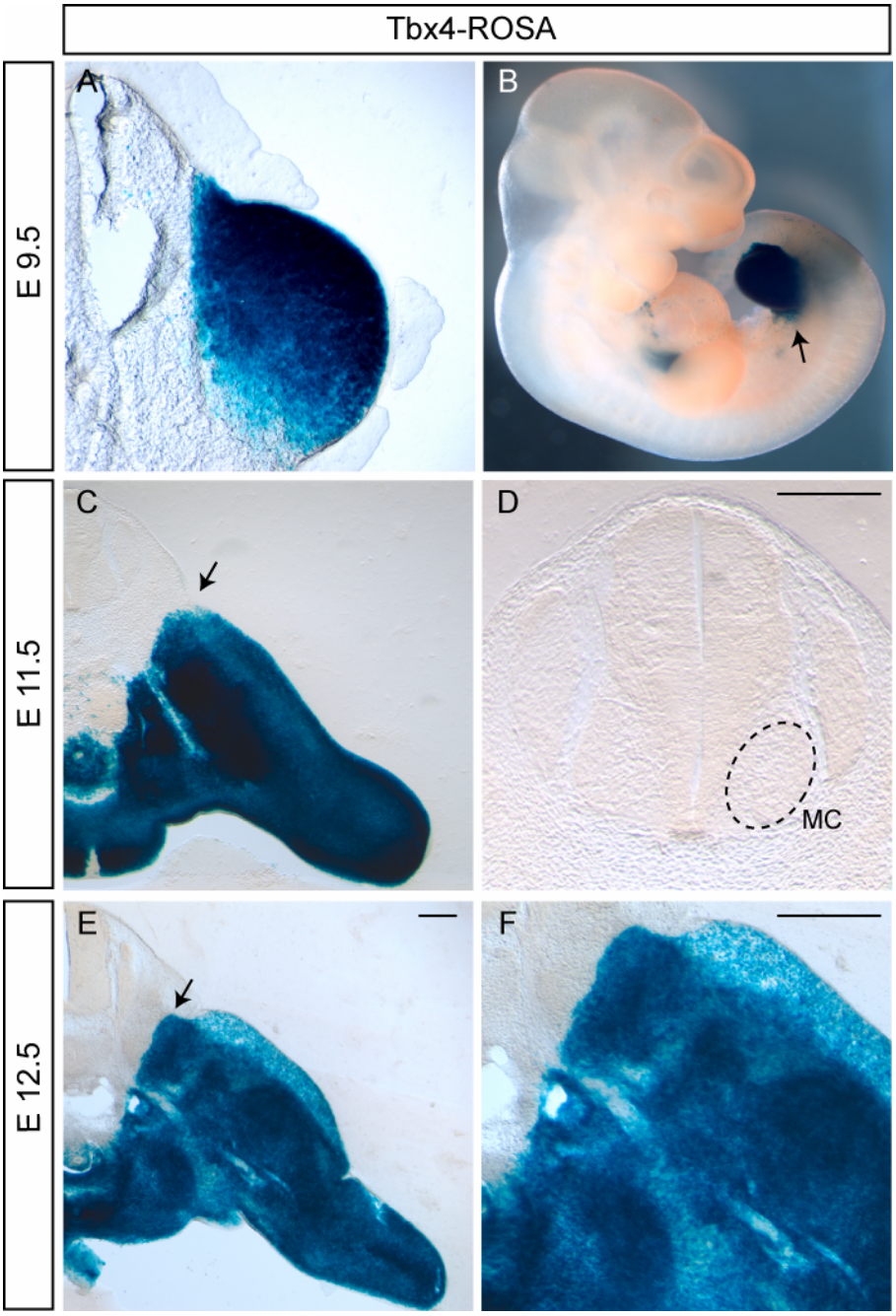

Figure 40 β-galactosidase activity in Tbx4-Cre;Rosa26R mice

β-galactosidase activity in whole mounts and sections of Tbx4-cre;Rosa26R (Tbx4-Rosa) transgenic embryos of the indicated stages at lumbar level. Specific and robust expression was detected at E9.5 (A and B). The signal was even more robust at E11.5 and E12.5 (C, E and F) and was completely absent from spinal cord or DRG neurons (D). Motor column (MC) is indicated with a stippled circle. Scale bars are 250 μm.

Figure 41 shows a preliminary test, where total cell lysates from wildtype embryo legs and spinal cords were probed for EphA4 and Ret. As expected, EphA4 protein was detected in both tissues, whereas Ret was only present in the spinal cord fraction. The amount of protein from the limb innervating axons can be disregarded.

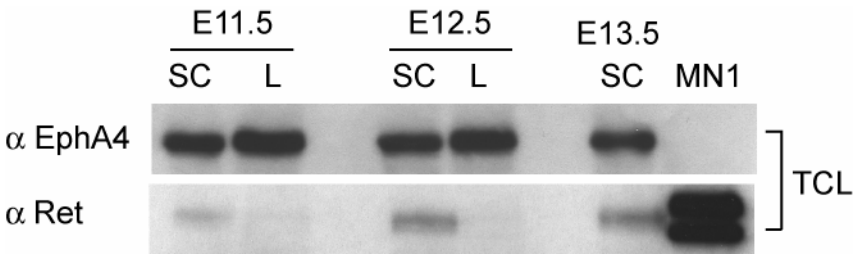

Figure 41 Spinal cord versus limb protein levels

Protein levels of EphA4 and Ret in spinal cord (SC) and hindlimb tissue of wildtype embryos at the indicated stages. EphA4 can be detected in both SC and limb mesenchyme, while Ret is only present in the SC sample. Lysates from MN1 cells were used as a positive control for Ret expression.

2.4.2 Motor neuron backfill technique allows the detection of single misguided axons

A described previousely (chapter 1.4. and 2.3.2.), most EphA4 knockout embryos display a mild axon guidance phenotype. If both axonal and mesenchymal EphA4 contribute to the correct pathway selection of LMC(l) axons, this phenotype would be expected to be even more mild in the conditional EphA4 mutants (Nes-EphA4$^{lx/lx}$ and Tbx4-EphA4$^{lx/lx}$). A very elegant and extremely sensitive way to discover misguided axons, is the motor neuron backfill technique. This method allows the detection of single misguided axons, which would be below the detection threshold in a whole mount neurofilament staining. To discover ventrally misrouted axons, the tibial nerve needs to be backfilled. So far only wildtype controls were filled to establish the method in the laboratory. Tibial nerves of Hb9-GFP$^{+/-}$ embryos were injured and a red dye (rhodamine-dextran) was applied at the site of nerve lesion using a fluorescent dissecting microscope to visualize motor axons (Figure 42A). Embryos were incubated for 7hrs in ACSF to allow retrograde transport of the dye into the cell bodies of the injured axons. In wildtype embryos, cell bodies of the LMC(m) were labeled, which can be seen in lumbar cross sections of treated Hb9-

GFP$^{+/-}$ embryos (Figure 42B, E and F). To prove that these cells indeed belong to the population of LMC(m), an antibody staining for Isl1 (a marker for LMC(m) neurons) will be done. A schematic drawing shows the expected result for mutants, displaying an axon guidance phenotype (Figure 42 C). Retrogradely labeled cell bodies of ventrally misguided LMC(l) axons will be located in the LMC(l) population and be devoid of Isl1 staining.

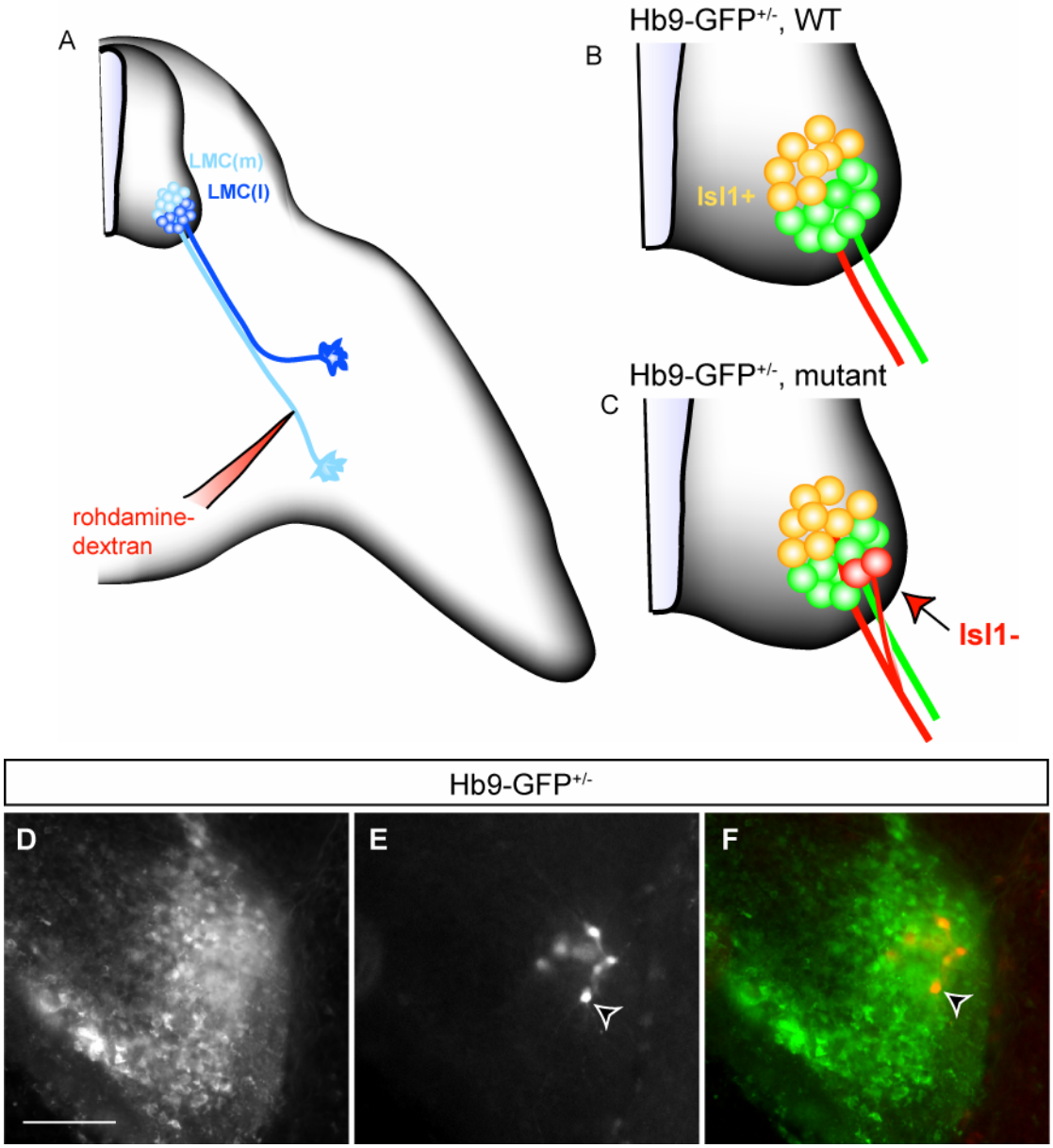

Figure 42 Motor neuron backfill

(A) Schematic drawing showing the injection of rhodamine-dextran dye into the axons of LMC(m) neurons. In wildtype embryos (B), only cell bodies of LMC(m) neurons are labeled

with the injected dye. Motor neurons can be visualized using Hb9-GFP$^{+/-}$ mice. In mutants, which have dorsaly-fated axons misguided into the ventral nerve branch, backfilled cell bodies can be detected in LMC(m) and LMC(l). The latter are well-defined by the absence of Isl1 staining (C). (D-F) Cryostat section of an E13.5 embryo at lumbar level showing Hb9-GFP in green (D and F) and backfilled cell bodies in red (E and F) in the area of the LMC(l). Scale bar is 100μm.

3 Discussion

The studies reported here identified novel guidance signals for topographic projections of specific motor axons to limb muscles. The main results are as follows: first, LMC(l) axons express high levels of Ret and project to a dorsal territory enriched in GDNF. Second, in mutant mice lacking GDNF or Ret, many LMC(l) axons are rerouted to an aberrant ventral trajectory. As shown by the LMC(l) marker Lim1, this phenotype is caused by a pathfinding defect and not by misspecification, reduced survival, or reduced axonal growth of LMC(l) neurons. Third, the requirement of Ret is likely to be cell-autonomous as shown by conditional removal of Ret in cells of the spinal cord. Fourth, the misprojection phenotype of limb-innervating axons is enhanced in mutant mice lacking both Ret and EphA4. Fifth, preliminary experiments using a biochemical approach provided evidence for an activity dependent interaction of EphA4 and Ret receptor and a capacity to trans-phosphorylate each other. Moreover, in collaboration with Cathy Krull it was shown that Ret, when overexpressed, is sufficient to reroute some LMC(m) axons inappropriately into the dorsal nerve trunk (Kramer, Knott et al. 2006). Taken together, these results suggest that Ret and EphA4 cooperate to enforce the precision of the same binary choice of LMC axons at the sciatic plexus, to project dorsally rather than ventrally.

In another approach, a strategy to reveal the contribution of axonal versus mesenchymal EphA4 for the guidance of hindlimb innervating motor neurons was developed.

3.1. Differential expression pattern of Ret and GDNF suggests a function in topographic mapping of hindlimb innervating motor axons

Establishing the connectivity between particular motor neurons and their target tissue is a highly complex process that can be broken down into modular steps requiring simple binary decisions (Dickson 2002). One example for such a binary decision is the dorsoventral choice of hindlimb innervating LMC axons. Here, axons from the LMC(l) and LMC(m) express high and low levels of EphA4 receptor, respectively, and ephrinA ligands are expressed at a higher density in the ventral than in the dorsal compartment of the limb (Eberhart, Swartz et al. 2000; Helmbacher, Schneider-Maunoury et al. 2000; Kania and Jessell 2003). Inactivation of the mouse *ephA4* gene (EphA4^{lacZ} allele) causes misprojection of dorsal (LMC(l)) axons into a ventral trajectory (Helmbacher, Schneider-Maunoury et al. 2000). The current model is that EphA4-expressing LMC(l) axons are repelled from ephrinA-positive ventral territory (Figure 12B). However, the severity of the EphA4-loss-of-funtion phenotype is somewhat variable depending on which *ephA4* allele is studied (Kullander, Mather et al. 2001; Leighton, Mitchell et al. 2001). This unsolved issue suggests the existence of yet unknown guidance cues that act in parallel to the EphA4 pathway. For a signaling system to coordinate the dorsoventral choice of LMC axons at the sciatic plexus, differential expression of the receptors in motor axons and of the ligand in hindlimb mesenchyme, similar to that which has been described for EphA4, would be expected.

This study presents immunostainings on mouse embryo sections with antibodies against the receptor tyrosine kinase Ret, which revealed striking similarities to the EphA4 expression pattern (Figure 13). In contrast to EphA4, which is absent in sensory neurons (see Figure 25 A and C), Ret was also expressed in cells of the DRGs. Because strong immunoreactivity for Ret was detected on very proximal aspects of the sciatic nerve, where axons exit the spinal cord through the ventral horn, and only weak Ret signal was detected on sensory axons coming from the DRGs, which join the common pathway later, the differential expression on limb innervating axons could be attributed to motor axon origin. Consistently, Ret mRNA levels were higher

in LMC(l) than LMC(m) motor neurons at the same developmental stage and almost no signal was detected in DRGs (Figure 14).

Analysis of GDNF expression in the hindlimb using specific antibodies and monitoring of β-galactosidase activity in $GDNF^{lacZ}$ mice revealed a differential distribution in the hindlimb mesenchyme. An important source of GDNF was detected in the territory immediately dorsal to the sciatic plexus where peroneal and tibial axons branch off from the common trajectory. The differential expression patterns raised the possibility that GDNF acts as a guidance signal for Ret-positive motor axons.

3.2. GDNF/Ret signaling is required for motor axon growth into the dorsal hindlimb

There is compelling evidence that the Ret receptor and GDNF family ligands mediate axon outgrowth *in vivo* and play an important role for motor neuron survival (Oppenheim, Houenou et al. 2000; Markus, Patel et al. 2002). Motor neurons respond to GDNF with robust axon outgrowth, and ectopic expression of GDNF in muscle in transgenic mouse models leads to local hyperinnervation of neuromuscular junctions (Nguyen, Parsadanian et al. 1998). More recent work has shown that GDNF in muscle promotes axon terminal branching that counteracts ongoing synapse elimination (Keller-Peck, Feng et al. 2001). Early in development, GDNF produced by distinct muscles induces the expression of the ETS transcription factor, PEA3, in specific motor neuron pools (Haase, Dessaud et al. 2002). PEA3 is required for the specification of motor neuron identity. In GDNF and Pea3 mutant mice, specific motor neuron cell bodies are mispositioned within the brachial region of the spinal cord and target innervation is perturbed secondarily (Livet, Sigrist et al. 2002). However, no previous reports have implicated GDNF in regulating topographic projections of motor axons. The only indirect evidence for a possible role of Ret in axon guidance comes from *in vitro* studies. It was shown that soluble GFRα1 protein produced by target cells can potentiate neurite outgrowth *in vitro* by capturing GDNF and presenting it to axonal Ret receptors (Ledda, Paratcha et al. 2002), suggesting that GFRα1 receptors can act as a chemoattractant for peripheral neurons. Similarly, the GDNF/Ret pathway is required for migration of enteric neuron precursor cells into the gut, also through a chemotactic mechanism (Natarajan,

Marcos-Gutierrez et al. 2002). Whether these *in vitro* findings have any physiological relevance for *in vivo* guidance of peripheral axons has not yet been investigated.

The results presented in this thesis provide genetic evidence that Ret signaling controls the dorsoventral choice of motor axons in the hindlimb and that GDNF is an essential ligand for this newly assigned function. Inactivation of the *ret* gene in all cells ($Ret^{-/-}$) leads to the reduction of the peroneal (dorsal) nerve. Since the amount of the peroneal nerve reduction varied, mutants were classified into three categories according to the severity of the phenotype (Cat I: mild, Cat II: intermediate and Cat III: strong). The majority of $Ret^{-/-}$ embryos fell into Cat II. Selective removal of Ret from the spinal cord using the conditional allele with a nervous-system-specific Cre (Nes-$Ret^{lx/lx}$) resulted in the same phenotype and showed that Ret acts in a cell-autonomous manner in neurons of the spinal cord. The phenotype, however, was slightly milder than in full knockouts with the majority of embryos in category I at E12.5 (Figure 23). This could be due to variability in the excision of Ret with Nestin-Cre. Indeed, a small signal for Ret could be detected in western blots of spinal cord lysates from Nes-$Ret^{lx/lx}$ embryos. Consistent with this, immunostainings of Nes-$Ret^{lx/lx}$ embryos revealed low levels of remaining protein in a few sections (Figure 21). In contrast to Ret *null* mice, which die on the day of birth due to kidney agenesis, Nes-$Ret^{lx/lx}$ mice are viable and fertile. Interestingly, they show an abnormally stiff position of the hindlimb, similar to the club-foot-phenotype in $EphA4^{lacZ/lacZ}$ mice. The reduction of the peroneal nerve may lead to misbalanced innervation of flexor and extensor muscles and thereby cause the stiff hindlimb. Of course, other factors such as increased cell death cannot be excluded and it is most likely that the abnormal foot position is a result of a very complex sequence of events.

The peroneal nerve reduction is a true axon guidance mistake, because in the absence of Ret, LMC(l) axon outgrowth is not diminished, but instead axons are rerouted to a ventral pathway as shown by Lim1-driven β-galactosidase activity, $EphA4^{PLAP}$-driven AP-staining and EphA4 immunostainings. GDNF knockout embryos display the same axon guidance phenotype. It must be noted that all analyses were carried out before the period of programmed cell death. Thus, these findings provide genetic evidence for a participation of the GDNF/Ret system in dorsal/ventral pathway selection by motor axons, although further *in vitro* experiments will be required to establish whether GDNF can directly influence the pathfinding of motor-axon growth cones. Although GDNF has previously been shown to induce the expression

of PEA3 thereby influencing neuronal specification and growth characteristics (Haase, Dessaud et al. 2002), the analysis of axon projections in Pea3 mutant embryos did not reveal dorsal/ventral pathfinding defects of hindlimb-innervating axons (data presented in my diploma thesis). Thus, the possibility that GDNF has indirect modulatory effects on hindlimb-innervating axons via the regulation of PEA3 can be excluded, but it is still possible that GDNF acts indirectly through another transcriptional regulator.

Further support for a requirement of GDNF/Ret in the guidance of LMC(l) axons comes from overexpression studies in the chick, which were carried out in collaboration with Cathy Krull. In the majority of cases, LMC(m) axons that expressed Ret ectopically projected aberrantly into the dorsal limb (Kramer, Knott et al. 2006).

3.2. Cooperation between GDNF/Ret and ephrinA/EphA4 in motor axon guidance

The genetic analyses of Ret and EphA4 suggest that both signals cooperate to direct motor axons towards a dorsal pathway (model Figure 43). Absence of either Ret or EphA4 produces phenotypes that vary in severity with some LMC(l) axons being misrouted and others reaching the dorsal compartment as in wildtype embryos. Absence of both Ret and EphA4 produces generally strong phenotypes with all LMC(l) axons misrouted into a ventral pathway (Figure 30). These findings provide a compelling example of true cooperation between different guidance signals to enforce the same pathway choice. As in the case of loss-of function mutants, the Ret overexpression phenotype in chick is similar to EphA4 overexpression, again confirming their common function in dorsal pathway selection. However, for most axon-guidance decisions, for which the molecular cues are beginning to be understood, a single required pathway is known (Williams, Mann et al. 2003). The observed cooperation between Ret and EphA4 in establishing proper hindlimb innervation raises the question whether Ret signaling can function in the absence of EphA4 signaling. The *in vivo* observations suggest that this is indeed the case. Strong pathfinding phenotypes were generally observed in the EphA4;Ret double knockout mutants, which are partially rescued in the EphA4 single mutants. Hence, the presence of Ret alone is sufficient for at least a fraction of peroneal axons to project

dorsally in a significant proportion of mutant embryos. Support for this conclusion also comes from the gain-of-function experiments in chick. Ectopic expression of Ret in LMC(m) neurons can redirect them to a dorsal pathway despite low levels of EphA4 that are subthreshold for mediating the repulsive effects of ephrinAs (Kramer, Knott et al. 2006). More definitive conclusions would, however, require *in vitro* explant growth/guidance assays with GDNF under conditions in which EphA4 expression is (largely) eliminated.

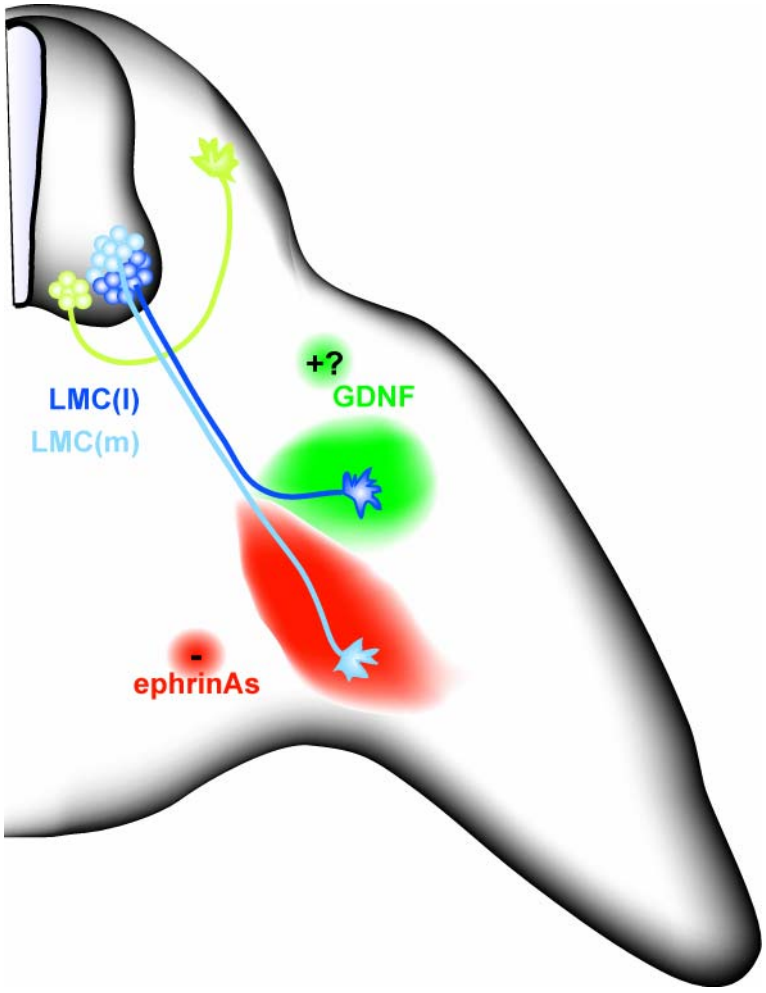

Figure 43 Model

Schematic drawing of a cross section at the level of the sciatic plexus. Neurons of the LMC(l), which have high levels of Ret and EphA4 are indicated in dark blue. Neurons of the LMC(m), which have low levels of Ret and EphA4 are indicated in light blue. EphrinAs in the ventral mesenchyme (red) repel LMC(l) axons into the dorsal compartment of the hindlimb. GDNF, indicated in green may be an attractive source for LMC(l) axons.

3.4. Molecular mechanisms underlying the cooperation between EphA4 and Ret

The possibility that Ret is required for maintaining EphA4 expression or vice versa can be excluded, because the levels of Ret and EphA4 proteins were not altered in the EphA4 and Ret *null* mutants, respectively (Figure 28 and 29). Ret may, however, be required for maintaining the expression of essential downstream components of EphA4 signaling. A candidate for such an effector could be ephexin1, a guanine nucleotide exchange factor (GEF), that is required for EphA4-mediated growth cone collapse (Sahin, Greer et al. 2005).

The first biochemical analysis, however, points to a rather direct influence of Ret and EphA4 signaling on each other. Constitutively active constructs of the long and short isoforms of Ret can clearly phosphorylate kinase-dead EphA4 receptor, and EphA4 can phosphorylate, although mildly, kinase-dead Ret receptor upon ephrinA ligand stimulation (Figure 32 and 33). Moreover, EphA4 can be detected in immunoprecipitations of Ret, when both receptors are fully activated (Figure 31), suggesting that the receptors can interact upon co-stimulation with GDNF and ephrinAs. Whether this interaction is direct, or indirect in a complex involving other molecules is so far unknown. Further experiments using a system, in which at least one receptor has physiological expression levels, and time-course stimulations will give important answers to many unsolved questions. Whatever the molecular interactions may be, the results suggest a positive interaction: Ret enhances and does not interfere with the ability of EphA4 to mediate repulsion. This would explain why in Ret null mutants, EphA4-positive axons turn into a ventral pathway despite the presence of repellent ephrinAs. Likewise, EphA4 should enhance, rather than interfere with, the ability of Ret to mediate an attractive activity of GDNF. This would be consistent with the fact that Ret-positive axons turn ventral despite the presence of GDNF at the branch point in EphA4 knockout mutants. Ret and EphA4 signaling pathways may converge at some point distal to the plasma membrane at the level of Src kinases. Src family kinases have been shown to interact with Ret and Ephs and appear to enhance both the neurite growth-promoting effects of GDNF and the repulsive effects of ephrinAs (Encinas, Tansey et al. 2001; Knoll and Drescher 2004). According to the preliminary biochemical results, the idea that Ret- and

EphA4-signaling pathways act independently and in parallel, ultimately regulating the cytoskeleton with opposing effects on actin and microtubule dynamics of growth cones appears to be less likely (Dent and Gertler 2003).

3.5. Deciphering EphA4/Ret interaction at the cellular level

To better understand what is going on in LMC motor neurons when they meet ephrinA and GDNF signals at the sciatic plexus, dissociated and explant cultures of motor neurons were established. With these tools in hand, antibody stainings could be done to trace the subcellular localization of Ret and EphA4 upon stimulation with ephrinAs or GDNF or both, and thereby obtain information about the mechanism underlying EphA4/Ret cooperation. Growth cone collapse assays using cultured motor neurons can give useful insights about the effect of ephrinA/GDNF stimulation on motor axons for example in a time course. To mimic the *in vivo* situation, only the population of neurons from the LMC will be used (explant cultures), and the repulsive cue will be presented as a localized source (e.g. Hela cells expressing ephrinAs). It will be exciting to compare the behavior of a motor neuron growth cone meeting an ephrinA-expressing cell in presence or absence of soluble GDNF using time-lapse microscopy. Is the expected growth cone collapse faster with co-stimulation of GDNF? Does the axon retract further, or can it recover within less time and thus perform better in deciphering other important guidance cues? It is possible that GDNF/Ret is not only necessary to support ephrinA/EphA4 signaling, but also to put the growth cone into an alerted state at the pathway selection point, and to support other so far unknown guidance signals.

3.6. The role of axonal and mesenchymal EphA4 in the dorsoventral choice of hindlimb innervating axons

We wanted to look at whether Ret could influence ephrinA reverse signaling. Previous reports have shown that LMC(l) axons at hindlimb levels not only express EphA4 receptors but also ephrinA ligands (Iwamasa, Ohta et al. 1999; Eberhart, Swartz et al. 2000). These factors exert opposing effects on growth cones *in vitro*: EphAs mediate growth cone collapse/repulsion, whereas ephrinAs signal motor-axon growth/attraction (Marquardt, Shirasaki et al. 2005). Because EphA4 is expressed by dorsal limb mesenchyme, it has been suggested that EphA4 interactions with axonal ephrinA induce reverse signaling and attract LMC(l) axons to the dorsal trajectory (Eberhart, Swartz et al. 2000; Eberhart, Swartz et al. 2002; Marquardt, Shirasaki et al. 2005). The mechanism of ephrinA-mediated growth or chemoattraction is not well understood. It is likely, however, that it involves ephrinA clustering and the tangential recruitment of other membrane proteins, possibly including Ret. EphrinAs and Ret may share downstream signaling components or even form a receptor complex that signals growth or attraction. Further genetic loss-of-function and in vitro growth/guidance experiments must be performed to test these hypotheses. It may be that LMC(l) axons are guided to the hindlimb by multiple attractive signaling pathways that direct them toward a dorsal trajectory and by repulsive signaling that repels them away from a ventral trajectory. One way to test the contribution of axonal and mesenchymal EphA4 is the specific deletion of EphA4 from the two tissues with subsequent analysis of hindlimb innervation using very sensitive techniques. The Tbx4-Cre turned out to be a very good tool to remove EphA4 (EphA4$^{lx/lx}$ allele) specifically from the hindlimb mesenchyme, without disturbing the axonal expression (Figure 40). Conversely, Nestin-Cre will be used to remove EphA4 from motor axons.

Mutants and control embryos will be intercrossed with Hb9-GFP mice to visualize all motor neurons. If both axonal EphA4 (mediating repulsion from ventral ephrinAs) and mesenchymal EphA4 (as attractive cue for axonal ephrinAs) contribute to the correct pathfinding of LMC(l) axons, a division of the already mild EphA4 hindlimb phenotype would be expected. Whole-mount neurofilament stainings do not provide enough resolution to detect such mild defects. The staining includes sensory and

motor axons, and changes in the diameter of peroneal and tibial nerves due to only one or three misguided axons would be undetectable. A very sensitive and elegant way to circumvent these problems is the backfill of motor neuron cell bodies. All axons of the ventral nerve are injured and a red dye is injected at the lesion site. The axons retrogradely transport the dye into their cell bodies, which are all located in the LMC(m) and positive for Isl1. If misguided axons have joined the ventral trajectory, they will also be labeled, but their cell bodies will be located in the fraction of the Isl1-negative LMC(l) neurons. Thus, even single misguided axons can be detected. In addition to Nes-EphA4$^{lx/lx}$ and Tbx4-EphA4$^{lx/lx}$ embryos, it is planned to additionally remove Ret from both conditional mutants to see, which of them leads to the enhanced "full" misguidance phenotype of LMC(l) axons.

4 Materials and Methods

4.1. Materials

4.1.1. Chemicals, enzymes and commercial kits

Chemicals were purchased from the companies Merck, Serva, Sigma, Fluka and Roth. All water used to prepare solutions was filtered with the "Milli-Q-Water System" (Millipore). Restrictions enzymes were purchased from Roche and New England Biolabs (NEB). Plasmid preparations, purifications or gel-extractions were done using the Qiagen Plasmid Mini/Maxi kit or PCR Purification kit, respectively. Special supplies and kits are mentioned in detail with the according method.

4.1.2. Bacteria

DH5α (Invitrogen)
TOP10 (Invitrogen)

4.1.3. Plasmids

Backbone/Insert	**Comment**	**Reference**
mammalian expression		
pcDNA3.1		
EphA4-wt	FL wt EphA4-Receptor	K. Kullander
EphA4-KD	Kinase dead EphA4-Receptor	K. Kullander
EphA4^{DSP}	EphA4-Receptor without SAM and PBM domains	K. Kullander
Ret51-wt	FL wt Ret51-Receptor	C. Ibañez
Ret51-KD	Kinase dead Ret51-Receptor	C. Ibañez

pJ7Ω

Ret9-wt	FL wt Ret9-Receptor	C. Ibañez
Ret51-M2A	Constitutively dimerized and thereby active Ret51-Receptor	C. Ibañez
Ret9-M2A	Constitutively dimerized and thereby active Ret9-Receptor	C. Ibañez
Ret9-M2A-KD	Constitutively dimerized kinase dead Ret9-Receptor	C. Ibañez

in situ probes

pBSKS

EphA4	digested XhoI; transcribed T7	F. Helmbacher
Ret	digested NotI ; transcribed T7	V. Pachnis

pBS-SK(-)

Lim1	digested EcoRI; transcribed T7	T. Fujii

pcDNA3.1

RALDH2	digested XhoI; transcribed T7	T. Jessell

4.1.4. Oligonucleotides

All small oligonucleotides were synthesized by MWG (www.mwg-biotech.com) and purified with HPSF.

Table 1 Primer

Name	Sequence
CreA	5` GCC TGC ATT ACC GGT CGA TGC AAC GA 3`
CreB	5` GTG GCA GAT GGC GCG GCA ACA CCA TT 3`
NesCreα	5` CGC TTC CGC TGG GTC ACT GTC G 3`
Cre3Nes	5` TCG TTG CAT CGA CCG GTA ATG CAG GC 3`
Rosa1	5` AAA GTC GCT CTG AGT TGT TAT 3`
Rosa2	5` GCG AAG AGT TTG TCC TCA ACC 3`
Rosa3	5` GGA GCG GGA GAA ATG GAT ATG 3`
lacZ-F	5` CCA GCT GGC GTA ATA GCG AA 3`
lacZ-R	5` CGC CCG TTG CAC CAC AGA TG 3`
Retgeno5	5` CCA ACA GTA GCC TCT GTG TAA CCC C 3`
Retgeno7	5` GCA GTC TCT CCA TGG ACA TGG TAG 3`
Retgeno6	5` CGA GTA GAG AAT GGA CTG CCA TCT CCC 3`
Ret3E	5` ATG AGC CTA TGG GGG GGT GGG CAC 3`
tauB1	5` CTG GCG GAG GGA ATA AAA AGA T 3`
tauB2	5` GCT GGC GAA AGG GGG ATG TGC T 3`
A4 WT-F	5` CAATCCGCTGGATCTAAGTGCCTGTTAGC 3`
A4WT-R	5` ACCGTTGCAAATCTAGCCAGT 3`
GFP-F	5` GCA CGA CTT CTT CAA GTC CGC CAT 3`
GFP-R	5` GCG GAT CTT GAA GTT CAC CTT GAT 3`

4.1.5. Cell lines

HeLa: Human epithelial adenocarcinoma cell line purchased from ATCC. For more information see www.atcc.org.
SK-N-BE2: Human neuroblastoma cell line from Cellzome (www.cellzome.com).

4.1.6. Media

4.1.6.1. Media and antibiotics for bacterial culture

Luria-Bertani (LB) medium

Bacto-Tryptone	10g
Bacto-Yeast extract	5g
NaCl	5g

Distilled water added to mark 1l. The pH was 7.5. Solution was sterilized by autoclaving and stored at RT.

LB plates

LB media	1l
Bacto-Agar	15g

Autoclavde and stored at 4°C.

Antibiotics (1000x stocks)

Ampicillin	100mg/ml
Kanamycin monosulfate	50mg/ml

4.1.6.2. Media and supplements for cell lines

Hela: DMEM, 10% FBS (1% FBS for starving medium), 1% Glutamine, 1% pen/strep

SK-N-BE2: OptiMEM with Glutamax, 10% ISCS (1%ISCS for starving medium), 1%pen/strep

4.1.6.3. Media and reagents for primary cell culture

Culture of dissociated mouse motor neurons

Medium M: L15 complete medium without bicarbonate (100 ml)

L15 medium	90 ml
Glucose	5 ml
Penicillin-streptomycin	1 ml
N2 100X	1 ml
Conalbumin	1 ml
Horse serum	2 ml

After preparation pH was corrected to red-orange colour using dry ice, sterile filtered (0.22 μm), and stored for up to one month at 4°C.

L15 medium with bicarbonate (250 ml)

L15 medium	244 ml
NaHCO3 7.5 % (Gibco)	6.25 ml

This medium was used to coat the wells.

Complete Neurobasal medium; prepared freshly (50ml)

NeuroBasal™ (Gibco)	47.5 ml
Glutamine	125 μl
Glutamate	50 μl
β-Mercaptoethanol	50 μl
Horse serum	500 μl
B27 supplement	500 μl

BSA 4% (w/v) in L15:

BSA 20g

BSA was dissolved in 500 ml of L15 medium. The BSA solution was first dialysed against PBS using Spectra/Por membranes (MWCO: 25 000, reference: 132 127, from Spectrum) o/n. The membranes were rinsed thoroughly with distilled water before use and dialysed against L15 medium for 2-3 days. The solution was then filtered and aliquoted (10 ml) and stored at -20°C.

Dnase I 1 mg/ml in L15; 500 μl aliquots; store at -20°C. A fresh aliquot was always used.

Glucose 72 mg/ml in L15 (filter); 20 ml aliquots; stored at -20°C.

Horse serum 2 ml aliquots; stored at -20°C, and kept at 4°C for no longer than a month.

L15 medium 500 ml bottles; stored at 4°C.

Laminin 1.5 mg/ml in PBS (500X) 50 µl aliquots; stored at -80°C.

Penicillin-streptomycin (5000 µg/ml) 5 ml aliquots; store at -20°C.

Poly-D,L-ornithine 3mg/ml 50 µl aliquots; stored at -20°C. A fresh aliquot was always used.

Trypsin (2.5%w/v) 50 µl aliquots; stored at -20°C.

L-Glutamine 70 µl aliquots; stored at -20°C.

Conalbumin 0.01% (w/v) 100 mg were dissolved in 10ml PBS.1 ml aliquots; stored at -20°C.

B27 500 µl aliquots; store at -20°C. Thawed at 4°C.

N2 supplement 500 µl aliquots; stored at -20°C.

Glutamate 25mM in L15, 500 µl aliquots; stored at -20°C.

2-mercaptoethanol 25mM in L15 500 µl aliquots; stored at -20°C.

Optiprep solution 10 ml aliquots; stored at -20°C. 50 ml were taken from the SIGMA bottle (60% w/v of iodixanol) and mixed with 450 ml of L15 medium, aliquoted and frozen.This aliquot can be stored for up to two weeks at 4°C. The SIGMA bottle can be stored at room temperature.

Culture of mouse motor neuron explants

MN culture medium 500ml (modified from Garces et al. 2000, J. Neurosci. 20: 4992)

Neurobasal medium	450 ml
B-27 supplement	to 1x from 50x stock
L-Glutamate (Sigma-Aldrich Nr.G8415)	0.5 mM
L-Glutamine (Invitrogen Nr. 25030-024)	25 mM
Penicillin-Streptomycin	to 1x from 100x stock
(optional: FCS, e.g. Invitrogen Nr. 10270106)	2%

4.1.7. Buffers and Solutions

Solutions for cell transfection

1M CaCl2

$CaCl_2 \cdot 2H_2O$	2.94g

Distilled water was added to 20 ml. Sterilized by filtration through a 0.22µm membrane and aliquots of 5 ml were stored at -20°C.

2x BES-buffer (2xBBS)

50 mM BES	> BES	1.07 g
280 mM NaCl	> NaCl	1.6 g
1.5 mM $Na_2HPO_4 \cdot 2H_2O$	> $Na_2HPO_4 \cdot 2H_2O$	0.027 g

Dissolved in 90 ml of distilled water. The pH was adjusted with NaOH to 6.96-7.22. The optional pH changed according to differences in size and preparation of the plasmid DNA. Then the volume was adjusted to 100 ml, sterilized through a 0.22µm membrane, aliquoted and stored at -20°C.

Solutions for agarose gel electrophoresis

50x TAE

2M Tris acetate

50mM EDTA

Gel loading buffer

Glycerol	25 ml
50x TAE	1 ml
Orange G	0.1 g
H_2O	24 ml

Solutions and buffers for western blot analysis

Lysis buffer

50 mM Tris pH 7.5	> 1M Tris pH 7.5	5 ml
150 mM NaCl	> 5M NaCl	3 ml
1% Triton	> Triton x100	1 ml

Distilled water was added to mark 100 ml. Store at 4°C.

Added freshly to 30 ml:

Protease inhibitor cocktail tablet (complete)		1 tablet
500 mM NaF	> NaF	1.05 g in 50 ml H_2O
200 mM NaPPi	> NaPPi	4.461 g in 50 ml H_2O
1 mM vanadate	> 100 mM Na_3VO_4	300 µl

SDS PAGE separating gel 7.5% (10 ml)

H_2O	4.85 ml
1.5M Tris pH 8.8, 0.4% SDS	2.6 ml
30% w/v Acrylamind/bisacrylamid	2.5 ml

10% APS	50 µl
TEMED	5 µl

Always prepared fresh.

SDS PAGE stacking gel 4% (5 ml)

H_2O	3.05 ml
1.5M Tris pH 6.8, 0.4% SDS	1.3 ml
30% w/v Acrylamind/bisacrylamid	0.65 ml
10% APS	50 µl
TEMED	5 µl

6x Sample buffer for reducing conditions

12% SDS	> SDS	3.6 g
300 mM Tris-HCl, pH 6.8	> 1.5M Tris	6 ml
600 mM DTT	> DTT	2.77 g
0.6% BPB	> BPB	0.18 g
60% Glycerol	> Glycerol	18 ml

Distilled water was added to 30 ml. Stored in 0.5 ml aliquots at -20°C.

5x Electrophoresis buffer

Tris base	154.5 g
Glycine	721 g
SDS	50 g

Distilled water was added to mark 10l. Stored at RT.

Protein transfer buffer

Tris base	3.03 g
Glycine	14.4 g
MetOH	200 ml

Approximately 650 ml of distilled water were added. Mixed to dissolve and made up to a final volume of 1l. Stored at 4°C.

Sodium phosphate buffer, pH 7.2

1M Na_2HPO_4	60.5 g
1M NaH_2PO_4	31.6 g
2% SDS	

Distilled water was added to mark 1l. Stored at RT.

PBS-Tween (PBST)

1x PBS

0.1% Tween®20

Stored at RT.

Blocking solution

5% BSA > BSA 2.5 g in 50 ml PBST

For blocking of first antibodies 0.05% NaN_3 was added.

Stripping buffer

5 mM Sodium Phosphate buffer, pH 7-7.4

2 mM β-Mercaptoethanol

2% SDS

Always prepared freshly for use.

Solutions for embedding of vibratome sections

0.1M Acetate buffer, pH 6.5

1M Sodium acetate 99 ml

1M Acetic acid 960 µl

pH adjusted and made up to a final volume of 1l. Stored at RT.

Embedding solution

1) Ovalbumin (Sigma, #A-S253) 90 g

0.1M Acetate buffer 200 ml

Albumine was dissolved in acetate buffer (needed stirring o/n) at RT. Then the solution was filtered through a gaze and undissolved albumin or air bubbles were removed.

2) Gelatine 1.5 g

0.1M Acetate buffer 100 ml

Gelatine was heated up in acetate buffer to dissolved. The solution was cooled down to RT and 1) and 2) were mixed without producing bubbles. Aliquots of 11 ml were made and stored at -20°C.

Solutions for in situ hybridisation

Proteinase K, 20mg/ml (w/v)

Proteinase K 100mg

H_2O	5 ml

50µl aliquots stored at -20°C

Formamide deio

Resin (#142-6425, BioRad)	25 g
Formamide	500ml

Stired for 45 min, filtered and stored (50ml aliquots) at -20°C.

Heparin solution, 50mg/ml (w/v)

Heparin	500mg
H_2O	10 ml

Stored in 500µl aliquots at -20°C.

4M $LiCl_2$

$LiCl_2$	169.56g
H_2O	1l

5% Chaps (w/v) 1g

Chaps (SIGMA C-3023)	0.25 g
distilled H_2O	5 ml

Always freshly prepared for use.

0.5M EDTA, pH 8.0

$Na_2EDTA{\cdot}2H_2O$	186.1g
H_2O	700ml

Adjusted pH with 10N NaOH (~50ml) to 8.0 and made up to a final volume of 1l.

20x SSC, pH4.5

Sodium Citrate	69.2g
Citric Acid	13.7g
NaCl	175g

Adjusted pH to 4.5, made up a final volume of 1l and stored at RT.

Prehybridisation solution

50% Formamide deio

0.2% Tween 20

0.5% Chaps

5mM EDTA pH 8.0

50µg/ml Heparin

50µg/ml t-RNA (SIGMA R-5636; Lot 082K9135)

5x SSC pH4.5

0.2% Blocking Reagent

Distilled water was added to mark 50 ml, dissolved with rocking at 70°C and stored at -20°C.

Solution I

50% Formamide deio

5x SSC pH4.5

0.2% Tween 20

0.5% Chaps

Distilled water was added to mark 50 ml. Always prepared fresh.

Solution II

50% Formamide deio

2x SSC pH4.5

0.2% Tween 20

0.1% Chaps

A final volume of 50 ml was made and always prepared fresh.

Solution III

2x SSC pH4.5

0.2% Tween 20

0.1% Chaps

Distilled water was added to mark 50 ml and always prepared fresh.

5x Maleic acid buffer (MAB)

Maleic acid	58g
NaCl	44g

Adjusted pH to 7.5: using 25-30 g NaOH pellets and then 5N NaOH. Made up a final volume of 1l and stored at 4°C.

MAB-Tween

1x MAB

0.1% Tween®20

Stored at RT.

Blocking solution (w/v)

1x MABT

0.2% Blocking Reagent (#1096 176, Roche)

Blocking reagent was dissolved while rocking at 70° (took 4-5 h) and kept on ice. Always prepared fresh.

NTMT (200 ml)

5M NaCl	4ml
1M Tris-HCl (pH 9.5)	20ml
1M Mg Cl_2	10ml
Tween®20	200µl

Developing solution (10ml)

BCIP	11 µl
NBT	14 µl
NTMT	10 ml

Solutions for lacZ stainings

1M MgCl2

MgCl2	50.83 g
H2O	250 ml

Solution A

0.2% Glutaraldehyde (25%)

5mM EGTA, pH 7.3

2mM MgCl2 (1M)

Mixed in Sodium phosphate buffer and adjusted to pH 7.2. Always prepared fresh.

Solution B

2mM MgCl2 (1M)

0.02% Nonidet-P40

Mixed in Sodium phosphate buffer.

Solution C

1mg/ml x-Gal (#1161, Bio Vectra)

4mM Potassium ferrocyanide

4mM Potassium ferricyanide

Dissolved in solution B and preserved from light. Stored at 4°C for not longer than 2 weeks.

BABB 100%

1 part Benzyl alcohol

2 parts Benzyl benzoate

Preserved from light and stored at RT.

BABB 50%

50% BABB

50% MetOH

Preserved from light and stored at RT.

Solutions for antibody stainings

Blocking solution

0.2% Gelatine

0.5% Tritonx100

50% NCS

in PBS.

PGT and TGT buffer

0.2% Gelatine

0.5% Tritonx100

in PBS or TBS, respectively.

Gelvatol mounting medium

20 g Airvol (Air products chemicals)

80 ml H_2O

40 ml glycerol

Optional: 3.37 g DABCO for anti fading property

Airvol was dissolved in water by stirring 24 h at RT. Glycerol was added and continued stirring for 24 h. Undissolved Airvol was removed by centrifugation for 30 min at 12000rpm. DABCO was added if medium needed to be anti fading, otherwise aliquoted directly in 15 ml tubes and stored at -20°C.

Solutions and reagents for MN backfills

ACSF buffer (4l)

NaCl	29.68 g
KCl	0.56 g
KH_2PO_4	0.64 g
$MgSO_4 \cdot 7H_2O$	1.28 g
$CaCl_2 \cdot 2H_2O$	1.4 g
$NaHCO_3$	8.4 g
D-glucose	7.2 g

Dissolved in the order shown above in distilled water. Made fresh and sure each compound was dissolved before adding the next one. Aerated before use with carbogen (95% O_2 and 5% CO_2) at least 15 min.

Dextrantetramethylrhodamine 3000MW, lysine fixable 20 mg/ml in PBS (Molecular Probes, #D3308)

4.1.8. Antibodies

Primary antibodies

Table 2 Primary antibodies

Antibody	Species	Company	Dilution	Appl
anti-Tubulin	mouse monoclonal	Sigma	1:10000	WB, IF
anti-phospho-Tyrosine	mouse monoclonal, clone 4G10	Upstate	1to 1000	WB
anti-EphA4 (anti-Sek)	mouse monoclonal	BD Pharmingen	1to 2000	WB
anti-EphA4	rabbit polyclonal	In house	1 to 2000 2µl	WB IP
anti-EphA4 (S20)	rabbit polyclonal	Santa Cruz	1 to 100 1 to 600	IF IHC
anti-hFC	goat polyclonal	R&D Systems	1 to 50	IF IHC
anti-GFP	rabbit polyclonal	Molecular Probes	1 to 1000	IF

anti-GFP	mouse monoclonal	Acris	1 to 200	IF
anti-Ret (H300)	rabbit polyclonal	Santa Cruz	1 to 50	IHC
anti-Ret (C19)	rabbit polyclonal	Santa Cruz	1 to 500	WB
anti-Ret (C20)	rabbit polyclonal	Santa Cruz	1 to 500	WB
anti-Gfrα–1	goat polyclonal	R&D Systems	1 to 50	IHC
anti-GDNF	goat polyclonal	R&D Systems	1 to 50	IHC
anti-Neurofilament 160	mouse monoclonal	Sigma	1 to 300	IHC

Secondary antibodies

Table 3 secondary antibodies

Antibody	Species	Company	Dilution	Appl.
anti-mouse-HRP	goat polyclonal	Jackson ImmunoResearch	1 to 500 1 to 5000	IHC WB
anti-rabbit-HRP	goat polyclonal	Jackson ImmunoResearch	1 to 5000	WB
anti-goat-HRP	rabbit polyclonal	DAKO	1 to 4000	WB
anti-mouse-Cy2	donkey polyclonal	Jackson ImmunoResearch	1 to 300	IF
anti-mouse-Cy3	donkey polyclonal	Jackson ImmunoResearch	1 to 300	IF
anti-rabbit-488	donkey polyclonal	Molecular Probes	1 to 300	IF
anti-rabbit-Cy3	donkey polyclonal	Jackson ImmunoResearch	1 to 300	IF
anti-hFc-Cy5	donkey polyclonal	Jackson ImmunoResearch	1 to 100	IF
anti-hFc-TxR	donkey polyclonal	Jackson ImmunoResearch	1 to 100	IF
Phalloidin-TxR		Invitrogen	1 to 100	IF

Phalloidin-488		Molecular Probes	1 to 100	IF
Phalloidin-634		Molecular Probes	1 to 100	IF

4.1.9. Mouse lines

$Ret^{lx/lx}$ (conditional Ret knockout) mice were generated by Edgar Kramer (Kramer, Knott et al. 2006) and maintained in a C57Bl6/J genetic background with contributions of S129/sv and CBA/J from the different Cre lines, $Lim1^{tlz}$ and $EphA4^{PLAP}$ transgenic crosses. Deleter-Cre mice were used to obtain Ret *null* mutants (Lallemand, Luria et al. 1998).

$EphA4^{lx/lx}$ mice were generated by Klas Kullander (unpublished) in collaboration with the transgenic service of the Max-Planck Institute for Neurobiology. EphA4 cDNA flanked with loxP sites was inserted into exon 3 of the ephA4 gene. Recombination using a deleter-Cre mouse line (PGK-Cre) leads to the loss of protein and PGK-$EphA4^{lx/lx}$ mice display the known EphA4 *null* phenotypes. The mice were maintained in a C57Bl6/J background.

$EphA4^{PLAP}$ (EphA4-/-) mice were generated by Philip A. Leighton with a gene trap approach (Leighton, Mitchell et al. 2001). This line was used for the analysis of the hindlimb phenotype in EphA4 single and Ret/EphA4 double knock out mutants.

$Lim1^{tlz}$ mice were generated by Artur Kania (Kania, Johnson et al. 2000). The mice were used to label LMC(l) motor axons in Ret-/- and conditional Ret mutants.

$GDNF^{-/-}$ mice were generated by Mark Moore (Moore, Klein et al. 1996) and embryos were kindly prepared and provided by Eric Dessaud. GDNF-/- embryos were used for neurofilament stainings and GDNF+/- embryos were used to follow GDNF expression by staining for the transgenic lacZ activity.

Hb9-GFP mice were generated by Hynek Wichterle (Wichterle, Lieberam et al. 2002) and received from the Jackson Laboratory. For more information see www.jax.org. These mice were used to visualize all motor neurons.

ROSA26R mice were generated by Philippe Soriano (Soriano 1999). This Cre reporter line was maintained in a C57Bl6/J background and used to monitor different Cre lines used in this study.

PGK-Cre mice were generated by Yvan Lallemand (Lallemand, Luria et al. 1998). The mice were kept heterozygous on a C57Bl6/J background and used to obtain Ret *null* mutants.

Nes-Cre mice were generated by Lyle Zimmerman (Zimmerman, Parr et al. 1994; Tronche, Kellendonk et al. 1999) and maintained heterozygous on a C57Bl6/J background. These mice were used to remove Ret or EphA4 specifically from the nervous system. For experiments, one parent of the intercross was chosen from a Cre free pedigree.

Hb9-Cre mice were generated by Xia Yang (Arber, Han et al. 1999; Yang, Arber et al. 2001) and received from Silvia Arber. These mice were used to remove Ret specifically from motor neurons.

Tbx4-Cre mice were generated and kindly provided by Artur Kania (unpublished). This Cre is expressed in the developing hindlimb mesenchyme (Khan, Linkhart et al. 2002) and was used to remove EphA4 selectively from hindlimb mesenchyme.

4.2. Methods

4.2.1. Molecular Biology

4.2.1.1. Preparation of plasmid DNA

Plasmid DNA was purified from small-scale (5ml, minipreparation) or from large-scale (200ml, maxipreparation) bacterial cultures. Single colonies of transformed bacteria were picked into LB medium containing 100µg/ml ampicillin or kanamycin and grown o/n shacking at 37°C. Harvesting and purification of Mini- and Maxipreparation was carried out according to Qiagen protocol, using Qiagen buffers. The DNA concentration was measured in a UV spectrometer at 260nm.

4.2.1.2. Generation and labeling of in situ probes

Digoxigenin-labeled RNA in situ probes were generated from plasmids containing RNA polymerase sites upstream and downstream of cDNA coding for the gene of interest. 10 µg of plasmid DNA was digested (3h to o/n at 37°C) with restriction enzymes cutting downstream (for sense probe) or upstream (for antisense probe) to linearize the plasmid. Following purification of the linearized DNA using Qiagen PCR purification kit, 2 µl of the DNA was incubated with 2 µl transcription buffer (Roche, *in situ* probe labeling kit), 2 µl of 0.1M DTT, 2 µl digoxigenin-conjugated dNTP`s, 1 µl RNAse inhibitor, and 1 µl of the specific RNA polymerase in a total volume of 20 µl for 3h at 37°C. To precipitate short RNAs, 10 µl LiCl (4m), 100 µl TE and 300 µl of EtOH were added to the mix and incubated for 30 min. at -20°. Subsequently, the mix was centrifuged for 20 min. at 4°C. The pellet was washed with 70% EtOH and dried on ice. After resuspending in 100 µl TE, aliquots were stored at -80°C. For hybridisation 10 -12 µl was used per ml of hybridisation buffer.

4.2.1.3. Preparation of competent E.coli

1 l of LB medium was inoculated with 1:100 from an over night culture of Dh5α cells. The bacteria were grown with vigorous shaking at 37°C until the OD reached 0.5 – 0.8 at 600nm. The flask containing the bacteria was chilled on ice for 30 min. followed by 15 min. centrifugation at 4000xg in a chilled centrifuge. The pellet was resuspended in 1l of cold water and centrifuged again. This step was repeated with 0.5l water. Subsequently, the pellet was resuspended in 20 ml of 10% glycerol and centrifuged as above. Finally, the bacteria were resuspended in 3 ml of 10% glycerol. Aliquots of 50 µl were frozen in liquid nitrogen and stored at -80°C.

4.2.1.4. Transformation of competent E.coli by electroporation

50 µl of competent bacteria was thawed on ice and 0.2-2 µl of plasmid DNA was added. The mix was transferred into a sterile, pre-chilled 0.2 cm cuvette without making bubbles. The gene pulser apparatus was set to 25 µF and 2.5 kV; the pulse controller to 200 Ω. After drying the cuvette it was placed into the chamber slide and pulsed once. Immediately, 150 µl of LB medium was added to the cells, which were then transferred to a reaction tube and shaken for 15 to 60 min. The bacteria were then plated on LB plates containing the appropriate antibiotics and grown o/n at 37°C.

4.2.1.5. TOPO cloning

Specific primers were used to amplify exon 12 from the Ret gene by PCR using PFU Turbo DNA polymerase (Invitrogen) and cloned into the pCRIITOPO vector according to the Invitrogen TOPO TA Cloning manual. Briefly, the TOPO mix contained 4 µl linearized DNA (PCR product), 1 µl 1:4 diluted salt solution and 1 µl TOPO vector. Following incubation at RT for 15 min. the mix was transformed into Dh5α cells.

Primer

Retseqex12	5` GTA CTG CCA CTC CCT GTC CAA G 3`
Retex12BglIIB	5` GTA TCT TCT ACT AGA TCT AGG TCC TCA C 3`

PCR program

1 = 94°C; 1 min
2 = 94°C; 1 min
3 = 60°C; 30 sec
4 = 72°C; 1 min
5 = Goto 2; 10 times
6 = 94°C; 1 min
7 = 60°C; 30 sec
8 = 68°C; 1 min + 5 sec /cycle
9 = Goto 6; 20 times
10 = 72°C; 7 min
11 = 10°C; for ever
12 = end

4.2.1.6. Tail DNA preparation and genotyping using PCR

PCR analysis was used to determine the genotype of mice and embryos. Tail biopsies (1-3 mm) were taken from mice at weaning age (~ 3 weeks). For genotyping embryos, the yolk sacks were collected and washed with PBS. The biopsies were incubated at 95°C three times for 20 min in 100 µl 25mM NaOH/ 0.2mM EDTA (pH 12) and vortexed thoroughly between heating steps. Once the samples were well digested, the remaining debris was pelleted and the mix neutralized with the addition of 100 µl 40mM Tris-HCl (pH 5) and stored at 4°C. 1 µl of DNA was used as template in the PCR reaction. The PCR was carried out in a total volume of 50 µl and contained 2.5 mM dNTPs, 50mM specific primers to amplify a sequence of genomic DNA specific for a given allele, 1x PCR buffer (NEB) and 0.5 µl of Taq polymerase (NEB).

Agarose gel electrophoresis was used to separate PCR products. For a large 2% gel, 6 g of agarose (Biomol, # 9012-36-6) was dissolved in 300 ml TAE by heating in the microwave and frequent shaking. When the agarose solution was cooled to the touch, 15 µl of ethidium bromide (Roth, #2218.2) was added to and poured into a gel chamber containing combs. Once the gel had solidified the combs were removed and the gel submerged in 1x TAE in an electrophoresis chamber. PCR products, RNA probes or products of enzymatic digestions were loaded into the wells together with gel loading buffer (10:1) and separated according to their size for 20- 40 min at ~ 200V. DNA was visualized under UV light using a gel documenting system (BioRad).

4.2.2. Cell culture

4.2.2.1. Propagation and freezing of mammalian cells

Cells were grown at 37°C with 5% CO_2 in growth medium on 100 mm cell culture dishes (Falcon). Confluent plates were washed with warm PBS, incubated with 1 ml Trypsine/EDTA (Invitrogen) for ~ 2 min and then gently resuspended with new medium. Cells were usually seeded in a 1:10 ratio.
HeLa cells were frozen in 10%DMSO and 90% FBS SK-N-BE2 cells were frozen in 10% DMSO and 90% iron supplemented calf serum. The cells were kept in the -80 freezer o/n and were then transferred to the liquid nitrogen tank. To recover cells from the liquid nitrogen tank, they were thawed quickly in growth medium, pelleted, resuspended in growth medium and seeded.

4.2.2.2. Transfection of cell lines using calcium phosphate precipitation

Transient transfection of cells was done using calcium phosphate precipitation. All solutions were pre-warmed to RT and plasmid DNA was mixed well and centrifuged briefly. Confluent plates of cells were split 1:10 on the evening before transfection. For each 100 mm dish, 5-8 μg of plasmid DNA (= x) were mixed with water (601.7 - x μl) and 85.8 μl $Ca0Cl_2$ (1M). 678.5 μl BBS (2x) was added and thoroughly vortexed for 10 sec. The reaction was incubated for 20 min at RT to allow precipitation and then gently applied to the cells. 12 – 16h after transfection, the medium was replaced with fresh growth medium several times (until precipitates were gone). Transfection efficiency was estimated by co-expressing GFP in each plate and checking the amount of fluorescent cells under the microscope.

4.2.2.3. Primary culture of dissociated mouse motor neurons

Coating: CVSs were treated with nitric acid for 24-36 hrs in order to smooth the surface. This was followed by extensive washing with water (two days). They were dried on a sheet of Whatman paper and baked o/n at 175°C. Time lapse chambers (nunc, #155380) or wells of 4 well plates (Nunc, #176740), containing CVSs, were coated under sterile conditions with poly-ornithin (diluted 1:1000 in water from stock) for 30 min at RT, air dried for another 30 min and covered with L15 medium

(+ bicarbonate) containing 5 µg/ml laminin. The CVSs were kept in the incubator at 37°C and 7.5% CO_2 at least 3 hrs before seeding the neurons.

Spinal cord open book preparation (see Figure 44) Embryos of embryonic day E12.5 were dissected in ice cold PBS and Hb9-GFP positive mutants were collected in Hibernate medium (www.siumed.edu) containing B27 (1:500) on ice. To obtain the whole spinal cord without DRGs and meninges, the embryos were decapitated. Then the spinal cord was opened along its whole length on the dorsal side and removed in one piece with a fast movement (similar to peeling a banana) using fine forceps. For one tube five – six spinal cords were pooled in HBSS and chopped in very small pieces of similar size.

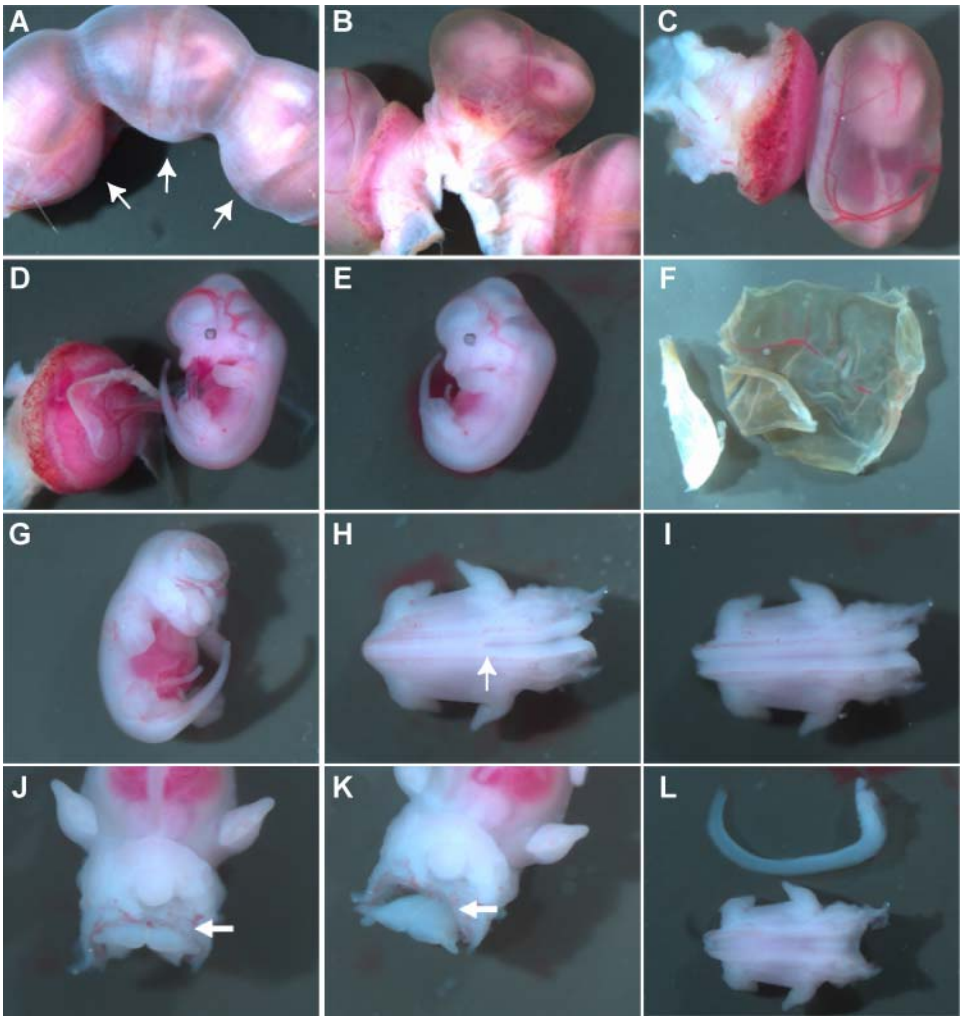

Figure 44 12.5 Spinal cord (SC) open book preparation

Panel (A) shows three embryos inside the uterus (arrows). (B) Uterus was removed and embryos with intact yolk sacs were separated (C). (D-F) Embryos were detached from the placenta and the yolk sac was retained for genotyping. (G-I) To isolate the SC, embryos were decapitated and turned onto the front side. Then the SC was carefully opened (arrow in H) with fine forceps along its whole length. (J-L) The remaining hindbrain was detached from the the meninges (arrows in J and K). Finally, the SC was removed by quickly pulling of the embryo while holding down the SC on the hindbrain area.

Purification: The spinal cord pieces were transferred from HBSS into 1 ml of HAM-F10 with a blue tip. The medium was replaced with 1 ml of fresh HAM-F10. 10 µl of trypsin (2.5% w/v) was added and the mix was incubated at 37°C for 10 min with frequent shaking. In the meantime, for each tube of cells with trypsin, a mix of 0.8 ml L15 complete medium without bicarbonate (medium M) + 100 µl BSA (4% w/v in L15) + 100 µl DNase (1 mg/ml in L15) and another 15 ml empty tube (transparent) = tube B was prepared.

Next, the medium was removed with a blue tip with the cells remaining in a pellet on the bottom of the tube. 1 ml of the fresh prepared L15 with BSA and DNase was added to the pellet and agitated vigorously until the tissue fragments were dissociated. The tissue fragments were triturated twice (gently) with a blue tip and then allowed to settle for two min. The supernatant was collected without taking any fragment from the bottom of the tube and transferred into the empty tube B. To each tube containing the residual fragments 0.9 ml of L15 complete medium without bicarbonate + 100 µl of BSA (4% w/v) + 20 µl of DNase (1 mg/ml in L15 medium) was added and triturated eight times with a blue tip. After two min, the supernatant was again collected and transferred to tube B. The procedure was repeated once more, if there were still tissue fragments remaining.

A 1.5 - 2 ml BSA (4% w/v) cushion was dispensed to the bottom of each tube containing the pooled supernatants using a long Pasteur pipette. The dissociated cells were pelleted by centrifugation for 5 min at 1500 rpm and resuspended 4 times with a blue tip in 1 ml medium M. Then 5 ml medium M was added and 2 ml Optiprep solution (final 6% w/v in L15) was gently added to the bottom of the tube using a long Pasteur pipette, creating a sharp interface between the two solutions.

The tube was centrifuged for 15 min at 2200 rpm (830 g) at room temperature. To reduce the vibration the brakes were switched off. After centrifugation the large motor neurons could be detected as a turbid band at the inter phase and were collected with a blue tip in 10 ml of medium M. The motor neurons were pelleted (always with a BSA cushion) for 5 min at 1500 rpm and resuspended in 4 ml of medium M. After the second washing step, the MNs were resuspended in 0.5 ml NB complete medium. The amount of neurons was counted on a Malassez slide and then multiplied by 1000 to give the noumber of cells per ml. Approximately 3000 neurons were seeded per CVS. Three growth factors were added to the NB complete medium for the seeding wells: BDNF (1 ng/ml), CNTF (10ng/ml) and GDNF (1 ng/ml).

4.2.2.4. Explant culture of mouse motor neurons

Coating of CVSs: Time lapse chambers or commercial (poly-D-lysine) pre-coated cover slips (BD, # 354086) were coated under sterile conditions with 50 µg/ml laminin. A drop of 30 – 40 µl laminin suspension was added to the surface of one CVS, which was then covered with a second CVS creating a uniform film of laminin suspension at the interface. The CVS "sandwiches" were incubated in a closed Petri dish for four -seven hrs at 37°C or alternatively o/n at 4°C. After incubation, CVSs were soaked in a drop of culture medium. The top CVS was removed, any excess laminin was washed away by repeatedly dipping into medium and placed coated face up into a well of a sterile tissue culture 24 well plate.

Dissection of motor column explants: The spinal cord was dissected in ice cold MN culture medium as described for dissociated motor neuron cultures (see also Figure 44). The whole spinal cords were collected in ice cold MN medium and then pinned down (ventral side facing up) with minuiten pines (FST, # 26002-10) in a silicon Petri dish (SYLGARD kit, # SYLG184). The excision of the LMC(l) was performed under a fluorescent stereomicroscope to visualize Hb9-GFP positive cells within the spinal cord (Figure 45). MNs were clearly visible as dense rostro-caudal columns. 2-3 mm cutting edge spring scissors were used to cut along the edge of the desired motor column. The excised column was then trimmed with a needle blade into small pieces. Three - six explants were seeded onto coated cover slips and incubated at 37°C and 5% CO_2.

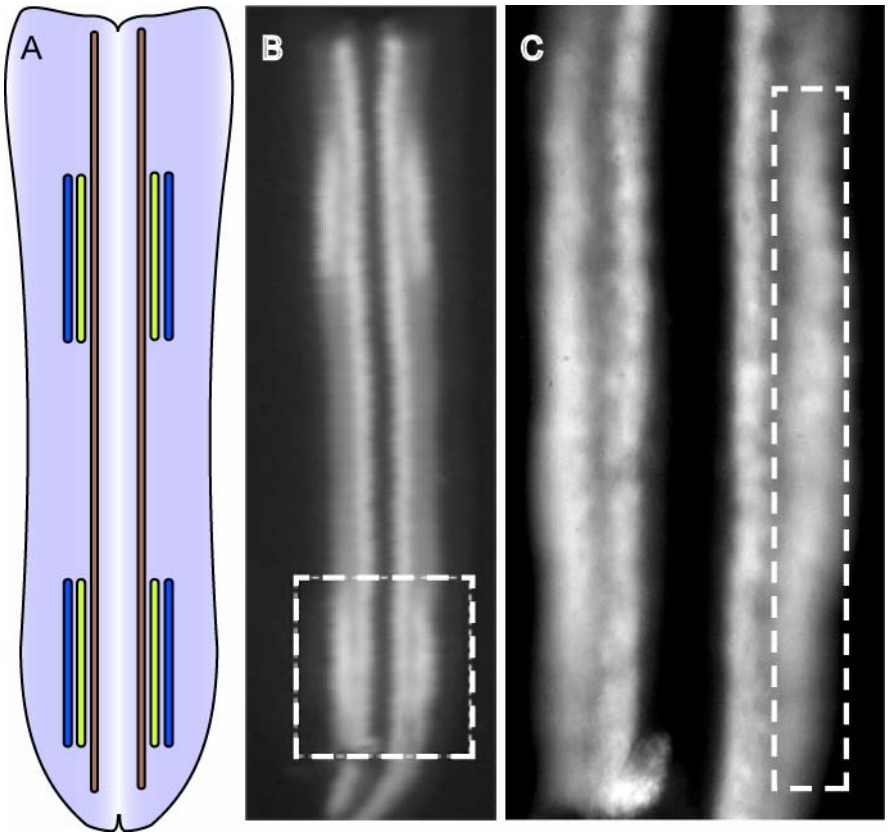

Figure 45 Excision of LMC(l)

Panel (A) shows a schematic representation of the spinal cord open book preparation. Lateral LMC is depicted in blue, medial LMC in green and MMC in brown columns. Top is rostral. (B) Open book preparation of an Hb9-GFP positive spinal cord. The boxed area in the lumbar region of the SC is enlarged in (C). Dashed box in (C) outlines roughly the area of the whole LMC, which can be cut out and dissected into several small explants.

4.2.2.5. Stimulation of cells and cultures with ephrin ligands and GDNF

Activation of Eph-receptors was induced with clustered multimeric ephrin ligands. Ephrin-Fc fusion proteins (R&D) Fc fragment as control were multimerized for 1 h at RT using 1:10 w/v anti-human Fc diluted in PBS. Pre-clustered ephrin-Fc was used at a concentration of 1 μg/ml.

Ret-receptors are endogenously expressed together with Gfrα 1 in SK-N-BE2 cells or motor neurons and were stimulated with 50 ng/ml GDNF. For HeLa cells transiently expressing Ret but not the co-receptor, Gfrα 1 was applied in a soluble form along with GDNF at a concentration of 50 ng/ml.

4.2.2.6. Time lapse imaging

Live-cell imaging of dissociated motor neurons or MN explants was performed using a Zeiss Axiovert 200M microscope equipped with a temperature controlled CO_2-incubation chamber. Temperature and humidity was set to 37°C and 5% CO_2, respectively. Phase contrast mages were acquired using a 40x oil immersion objective with a CoolSNAP-fx camera at a rate of one frame per minute. Images were processed using MetaMorph software (Visitron, Germany).

4.2.3. Biochemistry

4.2.3.1. Cell lysis and immunoprecipitation of proteins

Lysis: Previously transfected cells grown in 100 mm dishes were placed on ice, washed twice with 10 ml cold PBS and incubated on ice with 800 µl lysis buffer. After a 20 min incubation, cells were harvested using a blue tip, and transferred into a reaction tube and further lysed at 4°C on a rotating wheel for 30 min. Insoluble material was removed by centrifugation for 15 min at 13000rpm at 4°C. Spinal cords or other tissues were lysed in 3x volume to weight. Protein concentration was measured using the DC Protein Assay (BioRad) Supernatants were frozen in liquid nitrogen and stored at -80°C or used immediately.

Immunoprecipitation: Equal amount of protein from different TCLs were each incubated in a final volume of 1 ml with 2 µl of a specific antibody directed against the protein of interest. The samples were left on a rotating wheel at 4°C for two hours. 80 µl Protein-A coupled sepharose beads was added to each tube and incubated on the rotating wheel for another hour. The supernatants were discarded and the beads were washed three times with lysis buffer to remove uncoupled proteins from the lysate. 7 µl of 6x SDS sample buffer was added to the pelleted beads and the samples denatured by boiling at 95°C for 3 min before loading on a polyacrylamide-gel.

4.2.3.2. Immunoblotting

Protein samples obtained as described above were separated by SDS-PAGE on a 7.5% gel and transferred to a PVDF membrane (Amersham, # RPN303F) by semi-dry blotting (1 mA per cm^2 for 1 h). PVDF membranes were washed briefly with water, and incubated with blocking solution (5% BSA in PBST) for at least 30 min. Primary antibody was applied in blocking solution o/n at 4°C while rocking on a shaker. The membrane was washed 6 x 5 min with PBST before incubation with the secondary antibody for 1 h at RT. After 3 x 10 min PBST washes, the membrane was incubated with 1 ml of ECL solution (Santa Cruz) and exposed to X-ray films (Kodak, Biomax) to visualize the signal. If subsequent detection of another protein was necessary the membrane was incubated with stripping buffer for 30 min at 65°C and re-blotted as described above.

4.2.4. Mouse work

Mutant and control mice were maintained on a C57Bl6/J genetic background. Tail biopsies were taken to determine the genotype and mice were ear-tagged using 4-digit number ear tags (Hauptner und Herberholz). For experiments with embryos, breedings were set up with one male and two females. Vaginal plug checks were done starting the next morning after the start of the breeding. The presence plug was counted as day 0.5 of pregnancy. Embryos were dissected as described elsewhere in the methods section at day E11.5 – E13.5. Neuronal cultures of Hb9-GFP embryos were prepared from CD1 females, because of their higher number of embryos per litter. Except for Hb9-GFP mutants, which could be selected by fluorescence, yolk sac material was used to determine the genotype of embryos.

4.2.5. Histology

4.2.5.1. Vibratome sections

The caudal part of fixed E11.5 or E12.5 embryos including the hind legs was embedded in a gelatine-albumine (gel-alb) mixture in a small plastic chamber (Roth). 1 ml of gel-alb mix was polymerized with 50 µl of 25 % Glutaraldehyde. The embryo was placed on an ex ante prepared thin layer of gel-alb with the tail facing up. The embryo bud was dried thoroughly before gently pouring enough polymerizing gelatin-albumin mixture to cover the sample. After 5 min at RT the block was submersed in PBS and left at 4°C for 1 h to ensure complete polymerization. The gel-alb block was trimmed and glued to the vibratome platform and placed into the vibratome chamber filled with cold PBS. Razor blades (Wilkinson) were washed with acetone in order to remove the oil. 40-80 µm sections were cut at low speed and high vibration frequency. Vibratome sections were used for in situ hybridizations, antibody and lacZ stainings.

4.2.5.2. Cryostat sections

The caudal area of PFA fixed embryos was oriented as described for vibratome sections on a thin layer of OCT embedding medium (Tissue Tek). More OCT medium was poured on top and stored on ice for several hours to harden the medium. Sections were cut on a Leica Cryotome with chamber and object temperature between -16 to -20°C. Sections were either collected into PBS for staining of floating sections or collected on a coated glass slides (Menzel-Gläser, #J1800AMNZ). If processed later, sections were stored at -20°C.

4.2.5.3. Antibody staining

4.2.5.3.1. Whole mount Neurofilament staining

For whole mount anti-neurofilament stainings, embryos of embryonic day 11.5 or 12.5 were collected and fixed overnight in Dent's solution (1 part DMSO; 4 parts methanol) and genotyped from yolk sac DNA. The embryos were bleached in one part 30% H_2O_2, two parts Dent's Solution for several hours to o/n at RT. Three

washing steps (one hour each at RT) in PBS containing 0.2% Gelatin and 1% Triton X-100 (SIGMA) were followed by incubation with the primary antibody (mouse anti-NF160) overnight at RT. The antibody was diluted 1:300 in Blocking Serum (100ml NCS + 25 ml DMSO). After washing five times in TBS containing 1% Triton X-100 and 0.2% gelatin for one hour each, the embryos were incubated with the secondary antibody (anti-mouse-HRP) o/n at RT. The antibody was diluted 1:500 in Blocking Serum. Finally, embryos were washed and developed in diaminobenzidine (DAB) working solution. To obtain good pictures, embryos were cleared by going through 30 min incubations steps in 50% MetOH, 100% MetOH, 50% BABB and finally 100% BABB.

4.2.5.3.2. Staining of tissue sections

For immunostaining of mouse sections, embryos were collected and fixed for 1-2 h in 4% PFA and vibratome sectioned (40µm). To inactivate endogenous peroxidase, sections were dehydrated in MetOH, incubated in MetOH at -20°C for 2hrs and rehydrated including a step with 6% H_2O_2 treatment. Following three washes with PGT (PBS with 0.2% gelatine and 0.5% Triton) nonspecific antibody protein binding was blocked in 50% Serum in PGT for 1 h at RT. Primary antibodies were diluted in blocking solution and incubated at 4°C o/n. After several washing steps (2 x for 5 min followed by 2 x for 2 hrs), the slices were incubated with a biotinylated secondary antibody. The sections were finally stained using either a Tyramide Signal Amplification (TSA, NEN Life Sciences) or the Vectastain ABC Kit (Vector Laboratories) with horseradish peroxidase (HRP) or alkaline phosphatase (AP) as enzymes. Sections were mounted on slides, dried at RT and covered with Gelvatol Mounting medium and sealed with a square glass CVS.

4.2.5.3.3. Labeling of explant cultures and dissociated motor neurons

For fixation, a solution of 2% PFA and 15% sucrose in PBS was pre-warmed to 37°C. 500 µl pre-warmed fixant was added to each well containing 500 µl MN culture medium immediately after taking the 24 well dish from the incubator. The sucrose provides a gradual displacement of medium by fixant at the bottom of the wells, which is important to avoid morphological stress to growth cones. Following incubation for 30-45 min at RT, the top phase of the culture well was replaced gently

with another 500 ml of warm fixant and incubated 30 min to o/n at 4°C. The explants were washed three times for 10 min with PBS and incubated with primary antibody in 1% BSA in PBST (IgG free BSA). Primary antibody incubation for 2 h at RT (e.g. for surface markers) or o/n at 4°C was followed by 3-4 washing steps 5 min each. All secondary antibodies were diluted in the same blocking solution and incubated for 1-2 h at RT. Finally, explants were washed two – three times and mounted on a small drop of vectashield mounting medium (H-1000, Vector Laboratories) on glass microscopy slides.

4.2.5.4. LacZ staining

Whole embryos (E8.5 – E12.5) or whole spinal cords of E12.5 embryos were fixed in freshly made solution A for 30 min on ice and then washed 3 times 10 min each in solution B. Spinal cords and embryos were either incubated directly in solution C for staining or embedded in gelatin/albumin and vibratome sectioned into 40-60 μm thick slices before incubation in solution C. Staining was developed at RT or 37°C in the dark for 1 h, or o/n . Once the staining was complete, the samples were washed 3 times 5 min in solution B and eventually postfixed in 4% PFA. Clearing, as described in the neurofilament staining procedure was used for whole embryos. Spinal cords were mounted on glass object slides by using little plasticine feet to avoid squeezing of the sample in a mixture of 1:1 glycerol and 4% PFA. Sections were mounted as described in the staining of tissue sections procedure.

4.2.5.5. AP staining

Placental alkaline phosphatase (PLAP) activity in EphA4^{PLAP} mice was detected by AP staining. PLAP positive and control embryos (E11.5) were fixed in 4% PFA for 1 h on ice, washed with PBS and stored in 30% sucrose o/n at 4°C. Following gelatine/albumine embedding and vibratome sectioning as described before, sections were incubated in PBST for 2 h at 65°C to block endogenous AP activity. Post fixation for 1 h in 4% PFA was followed by several short washes in PBST and incubated in NTMT for 20 min. Finally sections were bathed in NTMT containing BCIP and NBT to develop the staining. Sections were mounted as described previously in the methods.

4.2.5.6. In situ hybridisation

All solutions used in the dissection or hybridisation procedure of the embryos were RNAse free. Whole embryos or spinal cords were dissected in ice cold PBS and fixed in 4% PFA o/n or longer (Figure 46). The exact age of the embryos was determined by counting the somites. After 3 washes for 5 min each in PBS, embryos were embedded in gelatine/albumine and vibratome sectioned or whole spinal cords were dissected. Sections and spinal cords were dehydrated through several methanol steps (25% MetOH for 5 min, 50% MetOH for 5 min, 75% for 5 min) and stored in 100% methanol at -20°C for a minimum of 2 hrs.

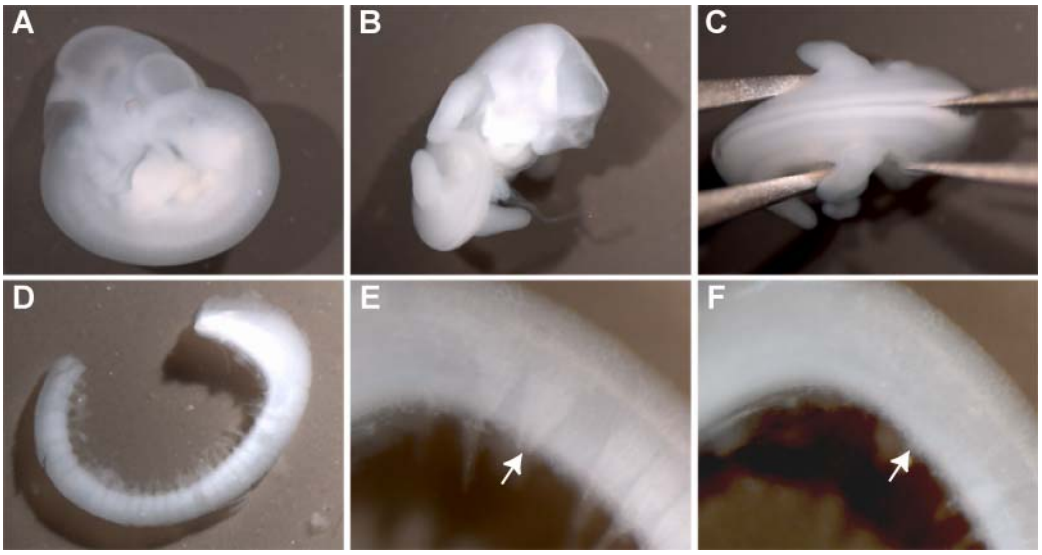

Figure 46 Dissection of E11.5 spinal cords (SC) for ISH

(A) Embryos were isolated from the uterus, yolk sacs were retained for genotyping and exact age was determined by counting the somites before proceding with disection. (B,C) Similar to the SC open book preparation at E12.5, embryos were decapitated and the SC was opened carefully using fine forceps. The SC was then separated from surrounding tissue and remaining dorsal root ganglia (arrow in E) were removed (arrow in F).

Day 1: Samples were taken from -20°C and incubated for 1 h at RT in a solution made of 80% Met-OH and 20% of a 30% H2O2 solution (makes 6% H2O2 final). Rehydration was continued in sequential methanol steps (50% MetOH for 5 min, 25% MetOH for 5 min) and sections or spinal cords were washed 3 x 5 min in PBST. To remove proteins from RNA, samples were treated with Proteinase K (20 µg/ml in PBST) at RT. Time of proteinase K treatment and subsequent post fixation with 4% PFA, 0.2% glutaraldehyde was chosen according to tissue (see table below).

Table 3 Time of Proteinase K treatment

sample	proteinase K treatment	time of post fixation
Vibratome sections (80 µm)	13 min	40 min
40-45 somite SC	20 min	1 h
48-55 somite SC	28 min	1.5 h
E12.5 SC	35 min	2 h
E11.5 embryos	45 min	2 h
E12.5 embryos	1 h	2.5 h

Samples were rinsed twice in PBST and transferred to prehybridisation solution for 1 h at 70°C with gentle rocking. Dig-labeled RNA probes were diluted in hybridisation solution (see probe labeling section), pre-heated to 70°C and incubated with the samples o/n at 70°C.

Day 2: Blocking reagent was dissolved in MABT at 70°C for several hours. Samples were washed 3 times in solution I at 70°C, followed by three 1 h wash steps in solution II at 66°C and three further 1 h washing steps in solution III at 68°C. After washing 3 times for 5 min in MABT at RT and twice for 30 min at 70°C to avoid background staining, samples were incubated with blocking solution for 1.5 hrs at RT. To detect dig-labeled RNA, samples were incubated o/n at 4°C with an anti-dig antibody conjugated with alkaline phosphatase (AP).

Day 3: Samples were rinsed and washed with MABT at least 8-10 times for 30 min at RT before incubation in NTMT. Following equilibration in NTMT for 10-20 min

developing solution was added. After the staining was developed, samples were rinsed in PBST and post fixed in 4% PFA. Sections and spinal cords were mounted on glass object slides as described before.

4.2.5.7. MN backfills

E13.5 embryos were dissected in aerated and preheated (30°C) ACSF at RT in a silicon Petri dish. To allow adequate diffusion of ACSF to muscle and neuronal tissues, embryos were eviscerated. Small spring scissors (FST, #15000-08) were used to open the embryo on the ventral side while pinned down lying on the back. All inner organs were gently removed using forceps and small scissors. Then embryos were fixed with the forelimbs and hindlimbs stretched to the side using minuiten pins. Damage of tissue was minimized to avoid possible labeling of other cells. A very fine glass pipette (WPI, #TW150F-6 11G S/N, pulled at heat 282) attached to short tubing and a mouth piece was filled with 8 µl rhodaminedextran. The tibial nerve of Hb9-GFP positive embryos was targeted using a fluorescent stereo microscope. The axons of the nerve were severed and a small amount of dye was injected into the ventral limb at the same time to allow the retrograde uptake into the cells of the injured axons. To allow the dye to travel to the motor neuron cell bodies, embryos were incubated in aerated ACSF at 30°C for 5 – 7 hrs in the dark. Once the retrograde labeling was complete, embryos were fixed in 4% PFA for 2 h at 4°C, washed in PBS and equilibrated in 30% sucrose o/n. Embryos were embedded and sectioned at 60 µm using a Cryostat. Sections were analyzed with a confocal microscope.

4.2.6. Quantifications

Anti-neurofilament stained embryos were grouped into three different categories depending on the strength of the phenotype:
E11.5 ***Cat I (mild):*** slightly shorter and/or scattered axons; *Cat II (intermediate):* clearly shorter and/or notably defasciculated axons; *Cat III (strong):* very short or absent and/or extremely defasciculated few axons.
E12.5 ***Cat I (mild):*** the peroneal nerve was slightly thinner and/or the fork-like branch at the distal end appeared atrophied; *Cat II (intermediate):* obvious reduction of the peroneal nerve structure in caliber and length and/or loss of the distal end-branch; **E12.5** ***Cat III (strong):*** length of the PN was reduced to at least half of the original length and distal branches were completely lost.

Quantification of the PN/TN nerve phenotype was done as follows: at E11.5, a vertical line was drawn distal to the sciatic plexus at the branch point of the tibial and peroneal nerves. The distances between this line and the distal end of each nerve were measured using the region measurement tool of the MetaMorph program (Visitron). The same tool was used to quantify the thickness of tibial and peroneal nerves at E12.5. Landmarks on both nerves were used to ensure that the measurement was performed at the same position in each embryo (see Figure 24).

5 Bibliography

(1997). "Unified nomenclature for Eph family receptors and their ligands, the ephrins. Eph Nomenclature Committee." Cell **90**(3): 403-4.

Airaksinen, M. S., A. Titievsky, et al. (1999). "GDNF family neurotrophic factor signaling: four masters, one servant?" Mol Cell Neurosci **13**(5): 313-25.

Arber, S., B. Han, et al. (1999). "Requirement for the homeobox gene Hb9 in the consolidation of motor neuron identity." Neuron **23**(4): 659-74.

Baloh, R. H., H. Enomoto, et al. (2000). "The GDNF family ligands and receptors - implications for neural development." Curr Opin Neurobiol **10**(1): 103-10.

Bergemann, A. D., L. Zhang, et al. (1998). "Ephrin-B3, a ligand for the receptor EphB3, expressed at the midline of the developing neural tube." Oncogene **16**(4): 471-80.

Brambilla, R., K. Bruckner, et al. (1996). "Similarities and differences in the way transmembrane-type ligands interact with the Elk subclass of Eph receptors." Mol Cell Neurosci **8**(2-3): 199-209.

Briscoe, J. and J. Ericson (1999). "The specification of neuronal identity by graded Sonic Hedgehog signalling." Semin Cell Dev Biol **10**(3): 353-62.

Briscoe, J., A. Pierani, et al. (2000). "A homeodomain protein code specifies progenitor cell identity and neuronal fate in the ventral neural tube." Cell **101**(4): 435-45.

Bruckner, K. and R. Klein (1998). "Signaling by Eph receptors and their ephrin ligands." Curr Opin Neurobiol **8**(3): 375-82.

Carvalho, R. F., M. Beutler, et al. (2006). "Silencing of EphA3 through a cis interaction with ephrinA5." Nat Neurosci **9**(3): 322-30.

de Graaff, E., S. Srinivas, et al. (2001). "Differential activities of the RET tyrosine kinase receptor isoforms during mammalian embryogenesis." Genes Dev **15**(18): 2433-44.

Dent, E. W. and F. B. Gertler (2003). "Cytoskeletal dynamics and transport in growth cone motility and axon guidance." Neuron **40**(2): 209-27.

Dickson, B. J. (2002). "Molecular mechanisms of axon guidance." Science **298**(5600): 1959-64.

Dottori, M., L. Hartley, et al. (1998). "EphA4 (Sek1) receptor tyrosine kinase is required for the development of the corticospinal tract." Proc Natl Acad Sci U S A **95**(22): 13248-53.

Drescher, U., C. Kremoser, et al. (1995). "In vitro guidance of retinal ganglion cell axons by RAGS, a 25 kDa tectal protein related to ligands for Eph receptor tyrosine kinases." Cell **82**(3): 359-70.

Durbec, P., C. V. Marcos-Gutierrez, et al. (1996). "GDNF signalling through the Ret receptor tyrosine kinase." Nature **381**(6585): 789-93.

Eberhart, J., J. Barr, et al. (2004). "Ephrin-A5 exerts positive or inhibitory effects on distinct subsets of EphA4-positive motor neurons." J Neurosci **24**(5): 1070-8.

Eberhart, J., M. Swartz, et al. (2000). "Expression of EphA4, ephrin-A2 and ephrin-A5 during axon outgrowth to the hindlimb indicates potential roles in pathfinding." Dev Neurosci **22**(3): 237-50.

Eberhart, J., M. E. Swartz, et al. (2002). "EphA4 constitutes a population-specific guidance cue for motor neurons." Dev Biol **247**(1): 89-101.

Egea, J., U. V. Nissen, et al. (2005). "Regulation of EphA 4 kinase activity is required for a subset of axon guidance decisions suggesting a key role for receptor clustering in Eph function." Neuron **47**(4): 515-28.

Encinas, M., M. G. Tansey, et al. (2001). "c-Src is required for glial cell line-derived neurotrophic factor (GDNF) family ligand-mediated neuronal survival via a phosphatidylinositol-3 kinase (PI-3K)-dependent pathway." J Neurosci **21**(5): 1464-72.

Enomoto, H., T. Araki, et al. (1998). "GFR alpha1-deficient mice have deficits in the enteric nervous system and kidneys." Neuron **21**(2): 317-24.

Enomoto, H., R. O. Heuckeroth, et al. (2000). "Development of cranial parasympathetic ganglia requires sequential actions of GDNF and neurturin." Development **127**(22): 4877-89.

Flanagan, J. G. and P. Vanderhaeghen (1998). "The ephrins and Eph receptors in neural development." Annu Rev Neurosci **21**: 309-45.

Gallo, G. and P. C. Letourneau (2004). "Regulation of growth cone actin filaments by guidance cues." J Neurobiol **58**(1): 92-102.

Gallo, G., H. F. Yee, Jr., et al. (2002). "Actin turnover is required to prevent axon retraction driven by endogenous actomyosin contractility." J Cell Biol **158**(7): 1219-28.

Gauthier, L. R. and S. M. Robbins (2003). "Ephrin signaling: One raft to rule them all? One raft to sort them? One raft to spread their call and in signaling bind them?" Life Sci **74**(2-3): 207-16.

George, S. E., K. Simokat, et al. (1998). "The VAB-1 Eph receptor tyrosine kinase functions in neural and epithelial morphogenesis in C. elegans." Cell **92**(5): 633-43.

Giehl, K. M. (2001). "Trophic dependencies of rodent corticospinal neurons." Rev Neurosci **12**(1): 79-94.

Golden, J. P., J. A. DeMaro, et al. (1999). "Expression of neurturin, GDNF, and GDNF family-receptor mRNA in the developing and mature mouse." Exp Neurol **158**(2): 504-28.

Goodman, C. S. (1996). "Mechanisms and molecules that control growth cone guidance." Annu Rev Neurosci **19**: 341-77.

Haase, G., E. Dessaud, et al. (2002). "GDNF acts through PEA3 to regulate cell body positioning and muscle innervation of specific motor neuron pools." Neuron **35**(5): 893-905.

Hall, A. and C. D. Nobes (2000). "Rho GTPases: molecular switches that control the organization and dynamics of the actin cytoskeleton." Philos Trans R Soc Lond B Biol Sci **355**(1399): 965-70.

Hattori, M., M. Osterfield, et al. (2000). "Regulated cleavage of a contact-mediated axon repellent." Science **289**(5483): 1360-5.

Helmbacher, F., S. Schneider-Maunoury, et al. (2000). "Targeting of the EphA4 tyrosine kinase receptor affects dorsal/ventral pathfinding of limb motor axons." Development **127**(15): 3313-24.

Henderson, C. E., H. S. Phillips, et al. (1994). "GDNF: a potent survival factor for motoneurons present in peripheral nerve and muscle." Science **266**(5187): 1062-4.

Himanen, J. P. and D. B. Nikolov (2003). "Eph receptors and ephrins." Int J Biochem Cell Biol **35**(2): 130-4.

Holland, S. J., N. W. Gale, et al. (1997). "Juxtamembrane tyrosine residues couple the Eph family receptor EphB2/Nuk to specific SH2 domain proteins in neuronal cells." Embo J **16**(13): 3877-88.

Hollyday, M. and V. Hamburger (1977). "An autoradiographic study of the formation of the lateral motor column in the chick embryo." Brain Res **132**(2): 197-208.

Holmberg, J., A. Armulik, et al. (2005). "Ephrin-A2 reverse signaling negatively regulates neural progenitor proliferation and neurogenesis." Genes Dev **19**(4): 462-71.

Huai, J. and U. Drescher (2001). "An ephrin-A-dependent signaling pathway controls integrin function and is linked to the tyrosine phosphorylation of a 120-kDa protein." J Biol Chem **276**(9): 6689-94.

Ishizaka, Y., F. Itoh, et al. (1989). "Human ret proto-oncogene mapped to chromosome 10q11.2." Oncogene **4**(12): 1519-21.

Iwamasa, H., K. Ohta, et al. (1999). "Expression of Eph receptor tyrosine kinases and their ligands in chick embryonic motor neurons and hindlimb muscles." Dev Growth Differ **41**(6): 685-98.

Iwamoto, T., M. Taniguchi, et al. (1993). "cDNA cloning of mouse ret proto-oncogene and its sequence similarity to the cadherin superfamily." Oncogene **8**(4): 1087-91.

Jing, S., D. Wen, et al. (1996). "GDNF-induced activation of the ret protein tyrosine kinase is mediated by GDNFR-alpha, a novel receptor for GDNF." Cell **85**(7): 1113-24.

Kalo, M. S. and E. B. Pasquale (1999). "Multiple in vivo tyrosine phosphorylation sites in EphB receptors." Biochemistry **38**(43): 14396-408.

Kania, A. and T. M. Jessell (2003). "Topographic motor projections in the limb imposed by LIM homeodomain protein regulation of ephrin-A:EphA interactions." Neuron **38**(4): 581-96.

Kania, A., R. L. Johnson, et al. (2000). "Coordinate roles for LIM homeobox genes in directing the dorsoventral trajectory of motor axons in the vertebrate limb." Cell **102**(2): 161-73.

Kawamoto, Y., K. Takeda, et al. (2004). "Identification of RET autophosphorylation sites by mass spectrometry." J Biol Chem **279**(14): 14213-24.

Keller-Peck, C. R., G. Feng, et al. (2001). "Glial cell line-derived neurotrophic factor administration in postnatal life results in motor unit enlargement and continuous synaptic remodeling at the neuromuscular junction." J Neurosci **21**(16): 6136-46.

Khan, P., B. Linkhart, et al. (2002). "Different regulation of T-box genes Tbx4 and Tbx5 during limb development and limb regeneration." Dev Biol **250**(2): 383-92.

Kim, D. and G. R. Dressler (2007). "PTEN modulates GDNF/RET mediated chemotaxis and branching morphogenesis in the developing kidney." Dev Biol **307**(2): 290-9.

Knoll, B. and U. Drescher (2002). "Ephrin-As as receptors in topographic projections." Trends Neurosci **25**(3): 145-9.

Knoll, B. and U. Drescher (2004). "Src family kinases are involved in EphA receptor-mediated retinal axon guidance." J Neurosci **24**(28): 6248-57.

Knoll, B., K. Zarbalis, et al. (2001). "A role for the EphA family in the topographic targeting of vomeronasal axons." Development **128**(6): 895-906.

Kramer, E. R., L. Knott, et al. (2006). "Cooperation between GDNF/Ret and ephrinA/EphA4 signals for motor-axon pathway selection in the limb." Neuron **50**(1): 35-47.

Kullander, K., S. D. Croll, et al. (2001). "Ephrin-B3 is the midline barrier that prevents corticospinal tract axons from recrossing, allowing for unilateral motor control." Genes Dev **15**(7): 877-88.

Kullander, K. and R. Klein (2002). "Mechanisms and functions of Eph and ephrin signalling." Nat Rev Mol Cell Biol **3**(7): 475-86.

Kullander, K., N. K. Mather, et al. (2001). "Kinase-dependent and kinase-independent functions of EphA4 receptors in major axon tract formation in vivo." Neuron **29**(1): 73-84.

Lallemand, Y., V. Luria, et al. (1998). "Maternally expressed PGK-Cre transgene as a tool for early and uniform activation of the Cre site-specific recombinase." Transgenic Res **7**(2): 105-12.

Lance-Jones, C. (1982). "Motoneuron cell death in the developing lumbar spinal cord of the mouse." Brain Res **256**(4): 473-9.

Lance-Jones, C. and L. Landmesser (1981). "Pathway selection by chick lumbosacral motoneurons during normal development." Proc R Soc Lond B Biol Sci **214**(1194): 1-18.

Landmesser, L. (1978). "The development of motor projection patterns in the chick hind limb." J Physiol **284**: 391-414.

Landmesser, L. T. (2001). "The acquisition of motoneuron subtype identity and motor circuit formation." Int J Dev Neurosci **19**(2): 175-82.

Ledda, F., G. Paratcha, et al. (2002). "Target-derived GFRalpha1 as an attractive guidance signal for developing sensory and sympathetic axons via activation of Cdk5." Neuron **36**(3): 387-401.

Lee, K. J. and T. M. Jessell (1999). "The specification of dorsal cell fates in the vertebrate central nervous system." Annu Rev Neurosci **22**: 261-94.

Lee, S. K. and S. L. Pfaff (2001). "Transcriptional networks regulating neuronal identity in the developing spinal cord." Nat Neurosci **4 Suppl**: 1183-91.

Leighton, P. A., K. J. Mitchell, et al. (2001). "Defining brain wiring patterns and mechanisms through gene trapping in mice." Nature **410**(6825): 174-9.

Lin, J. H., T. Saito, et al. (1998). "Functionally related motor neuron pool and muscle sensory afferent subtypes defined by coordinate ETS gene expression." Cell **95**(3): 393-407.

Lin, L. F., D. H. Doherty, et al. (1993). "GDNF: a glial cell line-derived neurotrophic factor for midbrain dopaminergic neurons." Science **260**(5111): 1130-2.

Livet, J., M. Sigrist, et al. (2002). "ETS gene Pea3 controls the central position and terminal arborization of specific motor neuron pools." Neuron **35**(5): 877-92.

Markus, A., T. D. Patel, et al. (2002). "Neurotrophic factors and axonal growth." Curr Opin Neurobiol **12**(5): 523-31.

Marquardt, T., R. Shirasaki, et al. (2005). "Coexpressed EphA receptors and ephrin-A ligands mediate opposing actions on growth cone navigation from distinct membrane domains." Cell **121**(1): 127-39.

Mey, J. and S. Thanos (2000). "Development of the visual system of the chick. I. Cell differentiation and histogenesis." Brain Res Brain Res Rev **32**(2-3): 343-79.

Miyazaki, K., N. Asai, et al. (1993). "Tyrosine kinase activity of the ret proto-oncogene products in vitro." Biochem Biophys Res Commun **193**(2): 565-70.

Moore, M. W., R. D. Klein, et al. (1996). "Renal and neuronal abnormalities in mice lacking GDNF." Nature **382**(6586): 76-9.

Myers, S. M., C. Eng, et al. (1995). "Characterization of RET proto-oncogene 3' splicing variants and polyadenylation sites: a novel C-terminus for RET." Oncogene **11**(10): 2039-45.

Natarajan, D., M. Grigoriou, et al. (1999). "Multipotential progenitors of the mammalian enteric nervous system capable of colonising aganglionic bowel in organ culture." Development **126**(1): 157-68.

Natarajan, D., C. Marcos-Gutierrez, et al. (2002). "Requirement of signalling by receptor tyrosine kinase RET for the directed migration of enteric nervous system progenitor cells during mammalian embryogenesis." Development **129**(22): 5151-60.

Nguyen, Q. T., A. S. Parsadanian, et al. (1998). "Hyperinnervation of neuromuscular junctions caused by GDNF overexpression in muscle." Science **279**(5357): 1725-9.

Noren, N. K. and E. B. Pasquale (2004). "Eph receptor-ephrin bidirectional signals that target Ras and Rho proteins." Cell Signal **16**(6): 655-66.

Nornes, H. O. and M. Carry (1978). "Neurogenesis in spinal cord of mouse: an autoradiographic analysis." Brain Res **159**(1): 1-6.

Novitch, B. G., H. Wichterle, et al. (2003). "A requirement for retinoic acid-mediated transcriptional activation in ventral neural patterning and motor neuron specification." Neuron **40**(1): 81-95.

Oppenheim, R. W. (1986). "The absence of significant postnatal motoneuron death in the brachial and lumbar spinal cord of the rat." J Comp Neurol **246**(2): 281-6.

Oppenheim, R. W., L. J. Houenou, et al. (1995). "Developing motor neurons rescued from programmed and axotomy-induced cell death by GDNF." Nature **373**(6512): 344-6.

Oppenheim, R. W., L. J. Houenou, et al. (2000). "Glial cell line-derived neurotrophic factor and developing mammalian motoneurons: regulation of programmed cell death among motoneuron subtypes." J Neurosci **20**(13): 5001-11.

Orioli, D. and R. Klein (1997). "The Eph receptor family: axonal guidance by contact repulsion." Trends Genet **13**(9): 354-9.

Pachnis, V., B. Mankoo, et al. (1993). "Expression of the c-ret proto-oncogene during mouse embryogenesis." Development **119**(4): 1005-17.

Paratcha, G., F. Ledda, et al. (2003). "The neural cell adhesion molecule NCAM is an alternative signaling receptor for GDNF family ligands." Cell **113**(7): 867-79.

Pfaff, S. L., M. Mendelsohn, et al. (1996). "Requirement for LIM homeobox gene Isl1 in motor neuron generation reveals a motor neuron-dependent step in interneuron differentiation." Cell **84**(2): 309-20.

Plaza-Menacho, I., G. M. Burzynski, et al. (2006). "Current concepts in RET-related genetics, signaling and therapeutics." Trends Genet **22**(11): 627-36.

Poliakov, A., M. Cotrina, et al. (2004). "Diverse roles of eph receptors and ephrins in the regulation of cell migration and tissue assembly." Dev Cell **7**(4): 465-80.

Riddle, R. D., M. Ensini, et al. (1995). "Induction of the LIM homeobox gene Lmx1 by WNT7a establishes dorsoventral pattern in the vertebrate limb." Cell **83**(4): 631-40.

Sahin, M., P. L. Greer, et al. (2005). "Eph-dependent tyrosine phosphorylation of ephexin1 modulates growth cone collapse." Neuron **46**(2): 191-204.

Sariola, H. and M. Saarma (2003). "Novel functions and signalling pathways for GDNF." J Cell Sci **116**(Pt 19): 3855-62.

Schmidt, A. and A. Hall (2002). "Guanine nucleotide exchange factors for Rho GTPases: turning on the switch." Genes Dev **16**(13): 1587-609.

Schneider, V. A. and M. Granato (2003). "Motor axon migration: a long way to go." Dev Biol **263**(1): 1-11.

Schuchardt, A., V. D'Agati, et al. (1994). "Defects in the kidney and enteric nervous system of mice lacking the tyrosine kinase receptor Ret." Nature **367**(6461): 380-3.

Scully, A. L., M. McKeown, et al. (1999). "Isolation and characterization of Dek, a Drosophila eph receptor protein tyrosine kinase." Mol Cell Neurosci **13**(5): 337-47.

Shamah, S. M., M. Z. Lin, et al. (2001). "EphA receptors regulate growth cone dynamics through the novel guanine nucleotide exchange factor ephexin." Cell **105**(2): 233-44.

Shirasaki, R. and S. L. Pfaff (2002). "Transcriptional codes and the control of neuronal identity." Annu Rev Neurosci **25**: 251-81.

Sockanathan, S. and T. M. Jessell (1998). "Motor neuron-derived retinoid signaling specifies the subtype identity of spinal motor neurons." Cell **94**(4): 503-14.

Soriano, P. (1999). "Generalized lacZ expression with the ROSA26 Cre reporter strain." Nat Genet **21**(1): 70-1.

Stapleton, D., I. Balan, et al. (1999). "The crystal structure of an Eph receptor SAM domain reveals a mechanism for modular dimerization." Nat Struct Biol **6**(1): 44-9.

Stein, E., A. A. Lane, et al. (1998). "Eph receptors discriminate specific ligand oligomers to determine alternative signaling complexes, attachment, and assembly responses." Genes Dev **12**(5): 667-78.

Takahashi, M. (2001). "The GDNF/RET signaling pathway and human diseases." Cytokine Growth Factor Rev **12**(4): 361-73.

Takahashi, M., Y. Buma, et al. (1989). "Isolation of ret proto-oncogene cDNA with an amino-terminal signal sequence." Oncogene **4**(6): 805-6.

Takahashi, M., J. Ritz, et al. (1985). "Activation of a novel human transforming gene, ret, by DNA rearrangement." Cell **42**(2): 581-8.

Tang, M. J., D. Worley, et al. (1998). "The RET-glial cell-derived neurotrophic factor (GDNF) pathway stimulates migration and chemoattraction of epithelial cells." J Cell Biol **142**(5): 1337-45.

Tessier-Lavigne, M. (1995). "Eph receptor tyrosine kinases, axon repulsion, and the development of topographic maps." Cell **82**(3): 345-8.

Tessier-Lavigne, M. and C. S. Goodman (1996). "The molecular biology of axon guidance." Science **274**(5290): 1123-33.

Thaler, J., K. Harrison, et al. (1999). "Active suppression of interneuron programs within developing motor neurons revealed by analysis of homeodomain factor HB9." Neuron **23**(4): 675-87.

Thanos, C. D., K. E. Goodwill, et al. (1999). "Oligomeric structure of the human EphB2 receptor SAM domain." Science **283**(5403): 833-6.

Thanos, S. and J. Mey (2001). "Development of the visual system of the chick. II. Mechanisms of axonal guidance." Brain Res Brain Res Rev **35**(3): 205-45.

Tosney, K. W. and L. T. Landmesser (1985). "Development of the major pathways for neurite outgrowth in the chick hindlimb." Dev Biol **109**(1): 193-214.

Treanor, J. J., L. Goodman, et al. (1996). "Characterization of a multicomponent receptor for GDNF." Nature **382**(6586): 80-3.

Tronche, F., C. Kellendonk, et al. (1999). "Disruption of the glucocorticoid receptor gene in the nervous system results in reduced anxiety." Nat Genet **23**(1): 99-103.

Trupp, M., E. Arenas, et al. (1996). "Functional receptor for GDNF encoded by the c-ret proto-oncogene." Nature **381**(6585): 785-9.

Trupp, M., N. Belluardo, et al. (1997). "Complementary and overlapping expression of glial cell line-derived neurotrophic factor (GDNF), c-ret proto-oncogene, and GDNF receptor-alpha indicates multiple mechanisms of trophic actions in the adult rat CNS." J Neurosci **17**(10): 3554-67.

Tsuchida, T., M. Ensini, et al. (1994). "Topographic organization of embryonic motor neurons defined by expression of LIM homeobox genes." Cell **79**(6): 957-70.

Wang, H. U. and D. J. Anderson (1997). "Eph family transmembrane ligands can mediate repulsive guidance of trunk neural crest migration and motor axon outgrowth." Neuron **18**(3): 383-96.

Wichterle, H., I. Lieberam, et al. (2002). "Directed differentiation of embryonic stem cells into motor neurons." Cell **110**(3): 385-97.

Wilkinson, D. G. (2001). "Multiple roles of EPH receptors and ephrins in neural development." Nat Rev Neurosci **2**(3): 155-64.

Williams, S. E., F. Mann, et al. (2003). "Ephrin-B2 and EphB1 mediate retinal axon divergence at the optic chiasm." Neuron **39**(6): 919-35.

Yang, X., S. Arber, et al. (2001). "Patterning of muscle acetylcholine receptor gene expression in the absence of motor innervation." Neuron **30**(2): 399-410.

Yin, Y., Y. Yamashita, et al. (2004). "EphA receptor tyrosine kinases interact with co-expressed ephrin-A ligands in cis." Neurosci Res **48**(3): 285-96.

Zhang, J. and S. Hughes (2006). "Role of the ephrin and Eph receptor tyrosine kinase families in angiogenesis and development of the cardiovascular system." J Pathol **208**(4): 453-61.

Zimmer, M., A. Palmer, et al. (2003). "EphB-ephrinB bi-directional endocytosis terminates adhesion allowing contact mediated repulsion." Nat Cell Biol **5**(10): 869-78.

Zimmerman, L., B. Parr, et al. (1994). "Independent regulatory elements in the nestin gene direct transgene expression to neural stem cells or muscle precursors." Neuron **12**(1): 11-24.